Politecnico di Torino

Politecnico di Torino

Master's Degree in Communication Engineering

Serial Bicode DSSS Pilot Channels for Satellite Navigation: Performance Analysis and Design

Candidate: ASSAF Mohammad Mahdi

Supervisors: Prof. GARELLO Roberto
Dr. NARDIN Andrea

Academic Year 2024/25

Summary

Serial Multicode Direct Sequence Spread Spectrum (DSSS) was originally introduced by Garello [1], who showed how embedding alternative spreading codes in a pilot channel can provide additional information to expedite synchronization tasks, such as resolving ambiguities in code phases. Building upon this idea, this thesis offers the following contributions:

Analytical Error Performance and Upper Bound for Serial Bicode/-Multicode DSSS: While the error probability under incoherent demodulation was originally presented by [1], we derive closed-form expressions for the error performance of Serial Bicode DSSS signals under coherent demodulation. Beyond the bicode case, we also provide an upper-bound analysis for generic Serial Multicode DSSS configurations, using a union bound approach to establish a tight bound (especially at medium to low error probabilities) by averaging pairwise error probabilities over all possible code combinations.

Table 1: Error performance for Serial Bicode/Multicode DSSS.

Demodulation Type	$\mathbf{P_b(e)}$	**Serial Multicode DSSS Union Bound**
Coherent	$\frac{1}{2}\operatorname{erfc}\left(\sqrt{\frac{L-R}{4\,\sigma^2}}\right)$	$\frac{1}{2^k}\sum_{i=1}^{2^k}\sum_{\substack{j=1\\ j\neq i}}^{2^k}\frac{d_H(v_i,v_j)}{k}\,\frac{1}{2}\operatorname{erfc}\left(\sqrt{\frac{(L-R_{ij})}{4\,\sigma^2}}\right)$
Incoherent	$f\left(\rho_{01}, k=1, \frac{E_b}{N_0}\right)$	$\frac{1}{2^k}\sum_{i=0}^{2^k-1}\sum_{l\neq i}\frac{d_H(\underline{v}_l,\underline{v}_i)}{k}\,f\left(\rho_{li}, k, \frac{E_b}{N_0}\right)$

Pilot Channel Application: Garello [1] demonstrated how Serial Bicode DSSS can embed patterns within a pilot channel to resolve ambiguities by detecting block transitions. These blocks are structured so that once a transition is identified, both the primary and the secondary code time ambiguities can be resolved.

In this thesis, we develop a statistical framework to evaluate the performance of

block detection, namely the probabilities of false alarm and missed detection. Note that this detection stage assumes knowledge of the delay and Doppler shift affecting the received signal. Consequently, the *acquisition* process, used to estimate delay and Doppler by computing the Cross Ambiguity Function (CAF), is also analyzed for pilot channels employing Serial Bicode DSSS. Specifically, we derive statistical metrics to evaluate the probability of false alarm and the probability of detection, both at the cell and decision level:

1. *Block Transition Detection:* We derive the probability of miss detection (P_{md}) and the probability of false alarm (P_{fa}) under both soft and hard decision rules, covering both coherent and incoherent demodulation strategies.

2. *Acquisition Analysis:* We assess the impact of alternative codes on the acquisition process under long non-coherent integrations. We derive, at the search space cell level, the probability of detection (P_{d}) and the probability of false alarm (P_{fa}); and at the decision level, the probability of detection (P_{D}) along with false alarm probabilities in two scenarios: (P_{FA}^{p}) when the signal is present and (P_{FA}^{a}) when the signal is absent.

Pilot Channel Design Methodology. Lastly, we propose a general method for designing pilot channels utilizing Serial Bicode DSSS technique by formulating the design problem as an optimization problem, thus improving synchronization time and accuracy in MEO GNSS systems. And we showcase three pilot channels with very good performance, each emphasizing a different aspect.

Block Transition Detection Results Table 2 summarizes the derived probabilities of miss detection (P_{md}) for Serial Bicode DSSS pilot channels when detecting block transitions, under various assumptions of demodulation and decision methods (coherent, incoherent, soft, hard). Table 3 then reports the corresponding probabilities of false alarm (P_{fa}).

Table 2: Block Transition Detection – Miss Detection Probability P_{md}.

Demodulation Type	$\mathbf{P}_{\text{md}}$
Coherent (Soft)	$P(T < t \mid H_1) = \frac{1}{2}\,\text{erfc}\Big(\frac{BL_s - t}{\sqrt{2\,BL_s\,\sigma^2}}\Big),$
Coherent (Hard)	$1 \;-\; \sum_{k=0}^{t} \binom{B}{k} (1-P_b)^{\,B-k}\,(P_b)^{\,k}$
Incoherent (Soft)	$1 \;-\; Q_1\Big(\frac{BL_s}{\sqrt{BL_s\,\sigma^2}},\; \frac{t}{\sqrt{BL_s\,\sigma^2}}\Big)$
Incoherent (Hard)	*(Similar to Coherent (Hard), but using the modified error probability for incoherent demodulation.)*

Table 3: Block Transition Detection – False Alarm Probability P_{fa}.

Demodulation Type	$\mathbf{P}_{\text{fa}}$
Coherent (Soft)	$\frac{1}{K-1}\sum_{j=1}^{K-1} \frac{1}{2}\,\text{erfc}\Big(\frac{t - c_j}{\sqrt{2\,BL_s\,\sigma^2}}\Big).$
Coherent (Hard)	$\sum_{k=0}^{t-1} \frac{1}{K-1} \sum_{i=0}^{K-1} \sum_{n=\max\left(0,\, k-(B-DP_i)\right)}^{\min(DP_i,\, k)} \binom{DP_i}{n} (1-P_b)^{\,n}\,(P_b)^{\,DP_i-n}$ $\times \binom{B-DP_i}{k-n} (P_b)^{\,k-n}\,(1-P_b)^{\,(B-DP_i)-(k-n)}$
Incoherent (Soft)	$\frac{1}{K-1}\sum_{i=1}^{K-1} Q_1\Big(\frac{c_i}{\sqrt{BL_s\,\sigma^2}},\; \frac{t}{\sqrt{BL_s\,\sigma^2}}\Big)$
Incoherent (Hard)	*(Similar to Coherent (Hard), but using the modified error probability for incoherent demodulation.)*

Acquisition Results The acquisition stage is analyzed under long non-coherent integration. We derive analytical expressions for the cell-level probabilities of detection P_d and false alarm P_{fa}. These metrics are then used to compute the

overall decision probabilities: P_{D} (probability of detection), P_{FA}^{p} (false alarm probability when the signal is present), and P_{FA}^{a} (false alarm probability when the signal is absent).

Table 4: Acquisition performance for Serial Bicode DSSS pilot channels under long non-coherent integration (cell-level probabilities).

Metric	**Expression**
Probability of Detection P_d	$\frac{1}{K}\sum_{m=1}^{K}\sum_{\tau=1}^{L}\frac{1}{L}\,Q_{N_c}\Big(\sqrt{\frac{\lambda^m(\tau)}{\sigma^2/(L\,N_c)}},\ \sqrt{\frac{t}{\sigma^2/(L\,N_c)}}\Big)$
False Alarm Probability P_{fa}	$\frac{\Gamma\Big(N_c,\ \frac{t}{2\,\sigma^2_{N_c}}\Big)}{\Gamma(N_c)}$

Table 5: Acquisition performance for Serial Bicode DSSS pilot channels under long non-coherent integration (decision-level probabilities).

Metric	**Expression**
Probability of Detection P_{D}	$P_d(t)$
Probability of Missed Detection P_{MD}	$\big[1-P_{\mathrm{fa}}(t)\big]^{M-1}\big[1-P_d(t)\big]$
False Alarm Probability (signal absent) P_{FA}^{a}	$1\ -\ \Big(1-P_{\mathrm{fa}}(t)\Big)^{M}$
False Alarm Probability (signal present) P_{FA}^{p}	$1\ -\ P_{\mathrm{D}}(t)\ -\ P_{\mathrm{MD}}(t)$

Pilot Channel Design Methodology as an Optimization Problem We formulate the pilot channel design as the following optimization problem:

$$\min Z$$

subject to

$$\sum_{j=iB+1}^{(i+1)B} p_j = m, \quad \forall i = 0, 1, \ldots, (b-1),$$

$$Z\ \geq\ \mathbf{P}_i\ \cdot\ \Big(\mathbf{S}_j\Big)^{\mathrm{T}}, \quad \forall i = 1, 2, \ldots, b, \quad \forall j = 1, \ldots, K, \quad j \neq (i-1)B+1.$$

Acknowledgements

First and foremost, I would like to express my deepest gratitude to my advisor, Professor Roberto Garello, for his invaluable guidance and unwavering support. Some encounters leave a lasting mark — Professor Garello helped me discover my own potential and inspired me to dream bigger. His mentorship has deeply influenced not only the development of this work but also my academic and professional aspirations.

I am also deeply thankful to Dr. Andrea Nardin, whose expertise and thoughtful discussions contributed greatly to this research. All our conversations were marked by warmth and curiosity, and he always seemed to have an interesting idea up his sleeve.

My thanks go as well to my colleagues and friends for the productive exchanges and enjoyable moments we've shared throughout this journey.

A special thanks goes to my family for their constant encouragement. Their belief in me, even during the most challenging moments, has been a strong source of motivation.

I want to thank my lifelong friend, Naim — without him, I might have never even begun to imagine myself standing where I am today.

And above all, I thank Hanay—for her presence, her patience, and her love. Without her, none of this would have held the same meaning.

Table of Contents

List of Tables

List of Figures

Acronyms

GNSS
Global Navigation Satellite System

TTFF
time to first fix

PVT
position, velocity, and time

RNS
radio navigation system

GPS
Global Positioning System

PNT
positioning, navigation and timing

SIS
signal in space

DSSS
direct sequence spread spectrum

LEO
low earth orbit

MEO
medium earth orbit

RF

Radio Frequency

IF

intermediate frequency

BPSK

binary phase shift keying

DSP

digital signal processing

STD

standard deviation

SNR

signal-to-noise ratio

CDMA

code division multiple access

TDMA

time division multiple access

FDMA

frequency division multiple access

3G UMTS

third generation universal mobile telecommunications system

AWGN

additive white Gaussian noise

Chapter 1

Introduction

Pilot channels are extensively utilized in GNSSs to improve the signal acquisition and tracking processes essential for receiver synchronization with satellite signals through delay and Doppler shift estimation [2, 3, 4]. However, until navigation data is demodulated, the receiver only obtains a relative timing marker rather than the absolute signal travel time. This relative marker's ambiguity primarily depends on the structure of GNSS signals and the processing capabilities of the receiver.

The absence of data bits on a pilot channel prevents, therefore, independent and unambiguous PVT estimation. Furthermore, incorporating a pilot channel introduces a trade-off, as the transmitted power must be shared between the data and pilot components [4]. However, pilot channels enable extended coherent integration times and improved carrier tracking, significantly enhancing receiver sensitivity [5]. As a consequence, the pilot component supports data channel processing and improves data demodulation performance. Efforts have also been made to design pilot signals that provide more synchronization-relevant information [6], also potentially contributing to an improved TTFF, a key performance indicator for GNSS services [7].

The work presented in [1] introduces *Serial Multicode DSSS*, as a promising alternative to parallel Multicode DSSS/CDMA [8, 9, 10, 11, 12]. The author in [1] demonstrates how we can embed a pattern into a pilot channel using a Serial Bicode DSSS to facilitate a faster extraction of key temporal information at the receiver, which in turn greatly accelerates initial synchronization. Moreover, this method offers flexibility in reducing time resolution ambiguity and, depending on the design parameters and application, may even be designed to provide absolute time information.

The core principle involves constructing a Serial Bicode DSSS pilot channel using two alternative spreading codes—one *legitimate* and one *alternative* code—that convey a synchronization information. Without loss of generality, we can consider a pilot channel made of a short, primary, and secondary code that form a tiered

code pattern, where the two alternative short codes are made of L_s chips, with L_s being an integer divisor of the primary code length $L_1 > L_s$. At the receiver, long non-coherent integration over several short code periods is employed to estimate Doppler shifts and code delays. However, this process leaves two ambiguities to be resolved: one associated with the primary code and another with the secondary code.

To address these ambiguities, the Serial Bicode DSSS signal is leveraged to embed a structured pattern within the pilot channel. This pattern is organized into distinct blocks that makes it easily recognizable. where transitions between consecutive blocks play a crucial role due to two key properties:

1. The transitions are consistently aligned with the primary code.

2. They provide a unique identification of the position within the secondary code.

By determining the position of a 1-block pattern, which is the sequence of spreading codes corresponding to a single block within the pilot channel and serves as a fundamental unit for transition detection, the transition between two consecutive blocks can be identified. This resolves the timing ambiguities in both the primary and secondary codes.

In this Thesis, we provide a comprehensive theoretical framework for evaluating the performance of pilot channels constructed using Serial Bicode DSSS, focusing on both acquisition and block transition detection. Furthermore, we propose a method for designing distinctive pilot channels based on Serial Bicode DSSS that are customized to optimize performance according to mission-specific requirements, yielding considerable improvement in both acquisition and block transition detection when compared to the channel originally proposed by the author in [1]. The work is organized as follows: In Chapter 2, we review Serial Multicode DSSS and its natural extension to CDMA. In Chapter 3, we analyze the performance of Serial Multicode DSSS under both coherent and incoherent demodulation. In Chapter 4, we provide the necessary GNSS background for understanding the subsequent chapters. In Chapter 5, we review the pilot channel construction introduced by Garello [1] for MEO and LEO cases. In Chapter 6, we present the statistical framework for block detection under different demodulation and detection schemes. In Chapter 7, we analyze the acquisition stage under Serial Bicode DSSS pilot channels and derive the corresponding statistical framework for performance evaluation. Finally, in Chapter 8, we propose a method to design various pilot channels using the same technique of utilizing Serial Bicode DSSS by formulating the design problem as an optimization problem, and we showcase three pilot channels with excellent performance, each emphasizing a different aspect. Chapter 9 outlines potential directions for future work.

Chapter 2

Serial Multicode DSSS

2.1 Direct Sequence Spread Spectrum (DSSS)

A spread-spectrum signal involves additional modulation that broadens the signal's bandwidth beyond what is necessary for the data modulation alone. Spread-spectrum communication systems [13] are particularly effective for suppressing interference, complicating interception, accommodating fading and multipath channels, and enabling multiple-access capabilities. The most widely used and practical methods in spread-spectrum communications are direct-sequence modulation in digital communications.

It may seem paradoxical at first to broaden the signal's bandwidth, since doing so would require a wider receive filter, potentially leading to an increase in noise entering the demodulator. However, when a signal passes through a filter designed to match it while accompanied by white Gaussian noise, the signal-to-noise ratio (SNR) depends on the noise power spectral density rather than the filter's bandwidth. Interestingly, this means that the filter's bandwidth and the corresponding noise power at its output do not affect the SNR, underscoring the practical advantages of spread-spectrum communication techniques.

In traditional Direct Sequence Spread Spectrum (DSSS), each user is given a distinct code consisting of a sequence of L chips, which is used to modulate the information sequence. By employing DSSS, the signal's bandwidth is expanded by a factor of L as a result of this encoding. This widening of the bandwidth greatly improves the system's ability to resist noise, interference, and jamming. However, this benefit comes at the cost of a lower information bit rate [13].

2.2 Serial Multicode DSSS

Serial Multicode DSSS assigns each user multiple spreading codes that are used sequentially rather than simultaneously. In this scheme, individual bits or groups of bits are mapped to distinct spreading codes, resulting in a single DSSS signal whose spreading code alternates in accordance with the transmitted data. This contrasts with the Parallel Multicode approach, where several coded streams are transmitted concurrently and the bit rate increases with the number of active codes [1].

At the receiver, a set of correlators—each matched to one of the potential spreading codes—is employed to detect the transmitted symbol. By selecting the correlator with the maximum output magnitude, the system identifies the code associated with the transmitted bit. This method decouples the information from the phase or sign of the spreading sequence, enabling incoherent demodulation. Such a design is especially beneficial in environments with high Doppler effects, for instance in satellite or UAV communications, where reducing receiver complexity and the need for stringent synchronization can significantly improve performance. Moreover, because only a single DSSS signal is transmitted at any given time, the scheme allows for dynamic bit rate adaptation without increasing the interference level among users [1].

2.2.1 Serial Bicode DSSS

In Serial Bicode DSSS, two distinct spreading codes of length L are assigned to each user. The legitimate code, $c_0 = (c_{01}, \ldots, c_{0L})$ where $c_{0j} \in \{-1, +1\}$, is used when the binary input is 0. Conversely, the alternative code, $c_1 = (c_{11}, \ldots, c_{1L})$ with $c_{1j} \in \{-1, +1\}$, is employed for a binary input of 1. This mapping directs each bit of the binary sequence $v = (v(0), v(1), \ldots, v(i), \ldots)$ with $v(i) \in \{0, 1\}$ to its corresponding code, creating a transmission sequence $s = (x(1), x(2), \ldots, x(i), \ldots)$. This method extends the traditional Direct Sequence Spread Spectrum (DSSS) by incorporating flexibility in the choice of spreading codes, thus generalizing the classic DSSS framework [1].

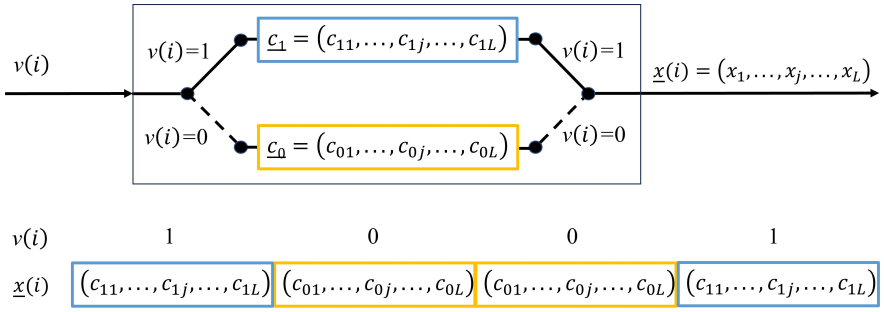

Figure 2.1: Serial Bicode DSSS. [1].

2.2.2 Serial Multicode DSSS

Extending the Serial Bicode framework, Serial Multicode DSSS allocates a set $\mathcal{H} = \{c_0, \ldots, c_{H-1}\}$ of spreading codes to each user, where the cardinality of $\mathcal{H}$, $H = 2^k$, represents the different codes available. A bijective function $f : \{0,1\}^k \to \mathcal{H}$ maps k-bit information vectors to these codes. The transmission sequence is thus constructed as $s = (x(0), x(1), \ldots, x(i), \ldots)$, with $x(i) = f(v(i))$ and the k-bit information vector defined as $v(i) = (v(ik), \ldots, v((i+1)k-1))$ [1].

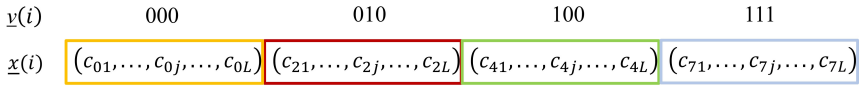

Figure 2.2: Serial Multicode DSSS [1].

2.3 Extension to Code Division Multiple Access (CDMA)

To address the reduction in bit rate caused by spreading in DSSS, multiple users can transmit simultaneously within the same frequency band using Code Division Multiple Access (CDMA) [1]. In CDMA, each user is assigned a unique code of L chips with favorable cross-correlation properties, ensuring minimal mutual interference among users. Information theory suggests that in an isolated cell, CDMA systems can achieve spectral efficiency comparable to that of TDMA or FDMA [13]. CDMA is widely used in systems such as the 3G UMTS mobile network and Global Navigation Satellite Systems (GNSS) like GPS and Galileo, which are crucial for one-way positioning.

In this sense, Serial Multicode DSSS extends naturally to CDMA, where each user is assigned multiple spreading codes. This approach, Serial Multicode CDMA,

is beneficial in scenarios where many coexisting users want to dynamically change their data rates without changing the spreading factor. Examples include satellite constellations and massive IoT applications [1].

In Serial Multicode CDMA, each user transmits a single DSSS signal characterized by a fixed spreading factor L. This design allows for dynamic adjustment of the bit rate while ensuring that any modifications do not lead to increased interference with other users. The fixed spreading factor maintains a consistent level of spreading regardless of bit rate changes, which is crucial for preserving overall system performance.

Furthermore, this approach is particularly well-suited for incoherent demodulation—a method often employed during the initial acquisition and synchronization phases of many communication systems. Incoherent demodulation simplifies receiver design by eliminating the need for phase tracking, thereby reducing both complexity and latency.

The robustness and flexibility inherent in Serial Multicode CDMA make it especially advantageous for applications such as the transmission of specific patterns or sporadic messages over pilot channels. This is particularly relevant in satellite navigation systems like GPS and Galileo, where reliable communication under challenging conditions (e.g., high Doppler shifts) is essential [1].

Chapter 3

Serial Bicode/Multicode DSSS Performance

3.1 Introduction

In this chapter, we will analyze the performance of Serial Bicode DSSS and Serial Multicode DSSS under two distinct demodulation schemes: coherent and incoherent demodulation. Our objective is to evaluate and compare the reliability and effectiveness of these systems in practical scenarios.

By exploring the performance of these systems under both demodulation techniques, we aim to provide a comprehensive understanding of how each method influences the overall system behavior, particularly in terms of bit error rate (BER). The following sections will present detailed theoretical analyses accompanied by simulation results.

3.2 Incoherent Demodulation

Incoherent Demodulation refers to a method in communication systems to detect signals where the phase of the carrier wave is unknown. This technique is commonly used when the signal phase cannot be accurately tracked due to rapid changes or when the system lacks a coherent reference signal. Incoherent detection focuses on using the magnitude of the received signal to make decisions, which simplifies the receiver design but typically results in requiring a higher signal-to-noise ratio threshold for reliable detection. [14]

3.3 Serial Bicode/Multicode DSSS Performance for Incoherent Demodulation

In incoherent demodulation, the optimal receiver computes the magnitude of the complex correlation for each spreading code $\underline{c_i} = (c_{i1}, \ldots, c_{iL})$ from the received complex vector $\underline{r} = (r_1, \ldots, r_L)$. This is given by:

$$|L_i| = \left| \sum_{j=1}^{L} r_j c_{ij} \right| \tag{3.1}$$

The receiver then selects the spreading code corresponding to the highest magnitude $|L_i|$.

3.3.1 Serial Bicode DSSS

Analytic Performance

For Serial Bicode DSSS, the error probability $P_b(e)$, under incoherent demodulation, as explored by Garello [1], is modeled as:

$$P_b(e) = f\left(\rho = \rho_{01}, k = 1, \frac{E_b}{N_0}\right) \tag{3.2}$$

where the function $f(\rho, k, \frac{E_b}{N_0})$ is defined by the expression:

$$f(\rho, k, \frac{E_b}{N_0}) =$$
$$\mathrm{Q}\left(ak\sqrt{\frac{E_b}{N_0}}, bk\sqrt{\frac{E_b}{N_0}}\right) - \frac{1}{2}\exp\left(-\frac{kE_b}{N_0}\frac{a+b}{2}\right) I_0\left(\frac{kE_b}{N_0}\sqrt{ab}\right) \tag{3.3}$$

with

$$a = \frac{1}{2}\left(1 - \sqrt{1 - |\rho|^2}\right) \quad b = \frac{1}{2}\left(1 + \sqrt{1 - |\rho|^2}\right)$$

Here, ρ_{li} is the normalized correlation (inner product) between the sequences c_l and c_i, computed as:

$$\rho_{li} = \frac{\sum_{j=1}^{L} c_{lj} c_{ij}}{L} \tag{3.4}$$

In this specific context, ρ_{01} is the normalized correlation between c_0 and c_1, i.e.,

$$\rho_{01} = \frac{\sum_{j=1}^{L} c_{0j} c_{1j}}{L} \tag{3.5}$$

Q is the Marcum Q-function and I_0 the modified Bessel function of the first kind. The most favorable scenario occurs when the two sequences are orthogonal ($\rho = 0$), simplifying the error probability to:

$$P_b(e) = \frac{1}{2}\exp\left(-\frac{1}{2}\frac{E_b}{N_0}\right) \tag{3.6}$$

Simulation

Following the theoretical development of the error probability for Serial Bicode DSSS, simulations were conducted to validate the analytical expressions and observe the system's behavior under varying conditions of E_b/N_0.

The simulation involved transmitting binary signals modulated according to the Serial Bicode DSSS scheme over a noisy channel (AWGN) and decoding them at the receiver using incoherent demodulation principles. The spreading codes c_0 and c_1 were randomly generated, and the system's bit error rate (BER) was estimated across a range of E_b/N_0 from 0 dB to 12 dB.

A total of 1000 bit errors were collected for each E_b/N_0 value to ensure statistical relevance. The idea of collecting a constant number of errors rather than fixing the number of simulations is that under low E_b/N_0, errors can be collected faster, making the simulation adaptable to the E_b/N_0 values. The received signals were affected by additive white Gaussian noise (AWGN) with varying noise levels corresponding to the E_b/N_0 values tested. The decision at the receiver was made based on the higher correlation between the received signal and the spreading codes.

The results of the simulation are plotted alongside the theoretical error probabilities calculated from the derived formulas. These results demonstrate the alignment between the theoretical predictions and the practical performance of the Serial Bicode DSSS system under incoherent demodulation conditions.

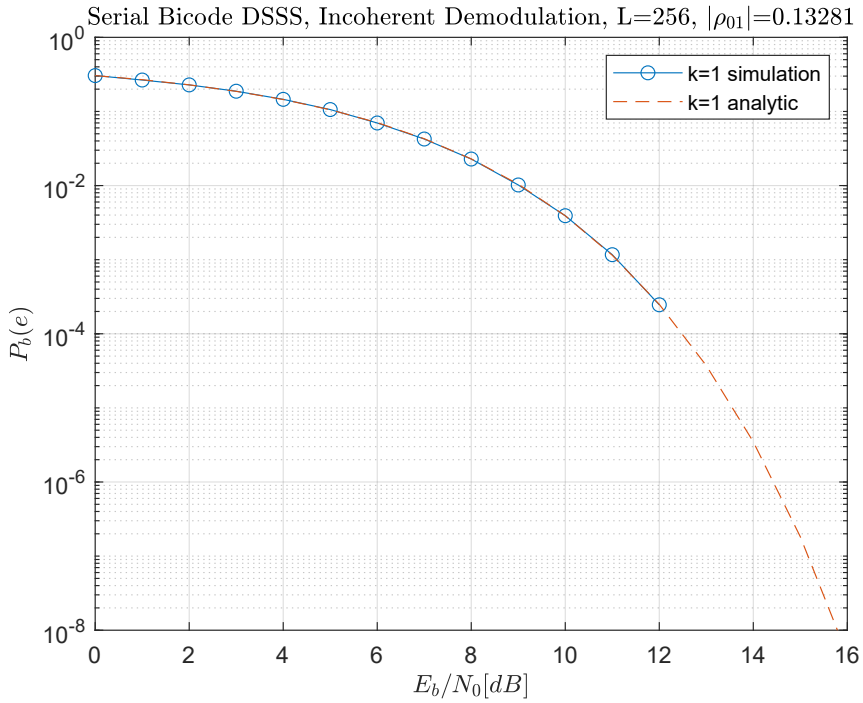

Figure 3.1: Bit error rate performance of Serial Bicode DSSS under incoherent demodulation. The figure shows both simulated and analytical error probabilities as functions of E_b/N_0, with random spreading codes of length $L = 256$ and normalized cross-correlation ρ_{01}.

3.3.2 Serial Multicode DSSS

Analytic Performance

For Serial Multicode DSSS configurations where each symbol represents multiple bits ($k > 1$), the error probability is analyzed using a union bound approach to establish an upper bound. This bound is particularly tight at medium to low error probabilities. The computation involves averaging the pairwise error probabilities across all possible combinations of 2^k spreading codes within the set $\mathcal{H}$:

$$P_b(e) \leq \frac{1}{2^k} \sum_{i=0}^{2^k-1} \sum_{l \neq i} \frac{d_H(\underline{v_l}, \underline{v_i})}{k} \cdot f(\rho_{li}, k, \frac{E_b}{N_0}) \tag{3.7}$$

where $d_H(v_l, v_i)$ is the Hamming distance between the vectors v_l and v_i, and ρ_{li} is their normalized cross-correlation defined in (3.4).

In the special case, when using 2^k orthogonal spreading codes, the error probability simplifies significantly due to uniformity in the distance profiles and congruence

in the decision regions. The simplified error probability expression becomes:

$$P_b(e) \leq 2^{k-2} \exp\left(-\frac{1}{2} k \frac{E_b}{N_0}\right) \tag{3.8}$$

Simulation

Following the theoretical framework, simulations were conducted to empirically validate the error probabilities for Serial Multicode DSSS under various E_b/N_0 conditions. The simulations leveraged a system with $L = 256$ spreading code length and $k = 2$ bits per symbol, reflecting a practical scenario where each short code can represent multiple bits. This setup aimed to test the system's error performance over an Additive White Gaussian Noise (AWGN).

The simulation involved generating $2^k = 4$ random spreading codes, each of length L. Each transmission involved selecting a code based on the binary representation of k-bit symbols, modulating this with a random phase, and transmitting over a noisy channel. The receiver then determined the most likely transmitted code by calculating the correlation between the received signal and each possible code. This process was repeated until 1000 bit errors were collected for each E_b/N_0 value to ensure statistical accuracy.

The bit error rate (BER) was computed for each E_b/N_0 value and plotted alongside the analytical predictions derived from the union bound described in (3.7). This provided a visual comparison between the theoretical predictions and the actual performance of the Serial Multicode DSSS system under noisy conditions.

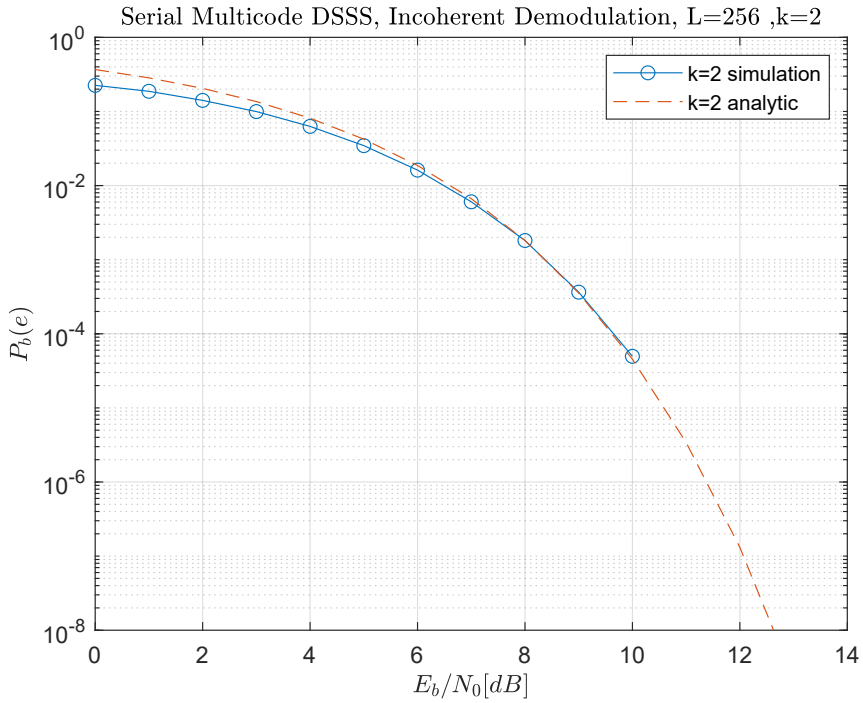

Figure 3.2: Performance of Serial Multicode DSSS in terms of bit error rate (BER) as a function of E_b/N_0. The plot shows simulation results with analytical predictions for a system with $L = 256$ and $k = 2$.

Finally, we compare the error performance of Serial Bicode and Multicode DSSS systems to observe the impact of different spreading techniques and dimensionalities on bit error rates.

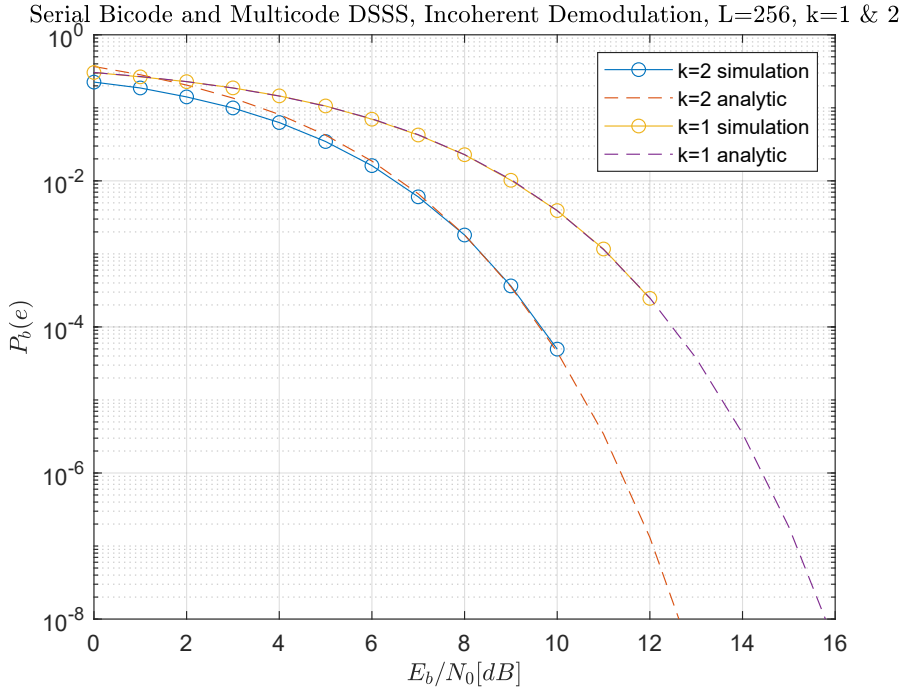

Figure 3.3: Error performance comparison between Serial Bicode and Multicode DSSS systems under incoherent demodulation. The graph displays BER as a function of E_b/N_0 for $L = 256$ with $k = 1$ and $k = 2$.

Figure 3.3 illustrates the effects of increasing the dimensionality (from $k = 1$ to $k = 2$) on system performance, highlighting the differences in error probabilities between the two systems.

3.3.3 Performance Analysis of Serial Multicode DSSS with Orthogonal Spreading Codes

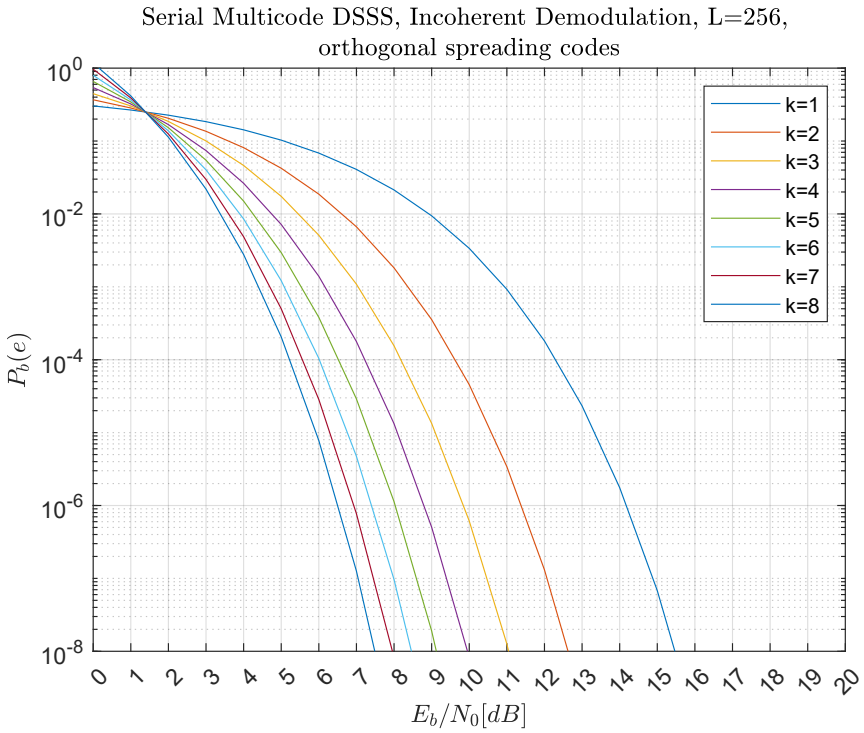

Figure 3.4: Bit error rate performance of Serial Multicode DSSS for different values of k using orthogonal spreading codes. The graph shows BER across a range of E_b/N_0 settings for $L = 256$.

This graph displays the BER for different coding complexities using orthogonal spreading sequences, indicating how increasing k influences error probabilities. Notably, as k increases, the BER decreases for medium to high E_b/N_0 values.

3.4 Coherent Demodulation

Coherent demodulation involves the receiver utilizing the phase of the carrier signal, alongside its amplitude, to decode the transmitted information. This method requires a reference signal or carrier synchronization at the receiver to align the phase. It is generally more complex but provides better sensitivity and accuracy compared to incoherent detection[14].

3.5 Serial Bicode/Multicode DSSS Performance for Coherent Demodulation

In coherent demodulation, the receiver calculates the correlation of the received signal $\underline{r} = (r_1, \ldots, r_L)$ with each spreading code $\underline{c}_i = (c_{i1}, \ldots, c_{iL})$:

$$L_i = \sum_{j=1}^{L} r_j c_{ij} \tag{3.9}$$

The code with the highest correlation L_i is selected by the receiver as the most likely transmitted signal.

3.5.1 Serial Bicode DSSS

Analytic Performance

For Serial Bicode DSSS, the bit error probability $P_b(e)$ is computed as:

$$P_b(e) = \frac{1}{2}\Big(P(e|\underline{c}_1 \text{ Tx}) + P(e|\underline{c}_0 \text{ Tx})\Big) \tag{3.10}$$

This is because we transmit $\underline{c}_1$ or $\underline{c}_0$ with equal probability.

Since $P(e|\underline{c}_1 \text{ Tx}) = P(e|\underline{c}_0 \text{ Tx})$ (because in Serial Bicode DSSS we have only 2 spreading codes $\underline{c}_0$ and $\underline{c}_1$), the overall bit error probability $P_b(e)$ can be expressed as:

$$P_b(e) = \frac{1}{2} \cdot 2 \cdot P(e|\underline{c}_1 \text{ Tx}) = P(e|\underline{c}_1 \text{ Tx}) \tag{3.11}$$

Let's compute $P(e|\underline{c}_1 \text{ Tx})$. When $\underline{c}_1$ is transmitted, an incorrect decision occurs when:

$$\sum_{i=1}^{L} r_i c_{1i} < \sum_{i=1}^{L} r_i c_{0i} \tag{3.12}$$

Here, $\underline{r} = (r_1, \ldots, r_L)$ is the received signal with $r_i = c_i + n_i$, where n_i is a Gaussian random variable with zero mean and variance $\sigma^2 = \frac{N_0}{2}$, representing channel Gaussian noise.

Define:

$$X = \sum_{i=1}^{L} r_i c_{1i} = \sum_{i=1}^{L} (c_{1i} + n_i) c_{1i} = \sum_{i=1}^{L} c_{1i} c_{1i} + \sum_{i=1}^{L} c_{1i} n_i = L + \sum_{i=1}^{L} c_{1i} n_i \tag{3.13}$$

$$Y = \sum_{i=1}^{L} r_i c_{0i} = \sum_{i=1}^{L} (c_{1i} + n_i) c_{0i} = \sum_{i=1}^{L} c_{0i} c_{1i} + \sum_{i=1}^{L} c_{0i} n_i = R + \sum_{i=1}^{L} c_{0i} n_i \tag{3.14}$$

where $\sum_{i=1}^{L} c_{1i}c_{1i} = L$ as $\underline{c_1}$ is bipolar sequence with length L, and R is the cross-correlation between c_0 and c_1 define as:

$$R = \sum_{i=1}^{L} c_{0i}c_{1i} \tag{3.15}$$

The terms $\sum_{i=1}^{L} c_{1i}n_i$ and $\sum_{i=1}^{L} c_{0i}n_i$ are both sums of L independent Gaussian random variables with mean 0 and variance σ^2, resulting in Gaussian random variables with mean 0 and variance $L\sigma^2$.

Thus, X and Y are Gaussian distribution: $X \sim \mathcal{N}(L, L\sigma^2)$ and $Y \sim \mathcal{N}(R, L\sigma^2)$. Now define $Z = X - Y$, which represents the decision variable.

Thus, an error occurs when:

$$Z = X - Y < 0$$

The variable Z is again a Gaussian random variable with:

$$E[Z] = E[X - Y] = E[X] - E[Y] = L - R$$

where $E[.]$ is the expected value operator, and

$$\text{var}(Z) = \text{var}(X) + \text{var}(Y) - 2 \cdot \text{cov}(X, Y)$$

where var(.) and cov(.) are the variance and the covariance operators respectively. The covariance between X and Y, $\text{cov}(X, Y)$, can be calculated as:

$$\text{cov}(X, Y) = E[XY] - E[X]E[Y]$$

Given:

$$X = L + \sum_{i=1}^{L} c_{1i}n_i \quad \text{and} \quad Y = R + \sum_{i=1}^{L} c_{0i}n_i$$

Expanding XY yields:

$$XY = \left(L + \sum_{i=1}^{L} c_{1i}n_i\right)\left(R + \sum_{i=1}^{L} c_{0i}n_i\right)$$

$$= LR + L\sum_{i=1}^{L} c_{0i}n_i + R\sum_{i=1}^{L} c_{1i}n_i + \sum_{i=1}^{L} c_{1i}n_i \sum_{i=1}^{L} c_{0i}n_i$$

Taking the expectation:

$$E[XY] = E\left[LR + L\sum_{i=1}^{L} c_{0i}n_i + R\sum_{i=1}^{L} c_{1i}n_i + \sum_{i=1}^{L} c_{1i}n_i \sum_{i=1}^{L} c_{0i}n_i\right]$$

Since $E[n_i] = 0$ for all i, the terms involving $E[n_i]$ vanish, leaving:

$$E[XY] = LR + E\left[\sum_{i=1}^{L} c_{1i}n_i \sum_{i=1}^{L} c_{0i}n_i\right]$$

we have:

$$E\left[\sum_{i=1}^{L} c_{1i}n_i \sum_{i=1}^{L} c_{0i}n_i\right] = E\left[\sum_{i=1}^{L}\sum_{j\neq i}^{L} c_{1i}c_{0j}n_i n_j + \sum_{i=1}^{L} c_{1i}c_{0i}n_i^2\right]$$

This can be further broken down as:

$$E\left[\sum_{i=1}^{L}\sum_{j\neq i}^{L} c_{1i}c_{0j}n_i n_j\right] + E\left[\sum_{i=1}^{L} c_{1i}c_{0i}n_i^2\right]$$

Since n_i and n_j are independent for $i \neq j$, the term $E\left[\sum_{i=1}^{L}\sum_{j\neq i}^{L} c_{1i}c_{0j}n_i n_j\right]$ simplifies to:

$$\sum_{i=1}^{L}\sum_{j\neq i}^{L} c_{1i}c_{0j}E[n_i n_j] = \sum_{i=1}^{L}\sum_{j\neq i}^{L} c_{1i}c_{0j}E[n_i]E[n_j] = 0$$

Therefore, we are left with:

$$E\left[\sum_{i=1}^{L} c_{1i}c_{0i}n_i^2\right] = \sum_{i=1}^{L} c_{1i}c_{0i}E[n_i^2] = \sigma^2 \sum_{i=1}^{L} c_{1i}c_{0i} = \sigma^2 R$$

Thus:

$$E[XY] = LR + \sigma^2 R \tag{3.16}$$

Subtracting $E[X]E[Y] = LR$, we get:

$$\mathrm{cov}(X, Y) = E[XY] - E[X]E[Y] = \sigma^2 R \tag{3.17}$$

This leads us to the variance of $Z = X - Y$:

$$\begin{aligned} \mathrm{var}(Z) &= \mathrm{var}(X) + \mathrm{var}(Y) - 2\mathrm{cov}(X, Y) \\ &= 2L\sigma^2 - 2R\sigma^2 \\ &= 2\sigma^2(L - R) \end{aligned} \tag{3.18}$$

Thus, Z is distributed as:

$$Z \sim \mathcal{N}(L - R, 2\sigma^2(L - R))$$

The probability of error when c_1 is transmitted ($P(e|\mathbf{c}_1 \text{ Tx})$) and an error occurs if $Z < 0$ is then given by:

$$\begin{aligned} P(e|\underline{c}_1 \text{ Tx}) = P(Z < 0) &= \frac{1}{2}\text{erfc}\left(\sqrt{\frac{(L-R)^2}{2(2\sigma^2(L-R))}}\right) \\ &= \frac{1}{2}\text{erfc}\left(\sqrt{\frac{L-R}{4\sigma^2}}\right) \end{aligned} \tag{3.19}$$

Using (3.11), we arrive at the final expression for the bit error probability:

$$P_b(e) = \frac{1}{2}\text{erfc}\left(\sqrt{\frac{L-R}{4\sigma^2}}\right) \tag{3.20}$$

Simulation

After theoretically deriving the error probability for Serial Bicode DSSS, we conducted simulations to validate these theoretical predictions with coherent demodulation. The simulations track the performance of the Serial Bicode DSSS system as it decodes signals in the presence of Gaussian noise.

The results of these simulations are visualized in the figure 3.5, which compares the simulated error probabilities against the analytical predictions.

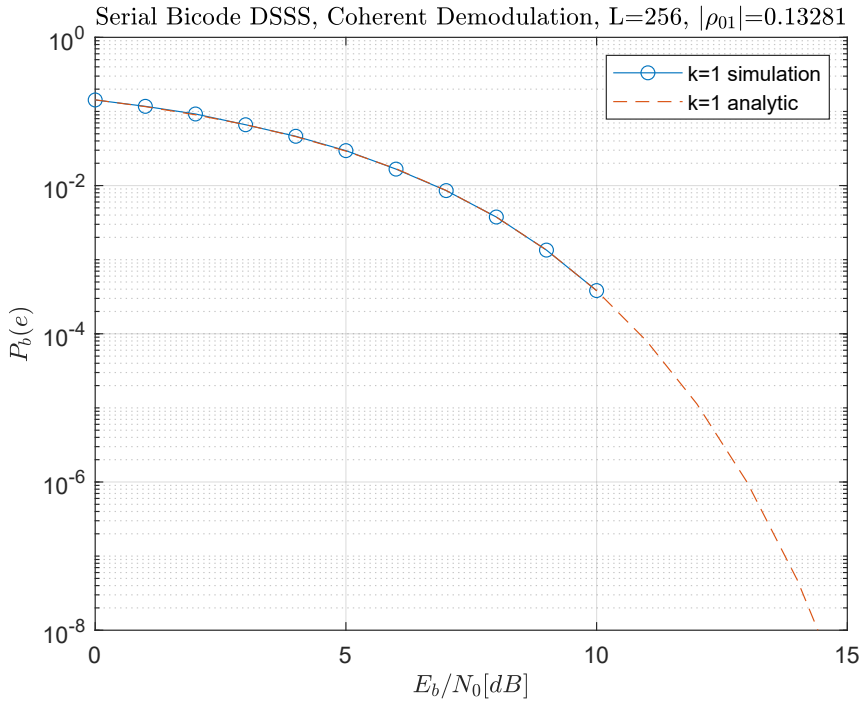

Figure 3.5: Comparison of simulated and theoretical bit error probabilities for Serial Bicode DSSS under coherent demodulation.

The simulation results align perfectly with the analytical predictions derived in the previous section, demonstrating the accuracy of our theoretical model for coherent demodulation performance in Serial Bicode DSSS.

3.5.2 Serial Multicode DSSS

Analytic Performance

The probability of error $P_{e,\text{multi}}$ for a Serial Multicode system with k-bit symbols can be estimated by averaging the pairwise error probabilities across all distinct code pairs. Using the pairwise error probability from Equation (3.20) and applying the union bound to establish an upper bound, we have:

$$P_{e,\text{multi}} \leq \frac{1}{2^k} \sum_{i=1}^{2^k} \sum_{j=1, j\neq i}^{2^k} \frac{d_H(v_i, v_j)}{k} \cdot \frac{1}{2} \text{erfc}\left(\sqrt{\frac{(L - R_{ij})}{4\sigma^2}}\right) \tag{3.21}$$

where R_{ij} is given in Equation (3.15).

This expression provides a bound on the probability of error which is tight at medium/low values of error probability.

Simulation

To validate the theoretical predictions of error probabilities, simulations were performed for coherent demodulation scheme. For this, we simulated a Serial Multicode DSSS system with $k = 2$, over a range of E_b/N_0 values. The bit error rates (BER) obtained from these simulations are plotted alongside the analytical predictions, providing a direct comparison between simulated outcomes and theoretical expectations.

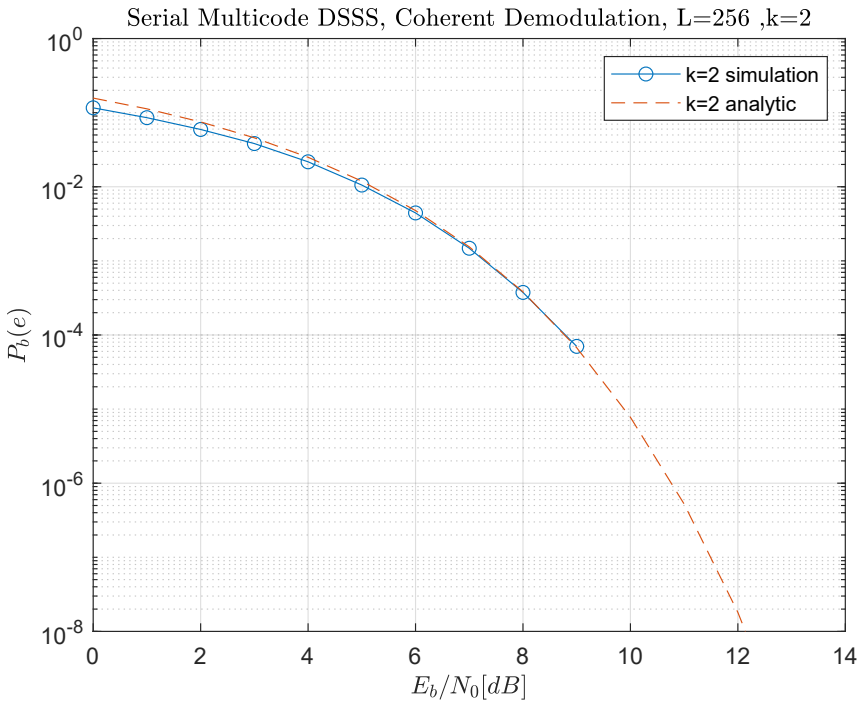

Figure 3.6: Bit error rate performance of Serial Multicode DSSS under coherent detection.

Combined Simulation for Serial Bicode and Multicode DSSS To provide a comprehensive analysis of the performance of Serial Bicode ($k = 1$) and Multicode ($k = 2$) DSSS systems under coherent demodulation conditions, we plot both bit error rate (BER) performances of Serial Bicode and Multicode DSSS under incoherent demodulation alongside each other. This approach enables a direct comparison, highlighting the impact of increasing code complexity from bicode to multicode on system performance. By examining the BER for both systems, we can illustrate how the increased complexity of multicode DSSS influences overall performance, emphasizing the effects of the increased complexity on the BER.

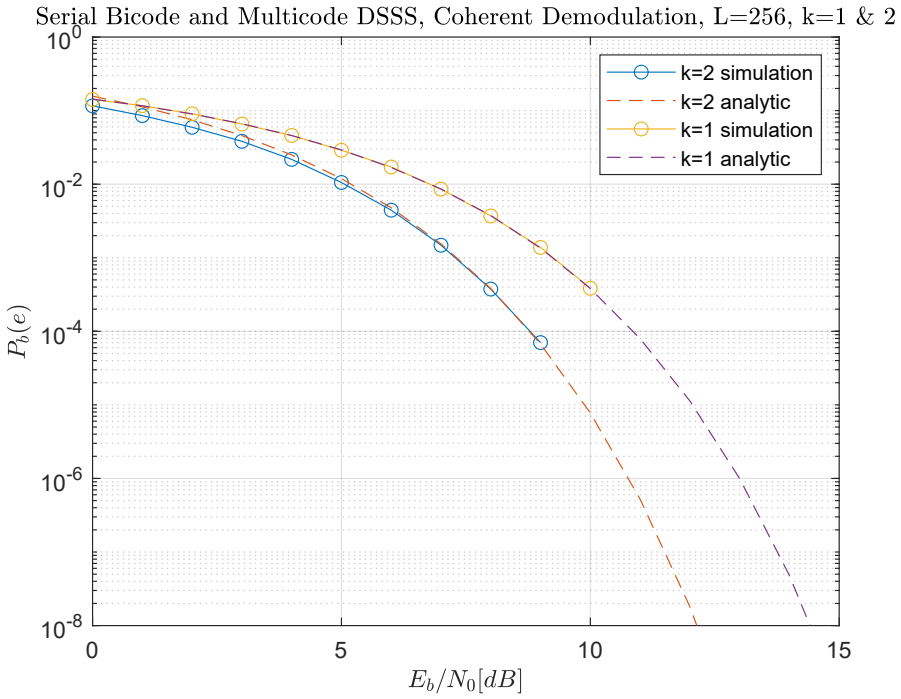

Figure 3.7: Comparison of bit error rate performance between Serial Bicode and Multicode DSSS under coherent demodulation.

Fig. 3.7 showcases BER as a function of E_b/N_0 for systems with $L = 256$ and varying k values, highlighting the differences in error probabilities with increasing complexity.

These results underscore how the increase in symbol complexity (k) impacts the system's error performance across different demodulation schemes. The comparison clarifies the performance enhancements when transitioning to a more complex coding scheme.

Chapter 4

GNSS Background

4.1 Introduction

Global Navigation Satellite Systems (GNSS) are indispensable for providing positioning, navigation, and timing (PNT) services globally [2]. These systems, comprising GPS, Galileo, GLONASS, and BeiDou, operate through a constellation of satellites that transmit signals to ground-based receivers. The receivers process these signals to determine location, velocity, and time [15]. This chapter establishes the foundational knowledge required to comprehend the acquisition process in GNSS receivers. It begins with an overview of the front-end stage of the receiver, followed by a detailed discussion on the acquisition process—the initial and crucial step in GNSS signal processing. This process involves detecting a satellite signal and making preliminary estimates of key parameters like code delay and Doppler frequency, essential for the subsequent tracking and position determination stages [16].

4.2 Receiver Architecture

A GNSS receiver's primary function is to measure the propagation time τ of signals transmitted by GNSS satellites, which is crucial for determining the range between the receiver and the satellites, and ultimately, the user's precise location [17]. Additionally, estimating the Doppler shift f_D is necessary to compute user velocity and clock drift.

The receiver must first identify which satellites are visible at any given moment. It continuously scans for radio signals to acquire and then track, ensuring the correct extraction of information needed to solve the Position, Velocity, and Timing (PVT) equations [18].

4.3 Front-End

Although GNSS receivers vary in design, their core components are largely consistent. The process starts with an antenna that captures the satellite signals in space (SIS), including any accompanying noise and interference. Once received, the signal undergoes front-end processing, including filtering, down-conversion, sampling, and quantization.

Initially, the front-end filters the incoming signal to eliminate out-of-band noise and interference, ensuring that only relevant frequency bands are processed. The signal is then amplified to strengthen the weak satellite signals, which are often below the noise floor due to their long travel distance.

Next, the signal is downconverted from the high-frequency carrier to a lower intermediate frequency (IF) or directly to baseband, simplifying digital processing. Following downconversion, the signal is sampled and quantized by an analog-to-digital converter (ADC), converting the continuous-time signal into a digital format suitable for the acquisition and tracking stages.

The design and performance of the front-end are pivotal in determining the GNSS receiver's sensitivity and accuracy, as it sets the foundation for all subsequent signal processing operations [19].

4.3.1 Signal Model at the Front-End Output

For the analysis that follows, relatively small coherent integration times are assumed, so certain second-order effects (e.g., Doppler impact on the spreading code) can often be safely neglected [20]. Likewise, the potential impact of the local oscillator on the sampling frequency remains out of scope given these short integration periods [20]. Note also that a complex sampling scheme is considered because with a real sampling, one would face additional summed-frequency components after mixing that could affect correlation results [21]. Nonetheless, results from real and complex sampling approaches remain reasonably close [22].

Consequently, at the output of the front end, considering a complex sampling approach, the received signal can be expressed as:

$$r_x(t) = \sqrt{2P_{RX}}\, D(t-\tau)\, c(t-\tau) \exp\Big(2\pi(f_{IF} + f_D)t + \Phi\Big) + \eta(t), \qquad (4.1)$$

where:

- τ represents the code delay due to signal propagation,
- f_D is the Doppler shift,
- $d(t-\tau)$ and $c(t-\tau)$ are the data and spreading code, respectively,

- f_{IF} is the intermediate frequency,
- Φ denotes the phase at the receiver,
- $\eta(t)$ accounts for noise modeled as zero-mean White Gaussian Noise (WGN),
- P_{RX} is the received power, considerably lower than the transmitted power due to various signal impairments.

For dataless pilot channels, the received signal does not include the data component. Thus, in our analysis, we model the post front-end signal for dataless pilot channels as follows (with the amplitude assumed to be unity, which does not impact the analysis):

$$r_x(t) = \alpha\, c(t-\tau)\exp\Big(2\pi(f_{IF}+f_D)t+\Phi\Big)+\eta(t), \quad \text{with } \alpha = 1. \tag{4.2}$$

4.4 Acquisition Stage

After being processed by the front end, the signal is directed to the acquisition and tracking stages, where digital signal processing (DSP) occurs. The acquisition stage serves as the preliminary phase, identifying the presence of satellites and initiating signal processing. The acquisition's output is passed to the tracking stage, where the delay of the local code replica—used for pseudorange computation—is precisely estimated [23]. Once the pseudorange is calculated, the PVT solution can be determined. It is important to highlight that acquisition and tracking are continuous, parallel processes. As satellites enter and leave the receiver's view, these operations are constantly updated to ensure accurate PVT calculations [24].

4.4.1 Signal Acquisition Process

The initial operation of a GNSS receiver is signal acquisition, which detects the presence of the signal under test and provides a rough estimation of the code delay and Doppler frequency of the incoming signal. Acquisition systems are based on correlating the received signal with a local replica, specifically through the evaluation and processing of the Cross Ambiguity Function (CAF). This involves a global search for approximate values of delay and Doppler shift. The CAF is a two-dimensional correlation function in the delay and Doppler domains that is used to compare the incoming signal with a local replica, yielding the best estimation of its parameters [25].

Cross Ambiguity Function (CAF)

The CAF in the discrete time domain is given by:

$$R(\hat{\tau}, \hat{f}_d) = \frac{1}{L} \sum_{n=1}^{L} r_x(nT_s) c(nT_s - \hat{\tau}) \exp\left(j2\pi(f_{IF} + \hat{f}_d) nT_s\right) \tag{4.3}$$

where $r_x(nT_s)$ is the received signal in the coherent window T_{coh}, sampled at intervals T_s.

In our analysis, we take $T_{coh} = L_s T_s = T_{short}$, where T_s is the sampling period, L_s is the number of chips of a short code and T_{short} is the duration of the short spreading code, obtaining 1 sample for each chip for the short code.

and $c(nT_s - \hat{\tau}) \exp\left(j2\pi(f_{IF} + \hat{f}_d) nT_s\right)$ is the local replica. f_{IF} is the intermediate frequency provided by the front-end receiver, and $\underline{c} \equiv \underline{c_0}$ defined as the legitimate code in chapter 1.

Let $\hat{F}_d = (f_{IF} + \hat{f}_d) T_s$ be the normalized frequency. Eq. (4.3) can be then written as:

$$R(\hat{\tau}, \hat{F}_d) = \frac{1}{L} \sum_{i=1}^{L} r_x(iT_s)\, c_0(iT_s - \hat{\tau}) \exp(-j2\pi \hat{F}_d i) \tag{4.4}$$

Which can be ordered as:

$$R(\hat{\tau}, \hat{F}_d) = Y_R(\hat{\tau}, \hat{F}_d) + jY_I(\hat{\tau}, \hat{F}_d)\ . \tag{4.5}$$

The phase of the received signal is unknown and is not estimated at this stage; hence, we consider the square modulus of the CAF to eliminate phase dependency, obtaining:

$$\begin{aligned} Y^2(\hat{\tau}, \hat{F}_d) &= \left| R(\hat{\tau}, \hat{F}_d) \right|^2 \\ &= Y_R^2(\hat{\tau}, \hat{F}_d) + Y_I^2(\hat{\tau}, \hat{F}_d)\ . \end{aligned} \tag{4.6}$$

Search Space and Grid

The CAF function is evaluated over a set of values that define the search space. The grid has the dimensions of delay (time) and Doppler shift (frequency). The search space contains bins, each representing a unique combination of delay and Doppler shift values.

The number of delay bins, N_τ, depends on the sampling frequency f_s and the coherent integration time T_{coh}, which is the time window taken into consideration for the calculation of the correlation function. The coherent integration time is a multiple of the code period. The number of delay bins is then:

$$N_\tau = f_s T_{coh} = \frac{T_{coh}}{T_s} = \frac{LT_s}{T_s} = L \tag{4.7}$$

where T_s is the sampling period.

The Doppler shift bins, Δf, take discrete values, and the optimal bin size depends on the integration time. An empirical rule used by many GNSS receivers is adopted to limit the loss when the actual Doppler shift is not one of the values tested [2, 26, 27, 25]. This rule ensures that, in the worst case, the loss is less than 3 dB. The empirical bin size is given by:

$$\Delta f = \frac{2}{3T_{coh}} \tag{4.8}$$

Then the Doppler domain $\mathcal{D}$ is given by:

$$\mathcal{D} = (f_{d,\min}, f_{d,\min} + \Delta f, \ldots, f_{d,\min} + i\Delta f, \ldots, f_{d,\max})$$

with $|\mathcal{D}| = H$, where H is the total number of Doppler bins.

4.4.2 Non-Coherent Integration

In order to reduce the impact of noise, we consider non-coherent integration, where we average the CAF evaluated over N_c coherent blocks, thereby reducing the noise variance by N_c [28]. This process enhances the detection probability of weak signals and improves the overall performance of the acquisition system.

The non-coherent integration of the CAF is given by:

$$X(\hat{\tau}, \hat{F}_d) = \frac{1}{N_c} \sum_{k=1}^{N_c} Y_k^2(\hat{\tau}, \hat{F}_d), \tag{4.9}$$

where $Y_k^2(\hat{\tau}, \hat{F}_d)$ is the squared modulus of the CAF evaluated for the k-th coherent integration. By averaging the squared modulus of the CAF over N_c blocks, we achieve a significant reduction in noise variance, improving the reliability of the signal acquisition process.

Search Strategy

In this context, the decision involves finding the maximum of the non-coherently integrated CAF:

$$\hat{p}_{\text{ML,NC}} = \arg\max_{\hat{p}} X(\hat{\tau}, \hat{F}_d), \tag{4.10}$$

where $\hat{p} = (\hat{\tau}, \hat{F}_d)$ represents the set of trial parameters.

There are different strategies to explore the search space. In our analysis, we adopt a strategy that involves evaluating the CAF over the entire search space. The decision is made based on the maximum of the ambiguity function. If the maximum value is greater than a predetermined threshold, the satellite signal is considered present and aligned. The estimated Doppler and code delay are those corresponding to the maximum value.

Chapter 5

Application of Serial Multicode DSSS to Pilot Channel Construction

5.1 Introduction

In this chapter, we discuss how Serial Multicode Direct Sequence Spread Spectrum (DSSS) can be applied to the design of pilot channels, which are crucial for improving the initial stages of position computation in Global Navigation Satellite Systems (GNSS) such as GPS and Galileo. Serial Multicode DSSS leverages alternative spreading codes to encode information within a DSSS pilot channel. Once these encoded patterns are detected, they provide precise temporal references, facilitating efficient system synchronization.

This method was originally proposed by Garello [1]. In this chapter, we revisit his approach to constructing pilot channels for both Medium Earth Orbit (MEO) and Low Earth Orbit (LEO) GNSS systems, employing Serial Bicode DSSS.

5.2 MEO GNSS Application

5.2.1 Scenario Overview

In typical Medium Earth Orbit (MEO) GNSS, each satellite sends out a data stream that includes:

- A primary code with a length $L_1 = 4000$ chips (as in the example of Fig. 5.1).
- A secondary code with a length $L_2 = 20$ chips (as in the example of Fig. 5.1).

These systems encounter challenges with time ambiguity in signal reception, which can delay or complicate synchronization.

At the receiver side, the following steps are essential:

1. Estimation of the Doppler shift and Code Delay values.
2. Alignment with the primary and secondary codes.
3. Data decoding.

For the first step, non-coherent integration is necessary, but this process is slowed down by data transitions with their change of sign. To address this issue, data-less pilot channels are used to speed up the acquisition process. By using these pilot channels, non-coherent correlations can be performed to estimate the Doppler shift and Code Delay values efficiently. Once these values are estimated, the primary and secondary code time ambiguities still need to be resolved to achieve proper alignment and synchronization with the primary and secondary code.

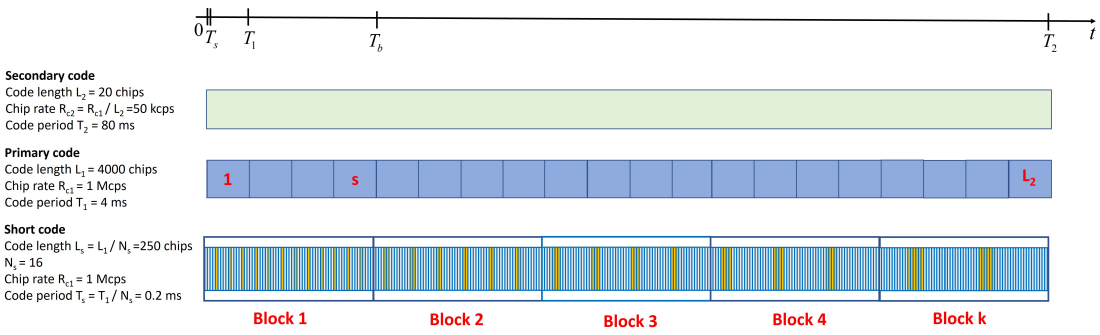

Figure 5.1: Construction of a data-less pilot channel by Serial Bicode DSSS for MEO GNSS [1].

Advantages of Data-less Pilot Channels: These channels accelerate the acquisition process by focusing solely on the essential synchronization signals, eliminating the complications introduced by unknown data modulation.

5.2.2 Construction of Serial Bicode DSSS Pilot Channel for MEO GNSS

The construction of pilot channels using Serial Bicode DSSS in MEO GNSS systems involves utilizing two distinct spreading codes to effectively resolve primary and secondary time ambiguities. This design leverages the simplicity of data-less pilot channels to enhance the speed and accuracy of satellite signal acquisition and synchronization.

Design Specifications The pilot channel employs two short spreading codes, each with a length $L_s = 250$ chips. The length of these codes is an integer divisor of the primary code length $L_1 = 4000$ chips. Both codes operate at the same chip rate R_{c1} as the primary code, without any overlay of secondary coding or data. This means that 16 short codes are required to cover the entire primary code length.

Pattern Embedding The Serial Bicode DSSS signal uses two short codes of the same length L_s: the legitimate code $\underline{c_0}$ (blue) and the alternative code $\underline{c_1}$ (orange). These codes embed a pattern $\underline{p}$ into the pilot channel $\underline{s}$, as illustrated in Fig. 5.1. For example, if $\underline{p} = (0,0,0,1)$, then $\underline{s} = (\underline{c_0}, \underline{c_0}, \underline{c_0}, \underline{c_1})$.

The patterns are structured in blocks, each block consisting of 64 symbols (short codes) and having a duration of $T_b = 16$ ms. Thus, five blocks are needed to completely cover the entire secondary code length in this example, yielding a total of 320 symbols modulated by Serial Bicode DSSS. Within each block:

- 52 '0' symbols are modulated by the legitimate code $\underline{c_0}$.
- 12 '1' symbols are modulated by the alternative code $\underline{c_1}$.

Each block has a unique discrete frequency characteristic, aiding synchronization.

Block Transitions and Code Alignment Each block is characterized by a different discrete frequency, making it easily identifiable. The transitions between consecutive blocks play a key role because:

- They are always aligned with the primary code.
- They uniquely identify the position within the secondary code.

By detecting the transition between two consecutive blocks, the receiver automatically achieves the correct alignment and resolves the time ambiguity of both the primary and secondary codes.

Designing Distinctive Pattern Blocks The pattern blocks facilitate quick and precise synchronization. Each block alternates between $\underline{c_0}$ and $\underline{c_1}$, creating a unique discrete frequency signature. This arrangement aids in distinguishing each block and achieving effective synchronization.

5.3 LEO GNSS Application

5.3.1 Scenario Overview

In this section, we describe the application of Serial Bicode DSSS to a LEO GNSS system. The system under consideration comprises:

- A 2-PSK modulated data channel with a primary spreading code having a code rate $R_c = 1.023$ Mchip/s and a code length of 4096 chips (code period of 4 ms), without a secondary code.
- A 2-PSK modulated pilot channel with Serial Bicode DSSS using short spreading codes, having a code rate $R_c = 1.023$ Mchip/s and a code length of 256 chips (code period of 4/16 ms).

As introduced by Garello [1], this scenario differs significantly from the MEO GNSS-like setup, where a secondary code is included. Here, a simpler pattern is sufficient to achieve synchronization because no secondary code ambiguity needs to be resolved.

5.3.2 Construction of Serial Bicode DSSS Pilot Channel for LEO GNSS

In a LEO GNSS system, where the signal-to-noise ratio is typically higher, secondary codes are generally not used. Even so, Serial Bicode DSSS can still enhance the receiver's acquisition performance by simplifying primary code synchronization. For this purpose, we can employ the pattern depicted in Fig. 5.2.

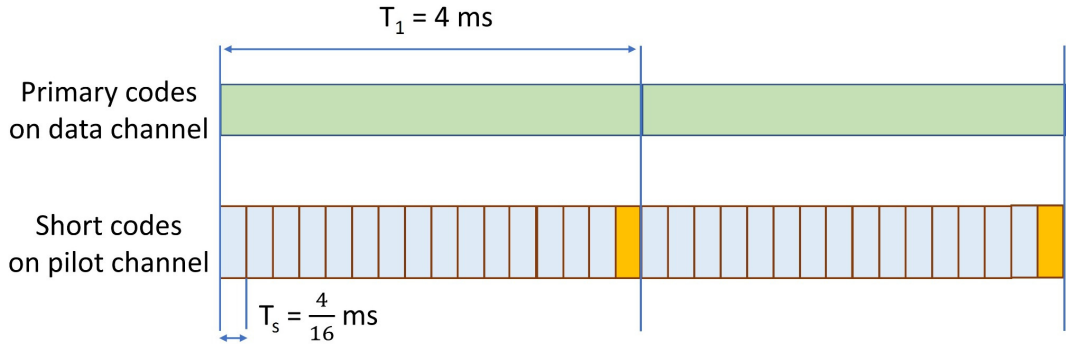

Figure 5.2: Pattern used for Serial Bicode DSSS in a LEO GNSS system [1].

Given that the primary code period is 16 times the short code period, a simplified pattern can be used. This pattern includes a single alternative short code placed in position number 8 out of 16. Once detected, this pattern automatically provides primary code synchronization [1].

Chapter 6

Block Transition Detection

As demonstrated by [1] and introduced in the previous chapter, block transitions are of paramount importance. Detecting the transition between two consecutive blocks (i.e., identifying a 1-block sequence) enables the receiver to achieve correct alignment and resolve the time ambiguity of both the primary and secondary codes.

In this chapter, we provide a statistical analysis for transition detection. We assume the pilot channel $\underline{s}$ is transmitted over an AWGN channel and that the receiver is already aligned with the short codes, having obtained the delay and Doppler estimates from the acquisition stage.

Generic Pilot Channel Model. The analysis is carried out for a generic pilot channel utilizing Serial Bicode DSSS. Such a channel consists of b blocks, each containing B short codes, resulting in a total of $K = b \times B$ short codes in the pilot channel. Although the derivations are performed generally, for the sake of performance comparison with simulation, we adopt the channel introduced by Garello in [1], which has $b = 5$, $B = 64$, and $K = 320$.

The analysis primarily focuses on the probability of false alarm $\left(P_{fa}\right)$ and the probability of missed detection $\left(P_{md}\right)$ for the first block. However, this methodology can be easily extended to other blocks by cyclically shifting the pilot channel such that the i-th block becomes the first block.

This approach effectively characterizes the entire process, since computing P_{md} and P_{fa} for all blocks allows us to determine the probability of detecting the i-th transition, $P_d^{(i)}$, as follows:

$$P_d^{(i)} = (1 - P_{md}^{(i)}) \prod_{\substack{j=1 \\ j \neq i}}^{b} (1 - P_{fa}^{(j)}), \tag{6.1}$$

where $P_{md}^{(i)}$ and $P_{fa}^{(i)}$ denote the probability of missed detection and false alarm for the i-th block, respectively, and b is the total number of blocks.

6.1 Block Transition Detection of MEO GNSS Pilot Channel with Soft Detection

In this section, we present a comprehensive analysis of block transition detection performance for patterns constructed using Serial Bicode DSSS in MEO GNSS applications. We focus on evaluating performance under both coherent and incoherent demodulation scenarios, specifically examining the key probabilities of false alarm (P_{fa}) and missed detection (P_{md}). This analysis emphasizes soft detection, in which the entire received signal is utilized to make a decision.

Scenario Description We consider a scenario involving a pattern $\underline{p}$ composed of $b = 5$ blocks (each of length 64 bits) that are spread using Serial Bicode DSSS to produce the pilot channel $\underline{s}$, as described earlier, where symbol 0 is mapped to the legitimate code $\underline{c_0}$ and symbol 1 to the alternative code $\underline{c_1}$. Both $\underline{c_0}$ and $\underline{c_1}$ are sequences of length L. We focus on the first block (1), being $B = 64$ symbols long. When this pattern $\underline{p_1}$ is spread using Serial Bicode DSSS, we refer to the resulting sequence as $\underline{s_1}$. We consider the signal $\underline{s_1}$ for further analysis.

We transmit a signal $\underline{s}$ of length KL over an AWGN channel, with the received signal given by:

$$\underline{r_x} = \underline{s} + \underline{n}$$

where $\underline{n} = (n_1, n_2, \ldots, n_i, \ldots, n_{KL})$ represents the noise vector, with $n_i \sim \mathcal{N}(0, \sigma^2)$, and we check if the sequence $\underline{s_1}$ is present within a window of length BL.

Hypotheses:

- **Null Hypothesis** H_0: The 1-block sequence is absent at the receiver. The received signal does not contain the 1-block sequence $\underline{s_1}$.
- **Alternative Hypothesis** H_1: The 1-block sequence $\underline{s_1}$ is present at the receiver.

6.1.1 coherent Demodulation

To evaluate the performance under coherent demodulation, we begin by testing the following statistic:

$$T = \sum_{i=1}^{BL} r_{x,i} s_{1,i}$$

We correlate the received signal with the 1- block sequence $\underline{s_1}$, and compare this against a threshold t. We decide:

$$\begin{cases} H_1 & \text{if } T \geq t, \\ H_0 & \text{if } T < t. \end{cases}$$

Under H_0:

$$T = \sum_{i=1}^{BL} (s_{t,i} + n_i) s_{1,i} = \sum_{i=1}^{BL} s_{t,i} s_{1,i} + \sum_{i=1}^{BL} n_i s_{1,i} \tag{6.2}$$

where $\underline{s_t}$ is a segment of length BL that could be any sub-sequence of the pilot channel $\underline{s}$, aligned with the short codes, and excluding $\underline{s}_1$, defined as follows:

First, let the pattern $\underline{p}$ embedded within the pilot channel $\underline{s}$ be represented as:

$$\underline{p} = (p_1, \ldots, p_i, \ldots, p_K) \qquad p \in \{0, 1\}$$

We then define the set $\mathcal{S}$ which contains all possible sub-sequences $\underline{s_t}$ of length BL within $\underline{s}$ (excluding $\underline{s}_1$), where:

$$\mathcal{S} = \left\{ \underline{s_t} = (x(p_{i \bmod K}), \ldots, x(p_{(i+B-1) \bmod K})) \mid 2 \leq i \leq K \right\}$$

where $x(\cdot)$ is a mapping from $0 \mapsto \underline{c}_0$, $1 \mapsto \underline{c}_1$. Here, the subscript indices are taken modulo K, ensuring that the segment wraps around to the start of $\underline{p}$ if $i + B - 1 > K$.

In Eq. (6.2) we have $s_{1,i} \in \{-1{,}1\}$, hence the second term is a sum of BL Gaussian random variables with mean 0 and variance σ^2, so $\sum_{i=1}^{BL} n_i s_{1,i}$ is Gaussian with mean 0 and variance $BL\sigma^2$.

For the first term, $\sum_{i=1}^{BL} s_{t,i} s_{1,i}$, the value depends on the specific transmitted segment $\underline{s_t} \in \mathcal{S}$. We compute correlations for all possible segments and collect the values c in a vector $\underline{c}$.

Let:

$$c_j = \sum_{i=1}^{BL} s_{(t,j),i} s_{1,i} \quad \forall \underline{s_{(t,j)}} \in \mathcal{S}. \tag{6.3}$$

Thus, under H_0:

$$T = c_j + \sum_{i=1}^{BL} n_i s_{1,i} \quad \text{with probability } \frac{1}{K-1}.$$

This means that the pdf of T under H_0 is an average of $(K-1)$ Gaussian distributions, each with variance $BL\sigma^2$ and mean $c_j \in \underline{c}$:

$$f_{H_0}(T) = \frac{1}{K-1} \sum_{i=1}^{K-1} \frac{1}{\sqrt{2\pi \cdot BL\sigma^2}} \exp - \frac{(T - c_i)^2}{2 \cdot BL\sigma^2}. \tag{6.4}$$

Under H_1:

$$T = \sum_{i=1}^{BL}(s_{1,i} + n_i)s_{1,i} = \sum_{i=1}^{BL} s_{1,i}s_{1,i} + \sum_{i=1}^{BL} n_i s_{1,i}$$

Since $\sum_{i=1}^{BL} s_{1,i}s_{1,i} = BL$, and $\sum_{i=1}^{BL} n_i s_{1,i}$ is Gaussian with mean 0 and variance $BL\sigma^2$, then T under H_1 is Gaussian with mean BL and variance $BL\sigma^2$,

$$T_1 \sim \mathcal{N}(BL, BL\sigma^2)$$
$$f_{H_1}(T) = \frac{1}{\sqrt{2\pi BL\sigma^2}} e^{\frac{-(T-BL)^2}{2\cdot BL\sigma^2}} \tag{6.5}$$

6.1.1.1 Probability of False Alarm (P_{fa})

The probability of false alarm (P_{fa}) refers to the event where the receiver incorrectly decides that the sequence $\underline{s}_1$ is present when it is actually absent, meaning it incorrectly accepts H_1 when H_0 is true [29].

In this section, we will present the analytical expression for P_{fa} and compare it with simulation results for coherent demodulation.

Analytical P_{fa}

The probability of false alarm, P_{fa}, is defined as $P(H_1|H_0)$, which represents the likelihood of deciding H_1 (the presence of the sequence $\underline{s}_1$) when H_0 (absence of the sequence) is actually true. Mathematically, this is expressed as $P(T \geq t|H_0)$.

As illustrated previously in (6.4), under H_0, the test statistic T is an average of $K-1$ Gaussian distributions, each with a variance of $BL\sigma^2$ and a mean $c \in \underline{c}$. Therefore, the probability of false alarm is given by:

$$P_{fa} = P(T \geq t \mid H_0) = \frac{1}{K-1} \sum_{j=1}^{K-1} \frac{1}{2} \operatorname{erfc}\left(\frac{t - c_j}{\sqrt{2\, BL\, \sigma^2}} \right).$$

This formulation allows us to compute the probability of false alarm by summing over the contributions of each Gaussian component..

Simulation of P_{fa}

To verify the analytical results, we generated $N_{sim} = 1{,}000{,}000$ simulation runs. In each simulation, a sub-sequence of $\underline{s}$ (a segment of length BL excluding the sequence $\underline{s}_1$), $\underline{s}_t$ was randomly selected from the pilot channel $\underline{s}$ to transmit. Gaussian noise with variance σ^2 was added to the selected segment, which was then correlated with the sequence $\underline{s}_1$ and the results were stored in a vector $\underline{T_0}$. For each threshold t, P_{fa} was estimated as the proportion of $\underline{T_0}$ values exceeding t. If fewer than 100

samples exceeded t, P_{fa} was not estimated for that threshold to ensure statistical reliability.

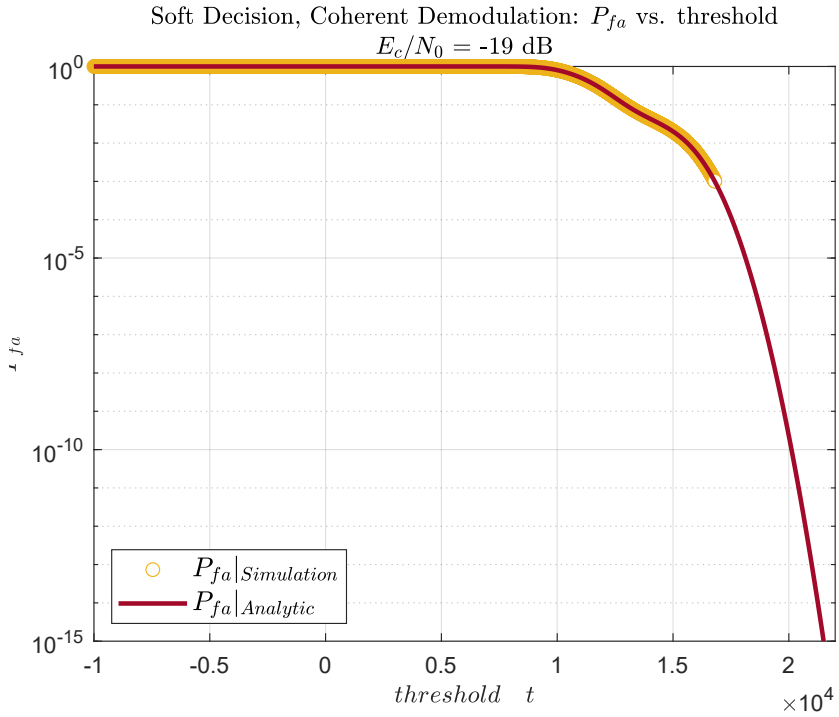

Figure 6.1: Comparison of analytical and simulated P_{fa} for soft detection coherent demodulation.

Fig. 6.1 demonstrates the alignment between the analytical and simulation results, validating the accuracy of the analytical expressions derived for the probability of false alarm. E_c is the energy of the chip.

6.1.1.2 Probability of Missed Detection (P_{md})

The probability of missed detection (P_{md}) occurs when the receiver incorrectly decides that H_0 (absence of the sequence $\underline{s}_1$) is true, even though H_1 (presence of the pattern) is correct. Mathematically, this is expressed as $P_{md} = P(H_0|H_1) = P(T < t|H_1)$.

Analytical P_{md}

As described previously in Eq. (6.5), under the alternative hypothesis H_1, the test statistic T follows a Gaussian distribution with a mean of BL and a variance of

$BL\sigma^2$. Therefore, the probability of missed detection is given by:

$$P_{md} = P(T < t|H_1) = \frac{1}{2}\,\mathrm{erfc}\left(\frac{BL - t}{\sqrt{2\,BL\,\sigma^2}}\right),$$

This formulation allows us to calculate P_{md} by evaluating the error function complement (erfc) based on the threshold t, the mean BL, and the variance $BL\sigma^2$.

Simulation of P_{md}

To validate the analytical results for the probability of missed detection (P_{md}), we conducted a simulation with $N_{sim} = 1{,}000{,}000$ simulation runs. In each simulation run, the test statistic T was calculated by computing the inner product of the pilot sequence $\underline{s}_1$ with itself including added Gaussian noise with variance σ^2, and the results were collected in vector $\underline{T}_1$ This simulates the scenario where the $\underline{s}_1$ is present at the receiver.

For each threshold t, P_{md} was estimated as the proportion of $\underline{T}_1$ values falling below t. If fewer than 100 samples were below t, P_{md} was not estimated for that threshold to ensure the statistical reliability of the results.

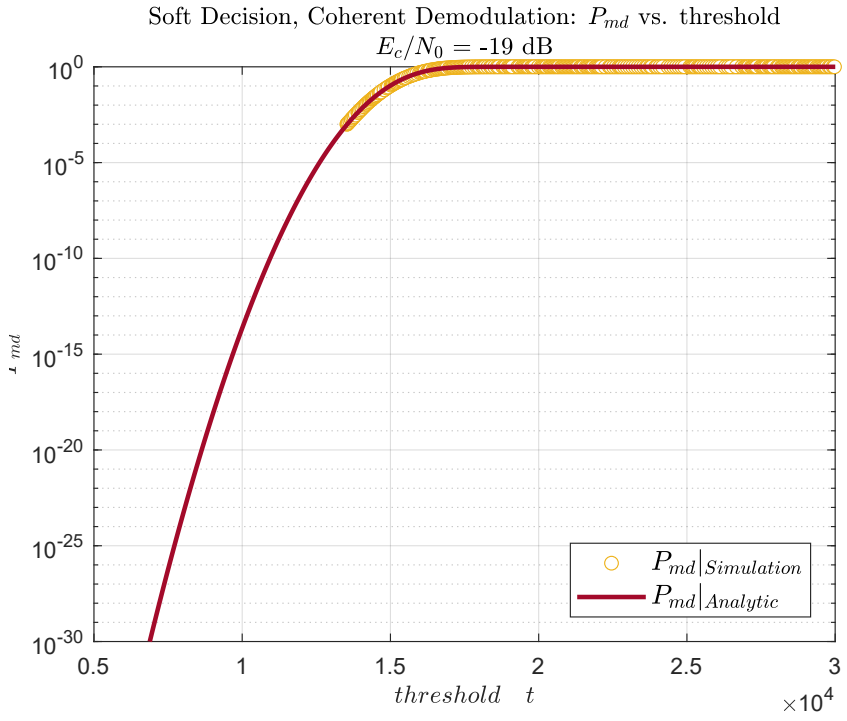

Figure 6.2: Comparison of analytical and simulated P_{md} for soft detection coherent demodulation.

Fig. 6.2 shows the alignment between analytical and simulation results, confirming the accuracy of the derived analytical expressions for the probability of missed detection.

Receiver Operating Characteristic (ROC) Curve

The Receiver Operating Characteristic (ROC) curve is a graphical representation of the trade-off between the probability of detection (P_d) and the probability of false alarm (P_{fa}). It illustrates the performance of the soft detection coherent demodulation system by plotting P_d against P_{fa} for various threshold values.

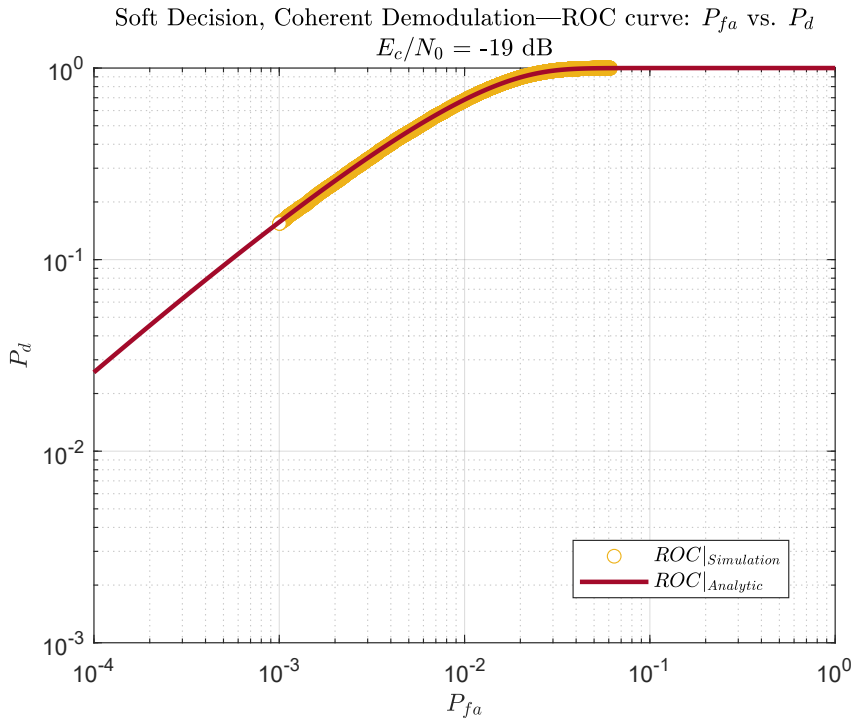

Figure 6.3: ROC curve for soft detection coherent demodulation.

The curve in Fig. 6.3 demonstrates the relationship between the probability of detection (P_d) and the probability of false alarm (P_{fa}), indicating the detection performance of the system.

6.1.2 Incoherent Demodulation

To evaluate the performance under incoherent demodulation, we begin by testing the following statistic:

$$T = \left| \sum_{i=1}^{BL} r_{x,i} s_{1,i} \right|$$

correlating the received signal with $\underline{s}_1$, and comparing the magnitude of this correlation against a threshold t. We decide for H_1 if $T \geq t$ and for H_0 otherwise.

Under H_0:

$$T = \left| \sum_{i=1}^{BL} r_{x,i} s_{1,i} \right| = \left| \sum_{i=1}^{BL} \left(s_{t,i} e^{j\Phi} + n_{\mathrm{r},i} + j n_{\mathrm{im},i} \right) s_{1,i} \right|, \quad \underline{s_t} \in \mathcal{S}$$

Expanding this, we get:

$$T = \left| \sum_{i=1}^{BL} \left((s_{t,i} \cos(\Phi) + n_{\mathrm{r},i}) + j(s_{t,i} \sin(\Phi) + n_{\mathrm{im},i}) \right) s_{1,i} \right|$$

Separating the real and imaginary parts, we have:

$$T = \left| \left(\cos(\Phi) \sum_{i=1}^{BL} s_{t,i} s_{1,i} + \sum_{i=1}^{BL} s_{1,i} n_{\mathrm{r},i} \right) \right.$$

$$\left. + j \left(\sin(\Phi) \sum_{i=1}^{BL} s_{t,i} s_{1,i} + \sum_{i=1}^{BL} s_{1,i} n_{\mathrm{im},i} \right) \right|$$

Let

$$X = \cos(\Phi) \sum_{i=1}^{BL} s_{t,i} s_{1,i} + \sum_{i=1}^{BL} s_{1,i} n_{\mathrm{r},i}$$

$$Y = \sin(\Phi) \sum_{i=1}^{BL} s_{t,i} s_{1,i} + \sum_{i=1}^{BL} s_{1,i} n_{\mathrm{im},i}$$

Given that $s_{1,i} \in \{-1, +1\}$, we have:

$$X \sim \mathcal{N} \left(\cos(\Phi) \sum_{i=1}^{BL} s_{t,i} s_{1,i}, BL\sigma^2 \right)$$

$$Y \sim \mathcal{N} \left(\sin(\Phi) \sum_{i=1}^{BL} s_{t,i} s_{1,i}, BL\sigma^2 \right)$$

Thus, the test statistic T can be expressed as:

$$T = |X + jY| = \sqrt{X^2 + Y^2} \sim \text{Rice}(\nu = \sum_{i=1}^{BL} s_{t,i}s_{1,i}, BL\sigma^2)$$

T follows a Rician distribution with parameters ν (the non-centrality parameter) and $BL\sigma^2$ (the variance).

For the non-centrality parameter, $\sum_{i=1}^{BL} s_{t,i}s_{1,i}$ depends on the specific transmitted sequence $\underline{s_t} \in \mathcal{S}$. Again, exactly as we did in (6.3) We calculate the correlations for all possible sequences, and we collect the values c in a vector $\underline{c}$.

Thus, under H_0:

$$T \sim \text{Rice}(\nu = c_j, BL\sigma^2) \text{ with probability } \frac{1}{K-1}.$$

Therefore, pdf of T under H_0 is an average of $(K-1)$ Rician distributions, each with variance $BL\sigma^2$ and non-centrality parameter c_i:

$$\begin{aligned} f_{H_0}(T) = \frac{1}{K-1} \sum_{i=1}^{K-1} \frac{T}{BL\sigma^2} \\ \times \exp{-\frac{T^2 + c_i^2}{4BL\sigma^2}} I_0\left(\frac{T \cdot c_i}{BL\sigma^2}\right) \end{aligned} \tag{6.6}$$

where $I_0(z)$ is the modified Bessel function of the first kind with order zero.

Under H_1

$$\begin{aligned} T = \Bigg| \left(\cos(\Phi) \sum_{i=1}^{BL} s_{1,i} \times s_{1,i} + \sum_{i=1}^{BL} s_{1,i} \times n_{\text{r},i}\right) \\ + j\left(\sin(\Phi) \sum_{i=1}^{BL} s_{1,i} \times s_{1,i} + \sum_{i=1}^{BL} s_{1,i} \times n_{\text{im},i}\right) \Bigg| \end{aligned}$$

Since $s_{1,i} \in \{-1, +1\}$, we have $\sum_{i=1}^{BL} s_{1,i}s_{1,i} = BL$. Thus, under H_1, the test statistic T follows a Rician distribution with a non-centrality parameter $\nu = BL$ and variance $BL\sigma^2$:

$$T \sim \text{Rice}(\nu = BL, BL\sigma^2)$$

The probability density function of T under H_1 is given by:

$$f_{H_1}(T) = \frac{T}{BL\sigma^2} \exp\left(-\frac{T^2 + (BL)^2}{2 \cdot BL\sigma^2}\right) I_0\left(\frac{T \cdot BL}{BL\sigma^2}\right) \tag{6.7}$$

where $I_0(z)$ is the modified Bessel function of the first kind with order zero.

6.1.2.1 Probability of False Alarm (P_{fa})

In this section, we will provide the analytical expression for P_{fa} and compare it with the simulation results for coherent demodulation.

Analytical P_{fa}

As previously illustrated in (6.6), under H_0, the test statistic T is a weighted average of $K-1$ Rician distributions, each with a variance of $BL\sigma^2$ and a non-centrality parameter $c \in \underline{c}$. Therefore, the probability of false alarm is given by:

$$\begin{aligned} P_{fa} &= P(T \geq t | H_0) \\ &= \frac{1}{K-1} \sum_{i=1}^{K-1} P\left(\text{Rice}(n=2, \nu = c_i, BL\sigma^2) > t\right) \end{aligned} \tag{6.8}$$

$$P_{fa} = \frac{1}{K-1} \sum_{i=1}^{K-1} Q_1\left(\frac{c_i}{\sqrt{BL\sigma^2}}, \frac{t}{\sqrt{BL\sigma^2}}\right) \tag{6.9}$$

where $Q_1(\cdot,\cdot)$ is Marcum Q-function of order 1.

Simulation of P_{fa}

To validate the analytical results for incoherent demodulation, we generated $N_{sim} =$ 1,000,000 simulation runs. In each simulation, a signal was randomly selected from the pilot channel for transmission (excluding the 1-block sequence). This signal was multiplied by a random phase shift and Gaussian noise with variance σ^2 was added. The noisy signal was then correlated with the sequence $\underline{s}_1$ and the magnitude of the correlation was computed. The results were then collected in vector $\underline{T_0}$

For each threshold t, P_{fa} was estimated as the proportion of T_0 values exceeding t. If fewer than 100 samples exceeded t, P_{fa} was not estimated for that threshold to ensure statistical reliability.

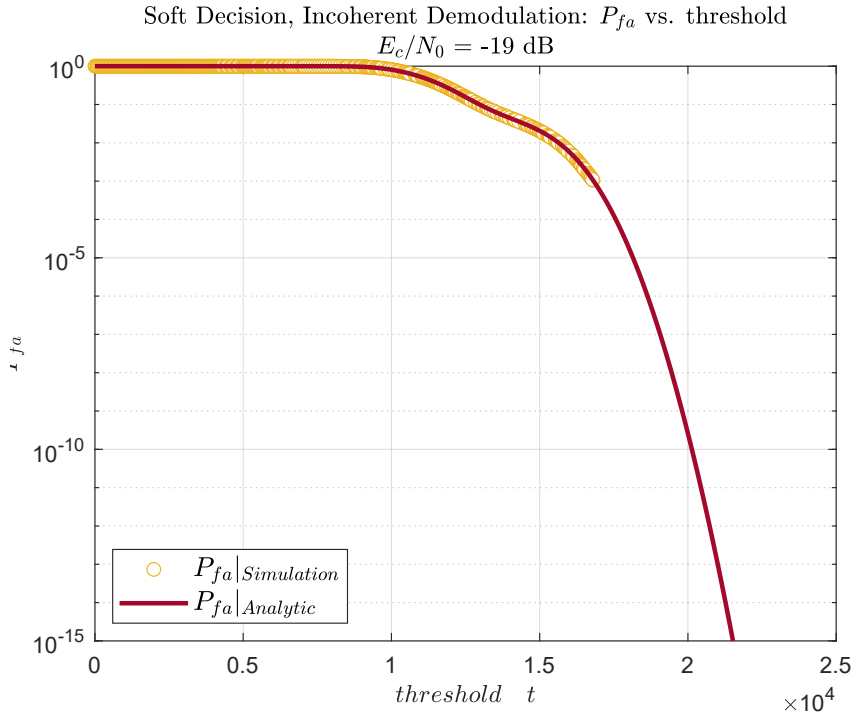

Figure 6.4: Comparison of analytical and simulated P_{fa} for soft detection incoherent demodulation.

Fig. 6.4 demonstrates the alignment between analytical and simulation results, confirming the accuracy of the derived analytical expressions for the probability of false alarm.

6.1.2.2 Probability of Missed Detection (P_{md})

In this section, we will provide the analytical expression for P_{md} and compare it with the simulation results for coherent demodulation.

Analytical P_{md}

As previously described in Eq. (6.7), under the alternative hypothesis H_1, the test statistic T follows a Rician distribution with a non-centrality parameter $\nu = BL$ and variance $BL\sigma^2$:

$$T \sim \text{Rice}(\nu = BL, BL\sigma^2)$$

Therefore, the probability of missed detection is given by:

$$P_{md} = P(T < t|H_1) = 1 - Q_1\left(\frac{BL}{\sqrt{BL\sigma^2}}, \frac{t}{\sqrt{BL\sigma^2}}\right) \tag{6.10}$$

where Q_1 is the Marcum Q-function of order 1.

Simulation of P_{md}

To validate the analytical results for the probability of missed detection (P_{md}) in incoherent demodulation, we conducted a simulation with N_{sim} = 1,000,000 simulation runs. In each simulation run, the test statistic T_1 was calculated by finding the magnitude of the inner product of the pilot sequence $\underline{s}_1$ including Gaussian noise with variance σ^2 and random phase with itself, then the results were collected in the vector $\underline{T}_1$. This setup simulates the scenario where the 1 pattern is present at the receiver.

For each threshold t, P_{md} was estimated as the proportion of $\underline{T}_1$ values falling below t. If fewer than 100 samples were below t, P_{md} was not estimated for that threshold to ensure the statistical reliability of the results.

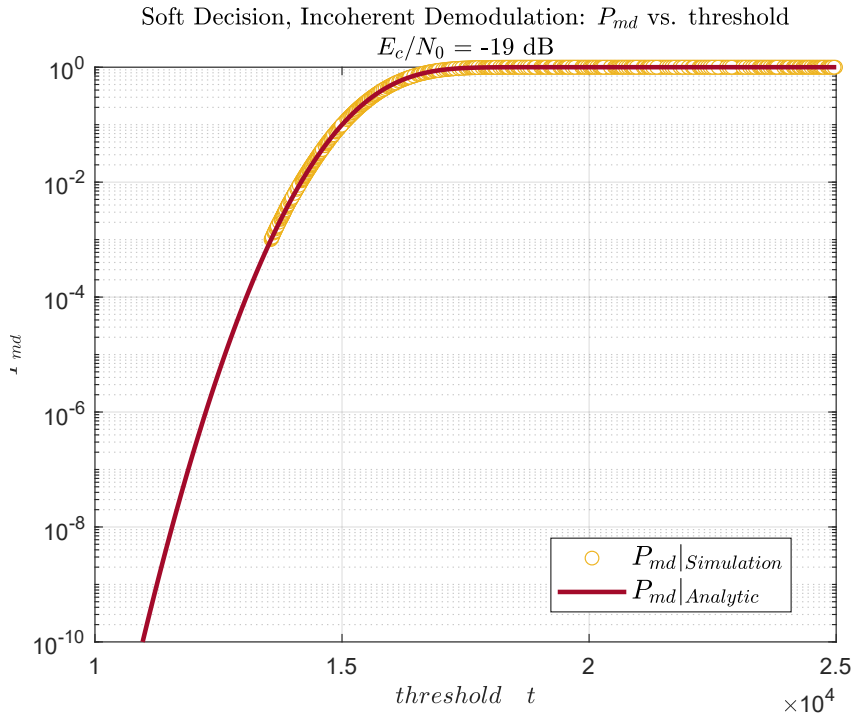

Figure 6.5: Comparison of analytical and simulated P_{md} for soft detection incoherent demodulation.

Fig. 6.5 demonstrates the alignment between analytical and simulation results, confirming the accuracy of the derived analytical expressions for the probability of missed detection with σ^2.

Receiver Operating Characteristic (ROC) Curve

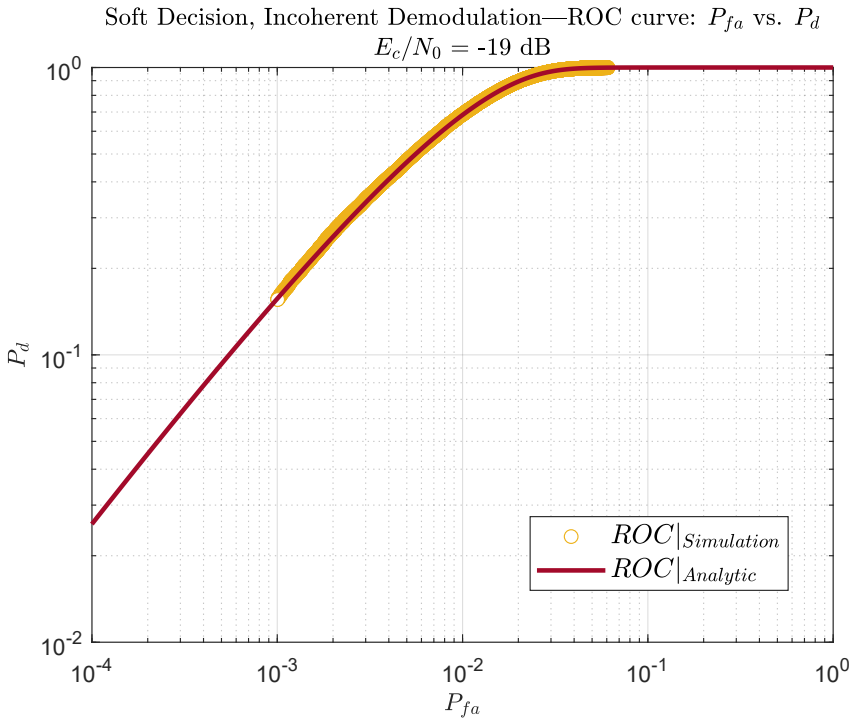

Figure 6.6: ROC curve for soft detection incoherent demodulation.

The curve in Fig. 6.6 shows the relationship between the probability of detection (P_d) and the probability of false alarm (P_{fa}), indicating the detection performance of the incoherent demodulation system.

6.2 Performance Analysis of MEO GNSS Pilot Channel with Hard Detection

In this section, we provide a detailed analysis of the performance metrics for patterns created using Serial Bicode DSSS in MEO GNSS applications. We evaluate the system's performance under both coherent and incoherent demodulation scenarios, focusing on two key probabilities: the probability of false alarm (P_{fa}) and the probability of missed detection (P_{md}). This analysis emphasizes hard detection, where each DSSS sequence is decoded, and decisions are made based on the resulting sequence. Hard detection involves decoding the spreading sequences, computing the Hamming distance between the received sequence and the expected pattern, and making decisions accordingly.

6.2.1 Coherent Demodulation

Scenario Description

We consider a scenario with a pattern $\underline{p}$ composed of $b = 5$ blocks, each $B = 64$ bits long, spread using Serial Bicode DSSS to form $\underline{s}$. We focus on the first block (1) of length B bits for the pattern $\underline{p}_1$. The first block features single consecutive 1's. This pattern is modulated using Serial Bicode DSSS, where bit 0 maps to c_0 (legitimate code) and bit 1 maps to c_1 (alternative code). Both c_0 and c_1 are sequences of length L, producing the signal $\underline{s}_1$.

We transmit a signal $\underline{s}$ of length KL over an AWGN channel, with the received signal given by $\underline{r_x} = \underline{s} + \underline{n}$ where $\underline{n} = (n_1, n_2, \ldots, n_i, \ldots, n_{KL})$ represents the noise vector, with $n_i \sim \mathcal{N}(0, \sigma^2)$, and we check if the sequence $\underline{s}_1$ is present within a window of length BL.

Hypotheses:

- **Null Hypothesis** H_0: The 1-block pattern is absent at the receiver.
- **Alternative Hypothesis** H_1: The 1-block pattern is present at the receiver.

We test the statistic $T = d_H(\underline{r}, \underline{p}_1)$, where $\underline{r}$ is a segment of length BL that we check for the presence of the pattern $\underline{p}_1$ within after decoding each L chips to either 0 or 1 according to Serial DSSS discussed before. Here, $d_H(\cdot, \cdot)$ represents the Hamming distance.

Under H_0

$$T = d_H(\underline{r}, \underline{p}_1)$$

Let $h(\cdot)$ be a function that maps each L chips according to Serial DSSS discussed in Section 3.4. Then $\underline{r} = h(\underline{r}_t)$ where $\underline{r}_t$ could be any segment of length BL.

The probability of a mistaken bit flip for coherent demodulation is given by Eq. (3.20).

The resulting Hamming distance T depends on the initial Hamming distance between the initial sequence $\underline{p_t} = h(\underline{s_t})$ and $\underline{p_1}$, representing the number of initially differnt bits. We can conceptualize this as flipping two sets of coins:

1. The first set is flipped $d_H(\underline{p_t}, \underline{p_1})$ times with a success probability of $1 - P_b$, representing the likelihood of a flipped bit remaining flipped and contributing to the final Hamming distance.
2. The second set is flipped $B - d_H(\underline{p_t}, \underline{p_1})$ times with a success probability of P_b, representing the likelihood of a correct bit becoming flipped and contributing to the Hamming distance.

Thus, under H_0, T is the sum of two binomial distributions:

$$T = X + Y$$

where $X \sim \text{Binomial}(d_H(\underline{p_t}, \underline{p_1}), 1 - P_b)$ and $Y \sim \text{Binomial}(B - d_H(\underline{p_t}, \underline{p_1}), P_b)$.

Let $d = d_H(\underline{p_t}, \underline{p_1})$. The probability $P(T = k)$ is given by:

$$P(T = k) = \sum_{n=\max(0,k-(B-d))}^{\min(d,k)} \binom{d}{n} (1 - P_b)^n P_b^{d-n}$$

$$\binom{B-d}{k-n} P_b^{k-n} (1 - P_b)^{(B-d)-(k-n)}$$

We collect all possible patterns $\underline{p_t}$ and compute their Hamming distance from $\underline{p_1}$, denoted as $d_H(\underline{p_t}, \underline{p_1})$. We then compile all unique values of these Hamming distances into DP (distance profile).
Let:

$$\underline{p} = (p_1, \ldots, p_i, \ldots, p_K)$$

We then define the set $\mathcal{P}$ which contains all the possible segments of length B within $\underline{p}$, excluding $\underline{p_1}$:

$$\mathcal{P} = \left\{ \underline{p_t} = (p_{(i) \bmod K}, p_{(i+1) \bmod K}, \ldots, p_{(i+B-1) \bmod K}) \mid 2 \leq i \leq K \right\}$$

The subscript indices are taken modulo K, ensuring that the segments wrap around to the start of $\underline{p}$ if $i + B - 1 > K$. Now we define

$$DP_i = d_H(\underline{p}_{t,j}, \underline{p}_1), \forall \underline{p_{t,j}} \in \mathcal{P}$$

The cardinality of DP, $|DP| = K - 1$.
Under H_0, the probability $P(T_0 = k)$ is:

$$\begin{aligned} P(T = k) = \frac{1}{K-1} \sum_{i=0}^{|DP|} \sum_{n=\max(0,k-(B-DP_i))}^{\min(DP_i,k)} & \binom{DP_i}{n} \\ & \times (1 - P_b)^n P_b^{DP_i - n} \binom{B - DP_i}{k-n} \\ & \times P_b^{k-n} (1 - P_b)^{(B-DP_i)-(k-n)} \end{aligned} \tag{6.11}$$

Under H_1

$$T = d_H(h(\underline{s}_1 + \underline{n}), \underline{p}_1)$$

Under H_1, We receive the signal $\underline{s}_1$, which is $\underline{p}_1$ spread according to Serial DSSS, with noise $\underline{n}$. In this scenario, since the initial Hamming distance $d_H(\underline{p}_1, \underline{p}_1)$ is 0, under H_1, T follows a binomial distribution:

$$T \sim \text{Binomial}(B, P_b)$$

The probability $P(T = k)$ is given by:

$$P(T = k) = \binom{B}{k}(1 - P_b)^{B-k} P_b^k \tag{6.12}$$

6.2.1.1 Probability of False Alarm (P_{fa})

In this section, we provide the analytical expression for P_{fa} and compare it with simulation results for hard detection coherent demodulation.

Analytical P_{fa}

For coherent demodulation hard detection, we compute the Hamming distance between the decoded received sequence and $\underline{p}_1$, and compare it to a threshold t. A false alarm occurs when, under H_0, the Hamming distance falls below the threshold t.

Using (6.11) it can be shown that the probability of false alarm is given by:

$$\begin{aligned} P_{fa} &= P(T < t|H_0) = P(T < t) \\ &= \sum_{k=0}^{t-1} \frac{1}{K-1} \sum_{i=0}^{K-1} \sum_{n=\max(0,k-(B-DP_i))}^{\min(DP_i,k)} \\ &\quad \times \binom{DP_i}{n}(1 - P_b)^n P_b^{DP_i - n} \\ &\quad \times \binom{B - DP_i}{k - n} P_b^{k-n}(1 - P_b)^{(B-DP_i)-(k-n)} \end{aligned} \tag{6.13}$$

Simulation of P_{fa}

To validate the analytical results for the probability of false alarm (P_{fa}), we conducted a simulation with $N_{sim} = 1{,}000{,}000$ simulation runs. In each simulation run, a signal $\underline{s_t}$ was selected from the matrix $\mathcal{S}$. Gaussian noise with variance σ^2 was added to the selected signal, and the received signal was decoded determining whether each L-chips segment corresponds to a 0 or 1. The Hamming distance T_0 between the decoded pattern and the expected pattern $\underline{p}_1$ was calculated.

For each threshold t, P_{fa} was estimated as the proportion of T_0 values falling below t. If fewer than 100 samples fall below t, P_{fa} was not estimated for that threshold to ensure statistical reliability.

Finally, we plot the simulation results against the analytical results to verify the accuracy of the analytical expression for P_{fa}.

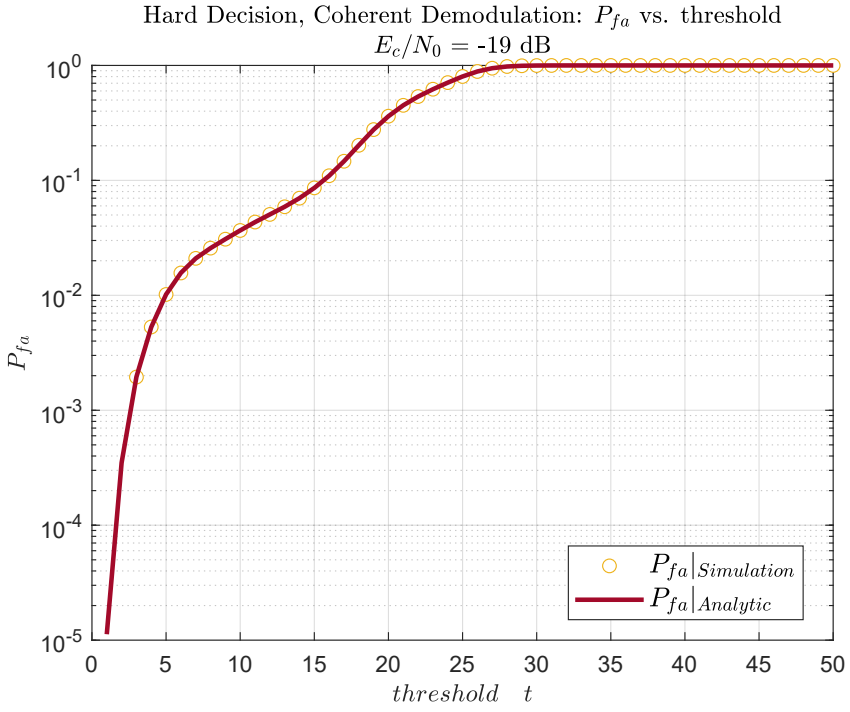

Figure 6.7: Comparison of simulated and analytical P_{fa} for hard detection coherent demodulation, demonstrating perfect alignment.

6.2.1.2 Probability of Missed Detection (P_{md})

The probability of missed detection (P_{md}) occurs when the receiver incorrectly concludes that H_0 (absence of the pattern p_1) is true, even though H_1 (presence of the pattern) is correct. Mathematically, this is expressed as $P_{md} = P(H_0|H_1) = P(T > t|H_1)$.

In this section, we provide the analytical expression for P_{md} and compare it with simulation results for hard detection coherent demodulation.

Analytical P_{md}

As previously described is Eq. (6.12), under the alternative hypothesis H_1, the test statistic T follows a binomial distribution:

$$T_1 \sim \text{Binomial}(B, P_b)$$

Therefore, the probability of missed detection is given by:

$$P_{md} = P(T_1 > t) = 1 - \sum_{k=0}^{t} \binom{B}{k} (1 - P_b)^{B-k} P_b^k \tag{6.14}$$

This formulation is used because t is typically much smaller than $B - k$, simplifying the calculation.

Simulation of P_{md}

To validate the analytical results for the probability of missed detection (P_{md}), we conducted a simulation with $N_{sim} = 1{,}000{,}000$ simulation runs . In each simulation run, the signal $\underline{s_1}$ was transmitted with added Gaussian noise having a variance σ^2. The received signal was then decoded by assessing each L-chips segment. The Hamming distance T_1 between the decoded pattern and the expected pattern $\underline{p_1}$ was computed.

For each threshold t, P_{md} was estimated as the proportion of T_1 values exceeding t. If fewer than 100 samples exceeded t, P_{md} was not estimated for that threshold to maintain statistical reliability.

Finally, we plot the simulation results against the analytical results to verify the accuracy of the analytical expression for P_{md}.

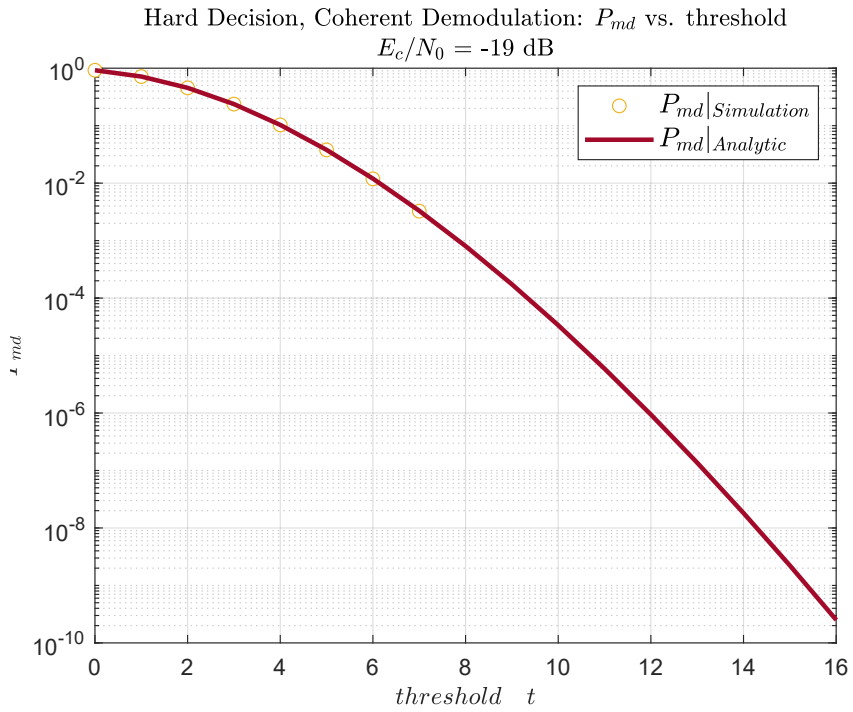

Figure 6.8: Comparison of simulated and analytical P_{md} for hard detection coherent demodulation, demonstrating perfect alignment.

Receiver Operating Characteristic (ROC) Curve

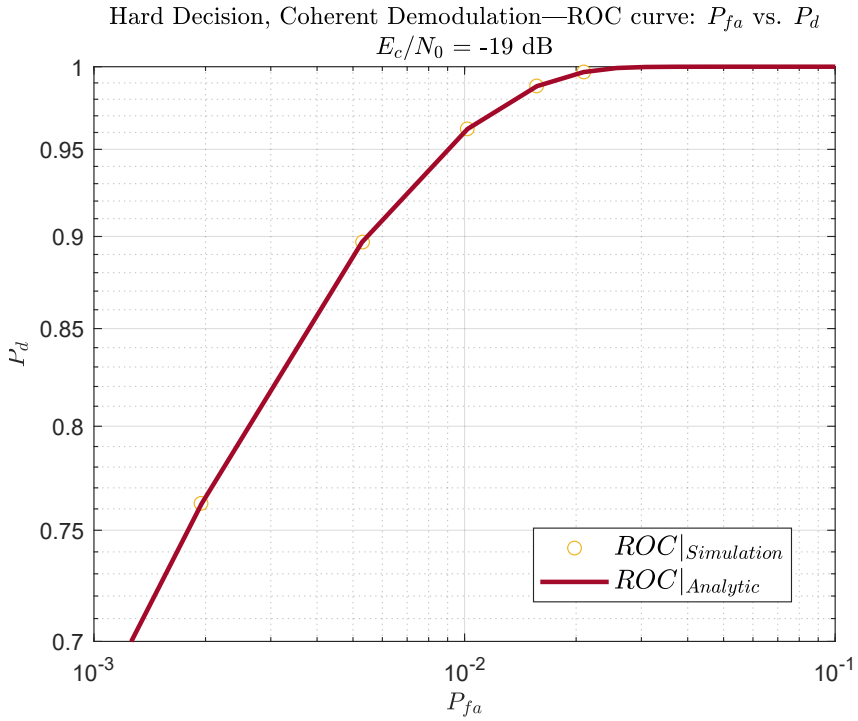

Figure 6.9: ROC curve for hard detection coherent demodulation.

The curve in Fig. 6.9 shows the relationship between the probability of detection (P_d) and the probability of false alarm (P_{fa}), indicating the detection performance of the hard detection coherent demodulation system.

6.2.2 Incoherent Demodulation

Scenario Description

The scenario is identical to the coherent demodulation case, with the exception that the probability of error $P_b(e)$ is now given by the error probability of Serial Bicode DSSS under incoherent demodulation, as expressed in Eq. (3.2).

The subsequent analysis follows the same approach as in the coherent demodulation case but with the modified error probability P_b.

Under H_0

$$P(T = k) = \frac{1}{K-1} \sum_{i=0}^{K-1} \sum_{n=\max(0,k-(B-DP_i))}^{\min(DP_i,k)}$$

$$\times \binom{DP_i}{n}(1-P_b)^n P_b^{DP_i-n} \times \binom{B-DP_i}{k-n} P_b^{k-n}(1-P_b)^{(B-DP_i)-(k-n)} \tag{6.15}$$

Under H_1

$$P(T=k) = \binom{B}{k}(1-P_b)^{B-k}P_b^k \tag{6.16}$$

6.2.2.1 Probability of False Alarm (P_{fa})

Analytical P_{fa}

The analytical expression for P_{fa} in incoherent demodulation is similar to that in coherent demodulation, with the modified error probability P_b, we now use P_b given in Eq. (3.2). It is given by:

$$\begin{aligned} P_{fa} &= P(T < t|H_0) = P(T < t) \\ &= \sum_{k=0}^{t-1}\sum_{i=0}^{K-1}\frac{1}{K-1}\sum_{n=\max(0,k-(B-DP_i))}^{\min(DP_i,k)} \\ &\quad \times \binom{DP_i}{n}(1-P_b)^n P_b^{DP_i-n} \\ &\quad \times \binom{B-DP_i}{k-n} P_b^{k-n}(1-P_b)^{(B-DP_i)-(k-n)} \end{aligned} \tag{6.17}$$

Simulation of P_{fa}

To validate the analytical expression for P_{fa}, a simulation with $N_{sim} = 1{,}000{,}000$ simulation runs was conducted. In each run, a signal $\underline{s_t}$ was randomly selected from $\mathcal{S}$, modulated with random phase, and combined with Gaussian noise. The received signal was then decoded to calculate the test statistic T_0, representing the Hamming distance from the expected pattern $\underline{p}_1$.

Finally, the simulation results were compared to the analytical results to ensure their accuracy.

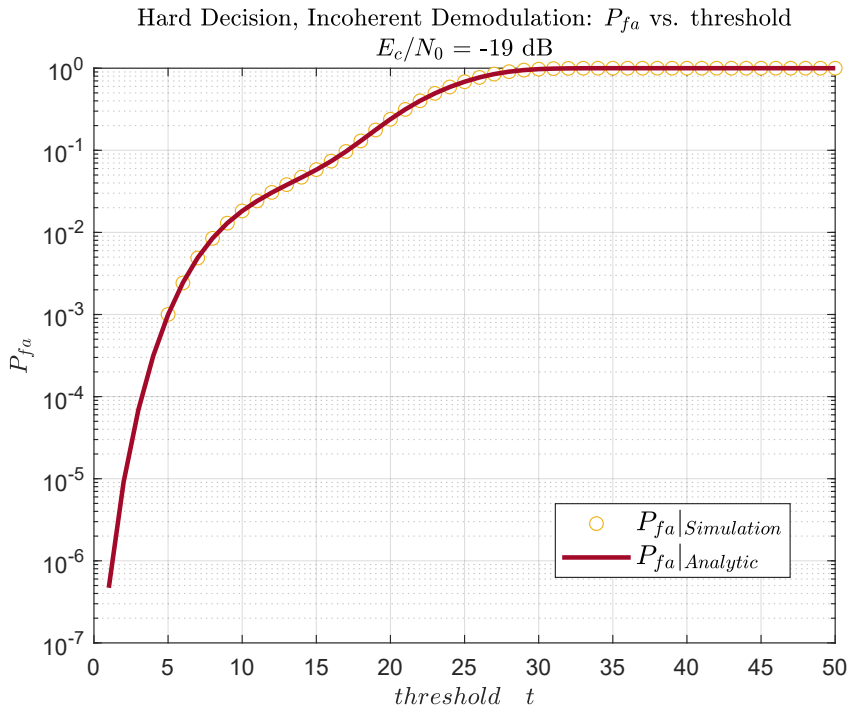

Figure 6.10: Comparison of simulated and analytical P_{fa} for hard incoherent demodulation, demonstrating perfect alignment.

6.2.2.2 Probability of Missed Detection (P_{md})

The probability of missed detection (P_{md}) measures the likelihood that the receiver fails to detect the presence of the pattern p_1 when it is actually present.

Analytical P_{md} For the incoherent demodulation scenario, the analytical expression for P_{md} is derived similarly to the coherent case, but with the modified error probability specific to incoherent demodulation:

$$P_{md} = P(T_1 > t) = 1 - \sum_{k=0}^{t} \binom{B}{k} (1 - P_b)^{B-k} P_b^k$$

Simulation of P_{md} To validate the analytical expression for P_{md}, a simulation was performed with $N_{sim} = 1{,}000{,}000$ simulation runs. For each run, the signal $\underline{s_1}$ was modulated with random phase and Gaussian noise, then decoded to compute the test statistic T_1. The statistic T_1 represents the Hamming distance from the expected pattern p_1.

The simulation results were compared to the analytical results to ensure their accuracy.

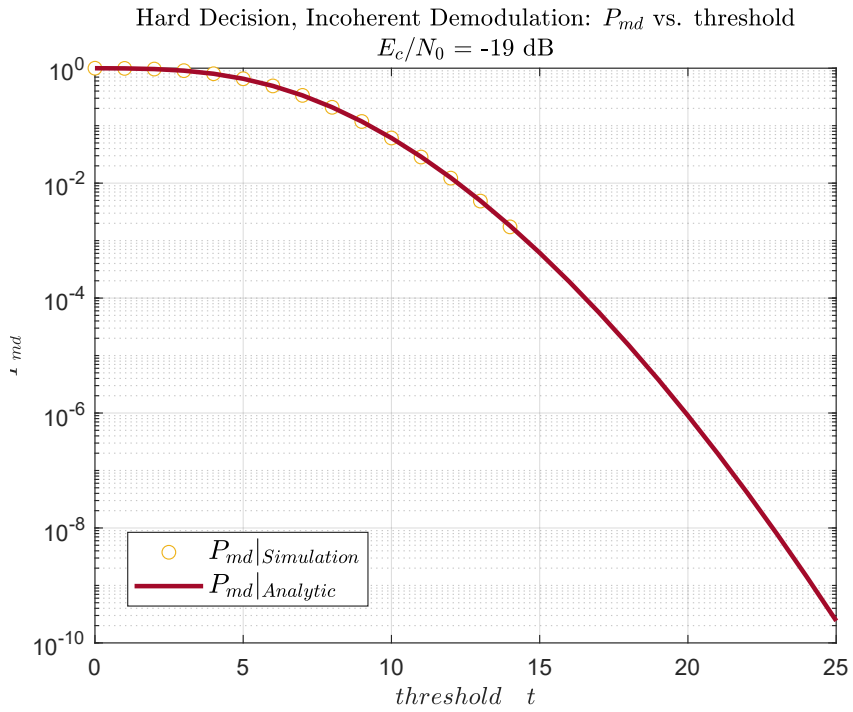

Figure 6.11: Comparison of simulated and analytical P_{md} for hard incoherent demodulation, demonstrating perfect alignment.

Receiver Operating Characteristic (ROC) Curve

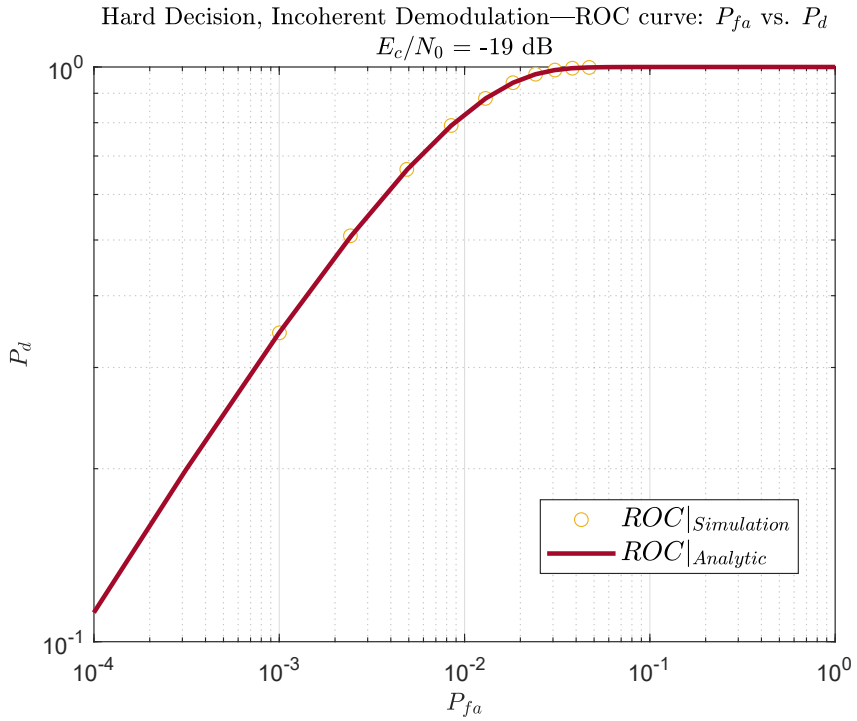

Figure 6.12: ROC curve for hard incoherent demodulation.

The curve in Fig. 6.12 shows the relationship between the probability of detection (P_d) and the probability of false alarm (P_{fa}), indicating the detection performance of the hard incoherent demodulation system.

6.3 Performance Analysis of LEO GNSS Pilot Channel with Soft Detection

In this section, we provide a comprehensive analysis of the performance metrics for patterns constructed using Serial Bicode DSSS in LEO GNSS applications. We focus on evaluating the system's performance under both coherent and incoherent demodulation scenarios, specifically targeting the key probabilities: probability of false alarm (P_{fa}) and probability of missed detection (P_{md}). This analysis emphasizes soft detection, where the entire received signal is utilized to make a decision.

6.3.1 Coherent Demodulation

Scenario Description

We consider a scenario involving a pattern $\underline{p}$:

$$\underline{p} = (0,0,0,0,0,0,0,1,0,0,0,0,0,0,0,0)$$

This pattern is spread using Serial Bicode DSSS to produce the pilot channel, where bit 0 is mapped to $\underline{c}_0$ (legitimate code) and bit 1 to $\underline{c}_1$ (alternative code). Both $\underline{c}_0$ and $\underline{c}_1$ are sequences of length L, forming the sequence $\underline{s}$:

$$\underline{s} = (\underline{c}_0, \underline{c}_0, \underline{c}_0, \underline{c}_0, \underline{c}_0, \underline{c}_0, \underline{c}_0, \underline{c}_1, \underline{c}_0, \underline{c}_0, \underline{c}_0, \underline{c}_0, \underline{c}_0, \underline{c}_0, \underline{c}_0, \underline{c}_0)$$

We continuously transmit a signal $\underline{s}$ of length $16L$ over an AWGN channel and check if the pattern $\underline{s}$ is present within a window of length $16L$.

Hypotheses

- **Null Hypothesis** H_0: The pattern within $\underline{s}$ is absent at the receiver. The received signal does not contain the pattern.
- **Alternative Hypothesis** H_1: The pattern within $\underline{s}$ is present at the receiver.

We test the statistic:

$$T = \sum_{i=1}^{16L} r_{x,i} s_i$$

where $\underline{r_x}$ is the received signal within a window of 16 short codes.

We correlate the received signal with the $\underline{s}$ block pattern and compare this against a threshold t.

The decision rule is:

$$\begin{cases} H_1 & \text{if } T \geq t, \\ H_0 & \text{if } T < t. \end{cases}$$

Under H_0

$$T = \sum_{i=1}^{16L} (s_{t,i} + n_i) s_i = \sum_{i=1}^{16L} s_{t,i} s_i + \sum_{i=1}^{16L} n_i s_i \tag{6.18}$$

where $\underline{s_t}$ is any cyclic shift of pattern $\underline{p}$ excluding the pattern itself, mapped into spreading codes with the mapping from $0 \to \underline{c}_0$ and $1 \to \underline{c}_1$. There are 15 possible segments for $\underline{s_t}$ as $\underline{p}$ consists of 16 bits.

In Eq. (6.18), the second term is a sum of $16L$ Gaussian random variables with mean 0 and variance σ^2, so $\sum_{i=1}^{16L} n_i s_i$ is Gaussian with mean 0 and variance

$16L\sigma^2$. The first term is the cross-correlation between $\underline{s}$ and $\underline{s}_t$. This can be easily computed by noticing that any cyclic shift $\underline{p}_t$ of the pattern $\underline{p}$ has $d_H(\underline{p}, \underline{p}_t) = 2$, and that $\underline{c}_0$ and $\underline{c}_1$ are sequences in $\{-1, 1\}$. Thus, the cross-correlation is:

$$\sum_{i=1}^{16L} s_{t,i}s_i = 14L + 2\sum_{i=1}^{L} c_{0,i}c_{1,i} = 14L + 2R \quad \forall \underline{s}_t \tag{6.19}$$

where R is given by Eq. (3.15).

This means that T under H_0 is a Gaussian distribution with variance $16L\sigma^2$ and mean $14L + 2R$:

$$f_{H_0}(T) = \frac{1}{\sqrt{2\pi 16L\sigma^2}} \exp\left(\frac{-(T - (14L + 2R))^2}{2 \cdot 16L\sigma^2}\right) \tag{6.20}$$

Under H_1

$$T = \sum_{i=1}^{16L}(s_i + n_i)s_i = \sum_{i=1}^{16L} s_i s_i + \sum_{i=1}^{16L} n_i s_i = 16L + \sum_{i=1}^{16L} n_i s_i \tag{6.21}$$

Similarly to before, the second term is a sum of $16L$ Gaussian random variables with mean 0 and variance σ^2, so it is Gaussian with mean 0 and variance $16L\sigma^2$.

Thus, T under H_1 is a Gaussian distribution with variance $16L\sigma^2$ and mean $16L$:

$$f_{H_1}(T) = \frac{1}{\sqrt{2\pi 16L\sigma^2}} \exp\left(\frac{-(T - 16L)^2}{2 \cdot 16L\sigma^2}\right) \tag{6.22}$$

Probability of False Alarm (P_{fa})

In this section, we will present the analytical expression for P_{fa} and compare it with simulation results for coherent demodulation.

Analytical P_{fa}

As illustrated previously in (6.20), T under H_0 is a Gaussian distribution with variance $16L\sigma^2$ and mean $14L + 2R$. Therefore, the probability of false alarm is given by:

$$P_{fa} = P\Big(T \geq t \mid H_0\Big) = \frac{1}{2}\operatorname{erfc}\left(\frac{t - \Big(14L + 2R\Big)}{\sqrt{2 \cdot 16L\sigma^2}}\right). \tag{6.23}$$

Simulation of P_{fa}

To verify the analytical results, we generated $N_{sim} = 1{,}000{,}000$ simulation runs. In each simulation, a segment of length $16L$, $\underline{s}_t$, was randomly selected to transmit. Gaussian noise with variance σ^2 was added to the selected segment, which was then correlated with the pilot $\underline{s}$. The results were stored in a vector $\underline{T_0}$. For each threshold t, P_{fa} was estimated as the proportion of $\underline{T_0}$ values exceeding t. If fewer than 1000 samples exceeded t, P_{fa} was not estimated for that threshold to ensure statistical reliability.

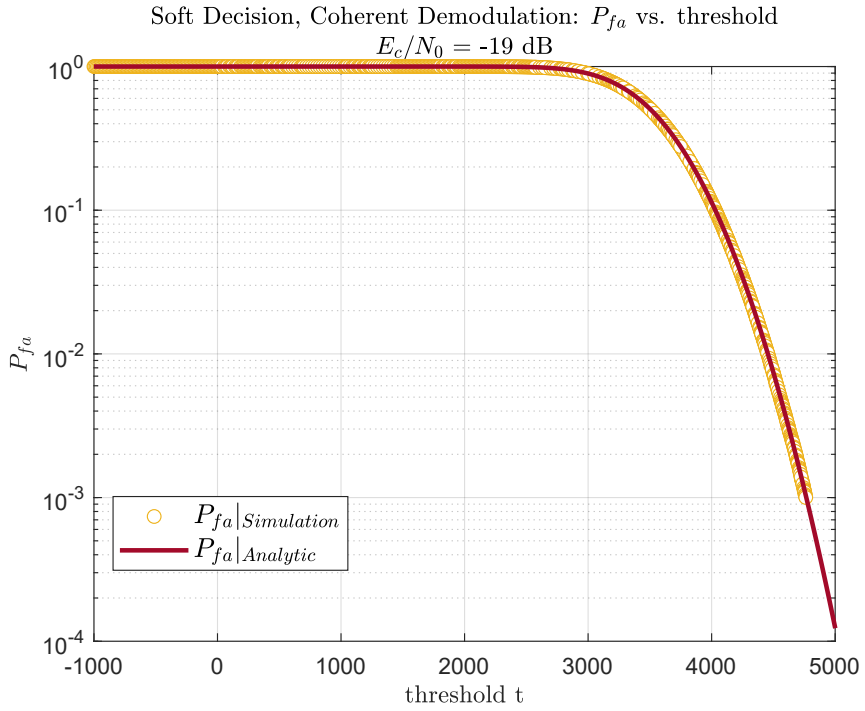

Figure 6.13: Comparison of analytical and simulated P_{fa} for soft detection coherent demodulation.

Probability of Missed Detection (P_{md})

In this section, we will present the analytical expression for P_{md} and compare it with simulation results for coherent demodulation.

Analytical P_{md}

As described previously, T under H_1 is a Gaussian distribution with variance $16L\sigma^2$ and mean $16L$. Therefore, the probability of missed detection is given by:

$$P_{md} = \frac{1}{2}\,\mathrm{erfc}\left(\frac{16L - t}{\sqrt{2 \cdot 16L\sigma^2}}\right) \tag{6.24}$$

Simulation of P_{md}

To validate the analytical results for the probability of missed detection (P_{md}), we conducted a simulation with N_{sim} = 1,000,000 simulation runs. In each simulation run, the test statistic T was calculated by summing the product of the pilot channel $\underline{s}$ with itself, including added Gaussian noise with variance σ^2. The results were collected in the vector $\underline{T_1}$.

For each threshold t, P_{md} was estimated as the proportion of $\underline{T_1}$ values falling below t. If fewer than 1000 samples were below t, P_{md} was not estimated for that threshold to ensure the statistical reliability of the results.

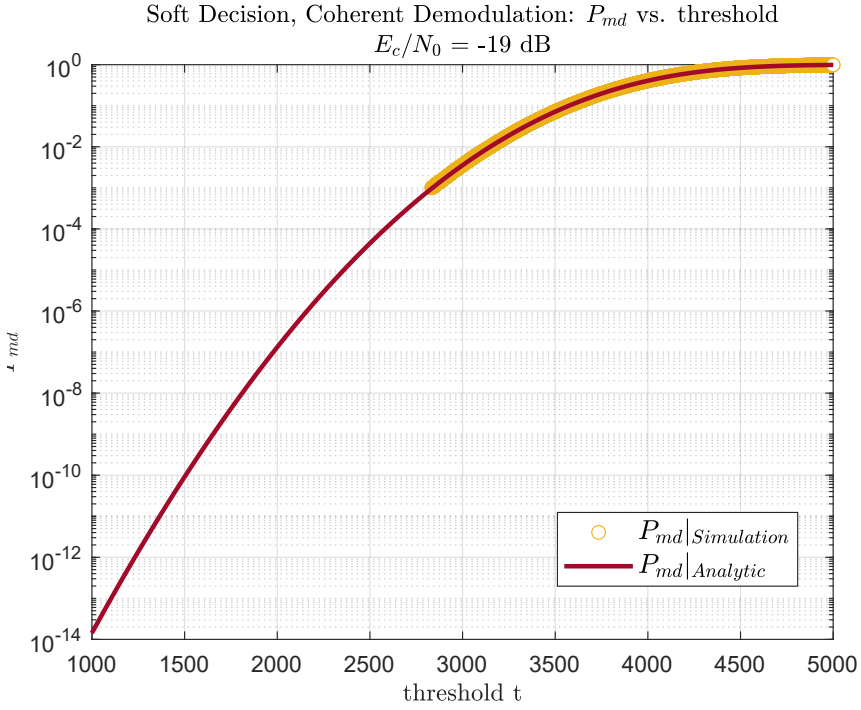

Figure 6.14: Comparison of analytical and simulated P_{md} for soft detection coherent demodulation.

The figure shows the alignment between analytical and simulation results,

confirming the accuracy of the derived analytical expressions for the probability of missed detection.

Receiver Operating Characteristic (ROC) Curve

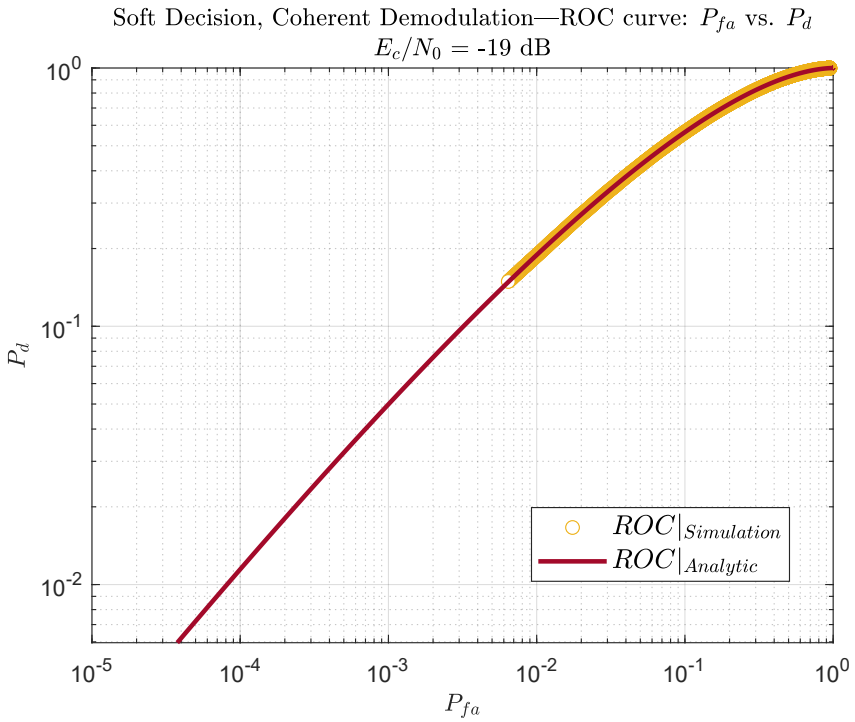

Figure 6.15: ROC curve for soft detection coherent demodulation.

6.3.2 Incoherent Demodulation

The scenario for incoherent demodulation is identical to the previously described scenario for coherent demodulation.

Hypotheses:

- **Null Hypothesis** H_0: The pilot $\underline{s}$ is absent at the receiver.
- **Alternative Hypothesis** H_1: The pilot $\underline{s}$ is present at the receiver.

For incoherent demodulation, we test the statistic $T = \left|\sum_{i=1}^{16L} r_{x,i} s_i\right|$, correlating the received signal with $\underline{s}$, and comparing the magnitude of this correlation against a threshold t. We decide for H_1 if $T \geq t$ and for H_0 otherwise.

Under H_0: By performing the same analysis as we did for the MEO case and noting that the cross-correlation between $\underline{s_t}$ and $\underline{s}$ is $14L + 2R$ for any segment $\underline{s_t}$, it can be found that the test statistic T under H_0 follows a Rician distribution with non-centrality parameter $\nu = 14L + 2R$ and variance $16L\sigma^2$.

Therefore, the probability density function of T under H_0 is given by:

$$f_{H_0}(T) = \frac{T}{16L\sigma^2}\exp\left(-\frac{T^2 + (14L + 2R)^2}{2 \cdot 16L\sigma^2}\right) I_0\left(\frac{T \cdot (14L + 2R)}{16L\sigma^2}\right) \tag{6.25}$$

where $I_0(z)$ is the modified Bessel function of the first kind with order zero.

Under H_1: Following the same analysis as for the MEO case, we find that under H_1, T follows a Rician distribution with non-centrality parameter $\nu = 16L$ and variance $16L\sigma^2$.

The probability density function of T under H_1 is given by:

$$f_{H_1}(T) = \frac{T}{16L\sigma^2}\exp\left(-\frac{T^2 + (16L)^2}{2 \cdot 16L\sigma^2}\right) I_0\left(\frac{T \cdot 16L}{16L\sigma^2}\right) \tag{6.26}$$

where $I_0(z)$ is the modified Bessel function of the first kind with order zero.

Probability of False Alarm (P_{fa})

In this section, we will provide the analytical expression for P_{fa} and compare it with the simulation results for incoherent demodulation.

Analytical P_{fa}

As previously illustrated in Eq. (6.25), the test statistic T under H_0 follows a Rician distribution with non-centrality parameter $\nu = 14L + 2R$ and variance $16L\sigma^2$. Therefore, the probability of false alarm is given by:

$$P_{fa} = P(T \geq t \mid H_0) = P\left(\text{Rice}(n = 2, \nu = 14L + 2R, 16L\sigma^2) > t\right)$$

$$P_{fa} = Q_1\left(\frac{14L + 2R}{\sqrt{16L\sigma^2}}, \frac{t}{\sqrt{16L\sigma^2}}\right) \tag{6.27}$$

where $Q_1(\cdot, \cdot)$ is the Marcum Q-function of order 1.

Simulation of P_{fa}

To validate the analytical results for incoherent demodulation, we generated $N_{sim} =$ 1,000,000 simulation runs. In each simulation, a segment of length $16L$, $\underline{s_t}$, was

randomly selected to transmit. This signal was multiplied by a random phase shift, and Gaussian noise was added. The noisy signal was then correlated with the pilot channel $\underline{s}$, and the magnitude of the correlation was computed. The results were then collected in the vector $\underline{T_0}$.

For each threshold t, P_{fa} was estimated as the proportion of $\underline{T_0}$ values exceeding t. If fewer than 1000 samples exceeded t, P_{fa} was not estimated for that threshold to ensure statistical reliability.

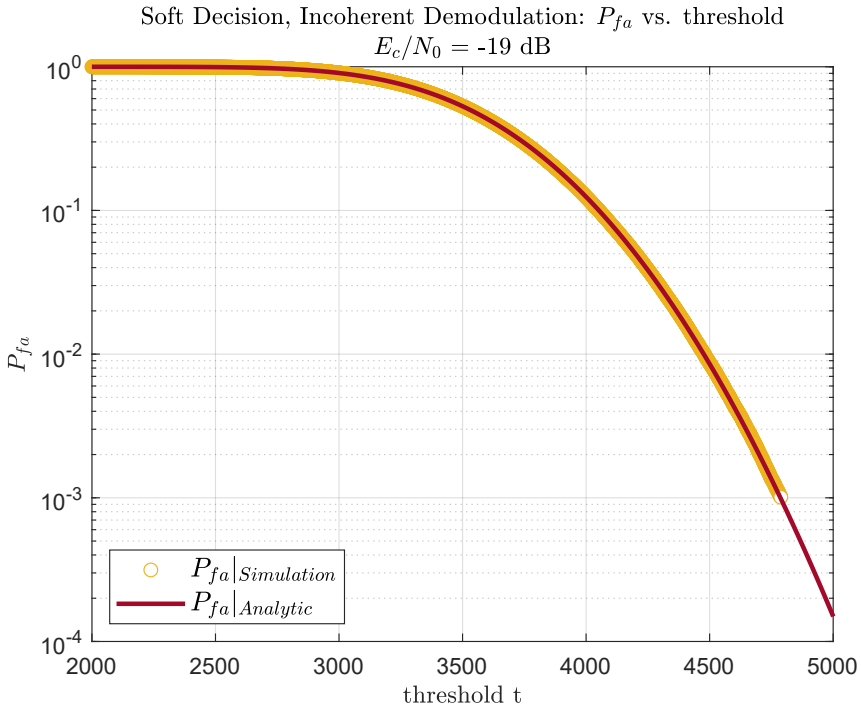

Figure 6.16: Comparison of analytical and simulated P_{fa} for soft detection incoherent demodulation.

Probability of Missed Detection (P_{md})

Analytical P_{md} As previously described in Eq. (6.26), under the alternative hypothesis H_1, the test statistic T follows a Rician distribution with a non-centrality parameter $\nu = 16L$ and variance $16L\sigma^2$:

$$T \sim \text{Rice}(\nu = 16L, 16L\sigma^2)$$

Therefore, the probability of missed detection is given by:

$$P_{md} = P(T < t \mid H_1) = 1 - Q_1\left(\frac{16L}{\sqrt{16L\sigma^2}}, \frac{t}{\sqrt{16L\sigma^2}}\right) \tag{6.28}$$

where Q_1 is the Marcum Q-function of order 1.

Simulation of P_{md}

To validate the analytical results for the probability of missed detection (P_{md}) in incoherent demodulation, we conducted a simulation with N_{sim} = 1,000,000 simulation runs. In each simulation run, the test statistic T_1 was calculated by finding the magnitude of the inner product of the pilot pattern $\underline{s}$, including Gaussian noise with variance σ^2, with itself. The results were collected in the vector $\underline{T}_1$.

For each threshold t, P_{md} was estimated as the proportion of $\underline{T}_1$ values falling below t. If fewer than 1000 samples were below t, P_{md} was not estimated for that threshold to ensure the statistical reliability of the results.

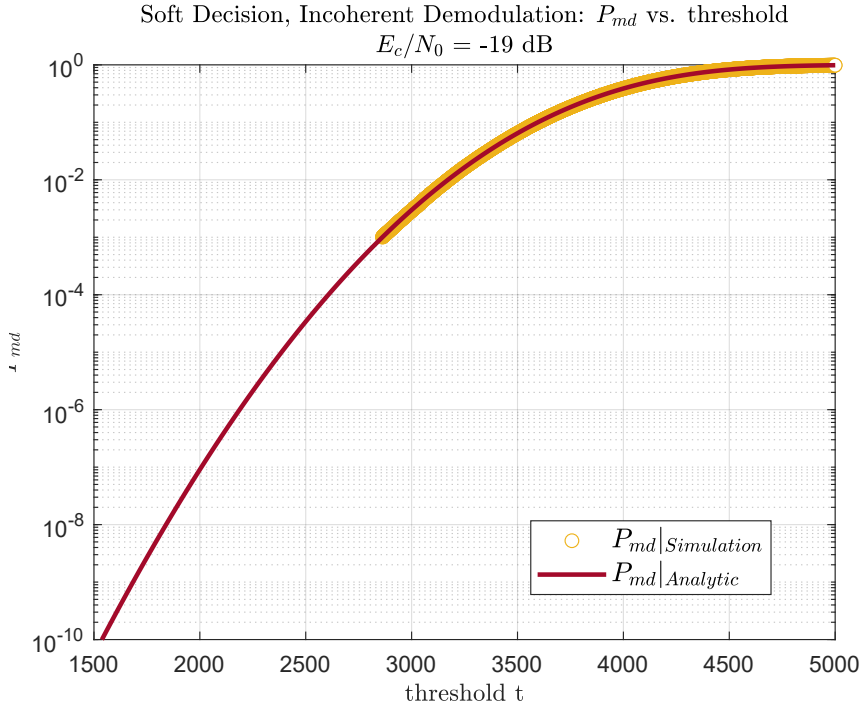

Figure 6.17: Comparison of analytical and simulated P_{md} for soft detection incoherent demodulation.

The figure shows the alignment between analytical and simulation results, confirming the accuracy of the derived analytical expressions for the probability of missed detection.

Receiver Operating Characteristic (ROC) Curve

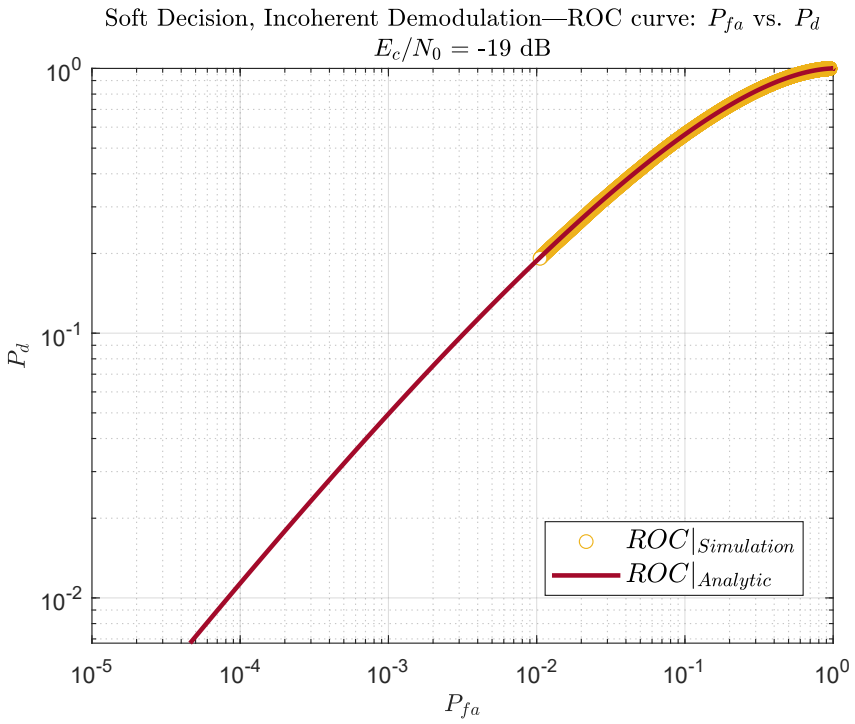

Figure 6.18: ROC curve for soft detection incoherent demodulation.

6.4 Performance Analysis of LEO GNSS Pilot Channel with Hard Detection

In this section, we provide a detailed analysis of the performance metrics for patterns created using Serial Bicode DSSS in LEO GNSS applications. We evaluate the system's performance under both coherent and incoherent demodulation scenarios, focusing on two key probabilities: the probability of false alarm (P_{fa}) and the probability of missed detection (P_{md}). This analysis emphasizes hard detection, where each DSSS sequence is decoded, and decisions are made based on the resulting sequence. Hard detection involves decoding the spreading sequences, computing the Hamming distance between the received sequence and the expected pattern, and making decisions accordingly.

6.4.1 Coherent Demodulation

Scenario Description

We consider a scenario involving a pattern $\underline{p}$:

$$\underline{p} = (0,0,0,0,0,0,0,1,0,0,0,0,0,0,0,0)$$

This pattern is spread using Serial Bicode DSSS to produce the pilot channel, where bit 0 is mapped to $\underline{c}_0$ (legitimate code) and bit 1 to $\underline{c}_1$ (alternative code). Both $\underline{c}_0$ and $\underline{c}_1$ are sequences of length L, forming the sequence $\underline{s}$:

$$\underline{s} = (\underline{c}_0, \underline{c}_0, \underline{c}_0, \underline{c}_0, \underline{c}_0, \underline{c}_0, \underline{c}_0, \underline{c}_1, \underline{c}_0, \underline{c}_0, \underline{c}_0, \underline{c}_0, \underline{c}_0, \underline{c}_0, \underline{c}_0, \underline{c}_0)$$

We continuously transmit a signal $\underline{s}$ of length $16L$ over an AWGN channel and check if the pattern $\underline{p}$ embedded within the received sequence is present a window of length $16L$.

- **Null Hypothesis** H_0: The pattern $\underline{p}$ embedded within $\underline{s}$ is absent at the receiver. The received signal does not contain the pattern.
- **Alternative Hypothesis** H_1: The pattern $\underline{p}$ embedded within $\underline{s}$ is present at the receiver.

We test the statistic $T = d_H(\underline{r}, \underline{p})$, where $\underline{r}$ is obtained from a segment of length $16L$ after decoding each L bits to either 0 or 1 according to the Serial DSSS method discussed before. Here, $d_H(\cdot, \cdot)$ represents the Hamming distance.

Under H_0

$$T = d_H(\underline{r}, \underline{p})$$

Following the same analysis we performed for the MEO case, and noticing that any cyclic shift $\underline{p_t}$ of pattern $\underline{p}$, excluding the pattern itself, has a Hamming distance $d_H(\underline{p_t}, \underline{p}) = 2$, it can be shown that under H_0, T is the sum of two binomial distributions:

$$T = X + Y$$

where $X \sim \text{Binomial}(d_H(\underline{p_t}, \underline{p}) = 2, 1 - P_b)$ and $Y \sim \text{Binomial}(16 - d_H(\underline{p_t}, \underline{p}) = 14, P_b)$.

Then, under H_0, the probability $P(T_0 = k)$ is:

$$P(T_0 = k) = \sum_{n=\max(0,k-14)}^{\min(2,k)} \binom{2}{n} (1 - P_b)^n P_b^{2-n} \binom{14}{k-n} P_b^{k-n} (1 - P_b)^{14-(k-n)} \quad (6.29)$$

Under H_1

Under H_1, T_1 follows a binomial distribution:

$$T_1 \sim \text{Binomial}(16, P_b)$$

The probability $P(T_1 = k)$ is given by:

$$P(T_1 = k) = \binom{16}{k}(1 - P_b)^{16-k} P_b^k \tag{6.30}$$

6.4.1.1 Probability of False Alarm (P_{fa})

In this section, we provide the analytical expression for P_{fa} and compare it with simulation results for hard detection coherent demodulation.

Analytical P_{fa}

For coherent demodulation hard detection, we compute the Hamming distance between the decoded received sequence and $\underline{p}$, and compare it to a threshold t. A false alarm occurs when, under H_0, the Hamming distance falls below the threshold t.

Using (6.29) it can be shown that the probability of false alarm is given by:

$$P_{fa} = P(T < t|H_0) = P(T_0 < t)$$

$$= \sum_{k=0}^{t-1} \sum_{n=\max(0,k-14)}^{\min(2,k)} \binom{2}{n}(1 - P_b)^n P_b^{2-n} \binom{14}{k-n} P_b^{k-n}(1 - P_b)^{14-(k-n)} \tag{6.31}$$

Simulation of P_{fa}

To validate the analytical results for the probability of false alarm (P_{fa}), we conducted a simulation with $N_{sim} = 1{,}000{,}000$ simulation runs. In each simulation run, a pattern $\underline{p_t}$ was selected randomly and encoded using serial bicode DSSS to form the transmitted signal. Gaussian noise was added to the selected signal, and the received signal was decoded by determining whether each L-chips segment corresponds to a 0 or 1. The Hamming distance T_0 between the decoded sequence and the expected pattern $\underline{p}$ was calculated and stored in the vector $\underline{T_0}$.

For each threshold t, P_{fa} was estimated as the proportion of $\underline{T_0}$ values falling below t. If fewer than 1000 samples fall below t, P_{fa} was not estimated for that threshold to ensure statistical reliability.

Finally, we plot the simulation results against the analytical results to verify the accuracy of the analytical expression for P_{fa}.

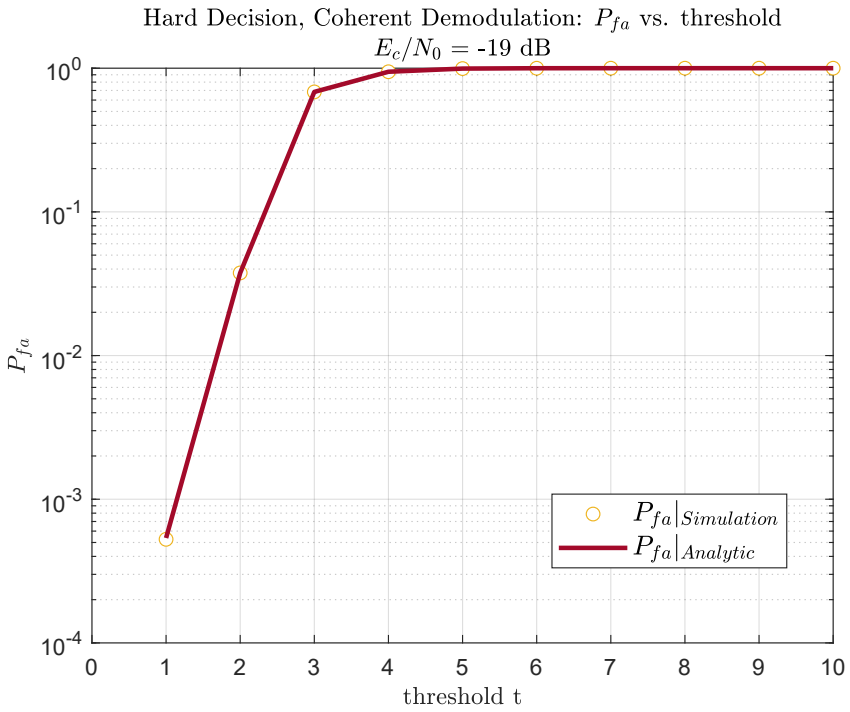

Figure 6.19: Comparison of simulated and analytical P_{fa} for hard detection coherent demodulation, demonstrating perfect alignment.

6.4.1.2 Probability of Missed Detection ((P_{md})

Analytic P_{md} As previously described is Eq. (6.30), under the alternative hypothesis H_1, the test statistic T follows a binomial distribution:

$$T_1 \sim \text{Binomial}(16, P_b)$$

Therefore, the probability of missed detection is given by:

$$P_{md} = P(T_1 > t) = 1 - \sum_{k=0}^{t} \binom{16}{k} (1 - P_b)^{16-k} P_b^k \tag{6.32}$$

This formulation is used because t is typically much smaller than $16-k$, simplifying the calculation.

Simulation of P_{md}

To validate the analytical results for the probability of missed detection (P_{md}), we conducted a simulation with $N_{sim} = 1{,}000{,}000$ simulation runs. In each simulation run, the signal $\underline{s}$ was transmitted with added Gaussian noise having a variance

σ^2. The received signal was then decoded by assessing each L-chips segment. The Hamming distance T_1 between the decoded sequence and the expected pattern $\underline{p}$ was computed and stored in the vector $\underline{T_1}$.

For each threshold t, P_{md} was estimated as the proportion of $\underline{T_1}$ values exceeding t. If fewer than 1000 samples exceeded t, P_{md} was not estimated for that threshold to maintain statistical reliability.

Finally, we plot the simulation results against the analytical results to verify the accuracy of the analytical expression for P_{md}.

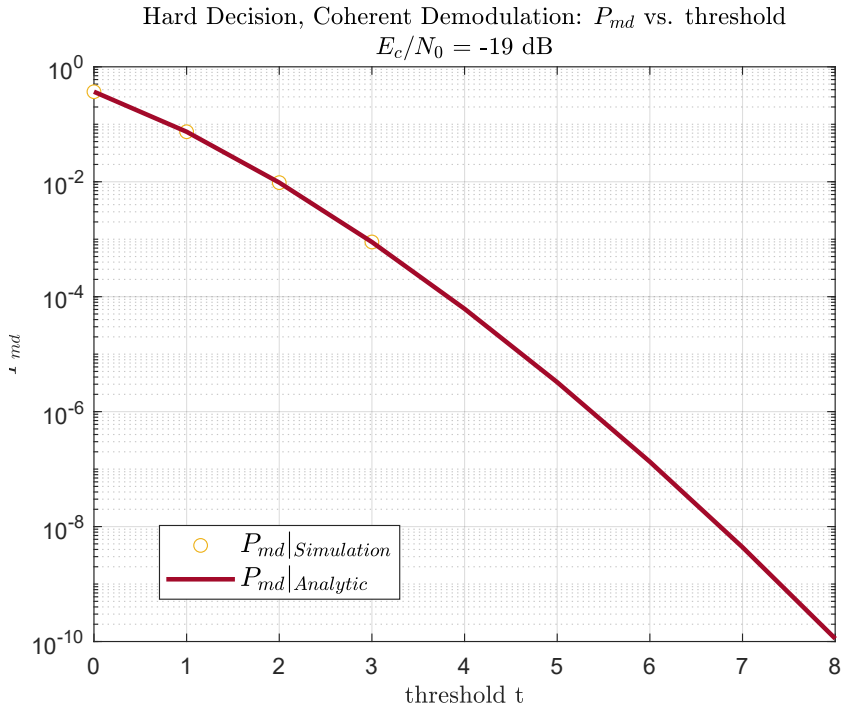

Figure 6.20: Comparison of simulated and analytical P_{md} for hard detection coherent demodulation

Receiver Operating Characteristic (ROC) Curve

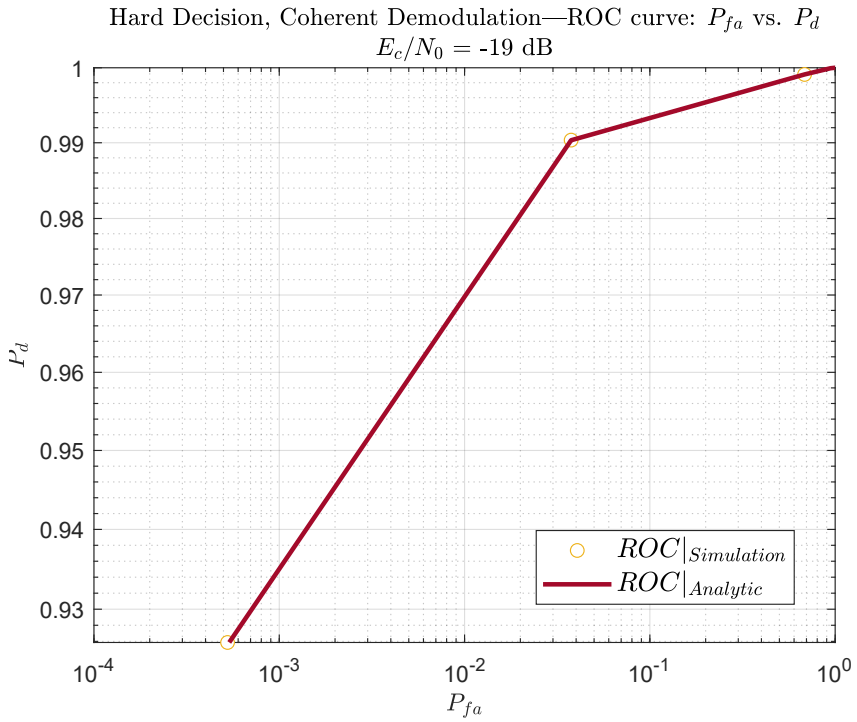

Figure 6.21: ROC curve for hard detection coherent demodulation.

6.4.2 Incoherent Demodulation

Scenario Description

The scenario is identical to the coherent demodulation case, with the exception that the probability of error $P_b(e)$ is given in Eq. (3.2).

The subsequent analysis follows the same approach as in the coherent demodulation case but with the modified error probability P_b.

Under H_0

$$P(T_0 = k) = \sum_{n=\max(0,k-14)}^{\min(2,k)} \binom{2}{n} (1-P_b)^n P_b^{2-n} \binom{14}{k-n} P_b^{k-n} (1-P_b)^{14-(k-n)} \quad (6.33)$$

Under H_1

$$P(T_1 = k) = \binom{16}{k} (1-P_b)^{16-k} P_b^k \quad (6.34)$$

6.4.2.1 Probability of False Alarm (P_{fa})

Analytical P_{fa}

The analytical expression for P_{fa} in incoherent demodulation is similar to that in coherent demodulation, with the modified error probability P_b, we now use P_b given in Eq. (3.2). It is given by:

$$P_{fa} = P(T < t|H_0) = P(T_0 < t)$$

$$= \sum_{k=0}^{t-1} \sum_{n=\max(0,k-14)}^{\min(2,k)} \binom{2}{n} (1-P_b)^n P_b^{2-n} \binom{14}{k-n} P_b^{k-n} (1-P_b)^{14-(k-n)} \quad (6.35)$$

Simulation of P_{fa}

To validate the analytical expression for P_{fa}, a simulation with $N_{sim} = 1{,}000{,}000$ simulation runs was conducted. In each run, a cyclic shift of pattern $\underline{p}$ was randomly selected and then encoded according to Serial Bicode DSSS to form the transmitted signal. This signal was then modulated with random phase and combined with Gaussian noise. The received signal was decoded to calculate the test statistic T_0, representing the Hamming distance from the expected pattern $\underline{p}$. The results were stored in the vector $\underline{T_0}$.

For each threshold t, P_{fa} was estimated as the proportion of $\underline{T_0}$ values falling below t. If fewer than 1000 samples fell below t, P_{fa} was not estimated for that threshold to ensure statistical reliability.

Finally, the simulation results were compared to the analytical results to ensure their accuracy.

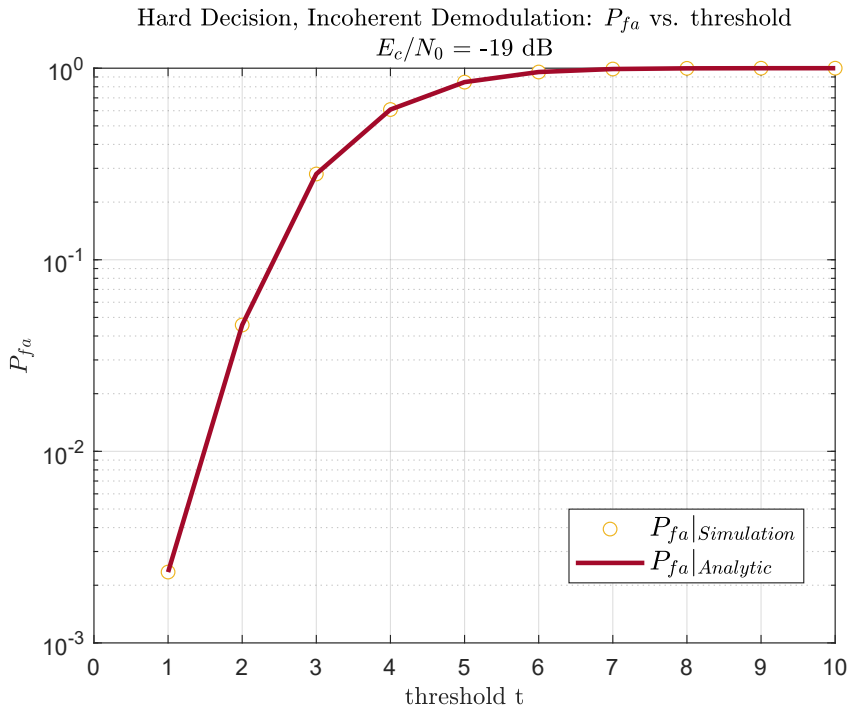

Figure 6.22: Comparison of simulated and analytical P_{fa} for hard incoherent demodulation.

6.4.2.2 Probability of Missed Detection (P_{md})

The probability of missed detection (P_{md}) measures the likelihood that the receiver fails to detect the presence of the pattern p embedded within the received signal when it is actually present.

Analytical P_{md} For the incoherent demodulation scenario, the analytical expression for P_{md} is derived similarly to the coherent case, but with the modified error probability specific to incoherent demodulation:

$$P_{md} = P(T_1 > t) = 1 - \sum_{k=0}^{t} \binom{16}{k} (1 - P_b)^{16-k} P_b^k$$

Simulation of P_{md} To validate the analytical expression for P_{md}, a simulation was performed with N_{sim} = 1,000,000 simulation runs. For each run, the pilot channel $\underline{s}$ was modulated with random phase and Gaussian noise, then decoded to compute the test statistic T_1. The statistic T_1 represents the Hamming distance from the expected pattern $\underline{p}$. The results were stored in the vector $\underline{T_1}$.

For each threshold t, P_{md} was estimated as the proportion of $\underline{T_1}$ values exceeding t. If fewer than 1000 samples exceeded t, P_{md} was not estimated for that threshold to ensure statistical reliability.

Finally, the simulation results were compared to the analytical results to ensure their accuracy.

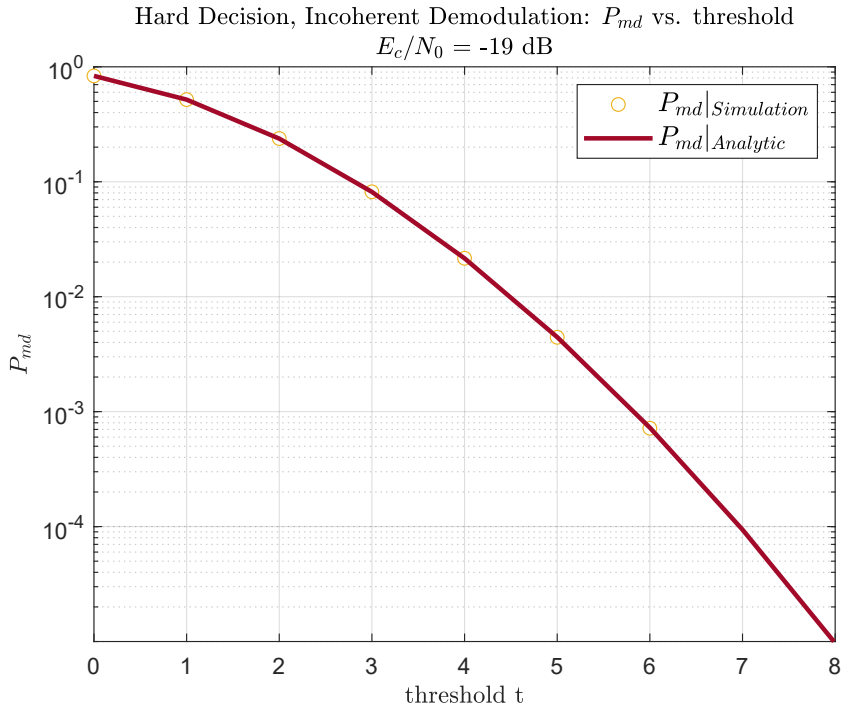

Figure 6.23: Comparison of simulated and analytical P_{md} for hard incoherent demodulation.

Receiver Operating Characteristic (ROC) Curve

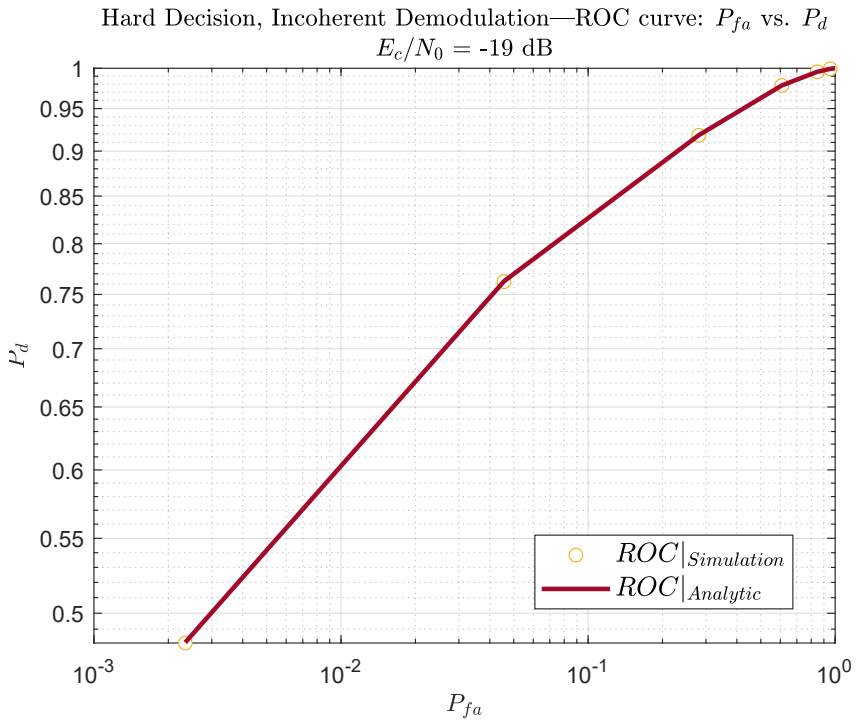

Figure 6.24: ROC curve for hard incoherent demodulation.

Chapter 7

Signal Acquisition for GNSS Serial Bicode DSSS Pilot Channels

7.1 Introduction

In the previous chapter, we examined the performance of block detection of pilot channels utilizing Serial Bicode DSSS for both MEO and LEO GNSS systems. Those analyses assumed that the Doppler shift and code delay values were already estimated. It was assumed that the receiver was aligned with the short code, facilitating a straightforward search and detection of the embedded patterns.

In this chapter, we turn our attention to the essential task of estimating the Doppler shift and code delay values, enabling the receiver to synchronize with the satellite signals. Unlike earlier scenarios, we no longer assume that the receiver is already aligned with the short codes. Instead, the acquisition process now seeks to determine these parameters, after which the receiver can decode and locate the embedded patterns in the GNSS signals. In the subsequent analysis, to evaluate the Cross-Ambiguity Function (CAF), we adopt the approach introduced in Chapter 4. Specifically, we compute the squared modulus of the CAF across the entire search space, accumulate these values over N_c coherent integrations, and then select the maximum value to make our decision. (Note that this analysis can be easily extended to other search strategies.) We begin by deriving a general model for acquisition performance, followed by a comparison of analytical and simulated results using the MEO and LEO pilot channels introduced by Garello in [1] and presented in Chapter 5.

7.2 General Framework

7.2.1 Introduction

In this section, we establish a general framework for analyzing the acquisition of GNSS Serial Bicode DSSS pilot channels. The received signal at the output of the front-end stage can be expressed as:

$$r_x(t) = c_r(t-\tau)\exp\Big(2\pi\big(f_{IF}+f_D\big)t+\Phi\Big) + n_R(t) + j\,n_I(t), \tag{7.1}$$

where $c_r(t-\tau)$ is the result of an unknown serial combination of the two codes $\underline{c_0}$ and $\underline{c_1}$. The different possible code patterns that may arise from this serial configuration will be discussed in detail in the following sections. The term $f_{IF}+f_D$ accounts for the sum of the intermediate frequency and Doppler shift, Φ is the carrier phase, and $n_R(t)+j\,n_I(t)$ represents complex-valued additive white Gaussian noise (AWGN).

7.2.2 Statistical Modeling and Cell Probabilities

The basic elements of the performance evaluation in our analysis are the detection and false alarm probabilities for a single cell of the non-coherent accumulation output, hereinafter referred to as P_d and P_{fa}, respectively. However, the overall performance depends on decisions made based on the entire search space. Consequently, the overall detection and false alarm probabilities, denoted hereafter as P_D and P_{FA}, respectively, are also evaluated.

We distinguish between two hypotheses:

- a *null hypothesis*, H_0, where the signal is not present or does not align with the local replica; and
- an *alternative hypothesis*, H_1, where the signal is present and correctly aligned with the local replica.

We assume that the ambiguity function is null in the absence of noise for $\hat{\tau}_n \neq \tau$ and $\hat{F}_{dn} \neq F_d$, where (τ, F_d) is the cell in which the signal is present and aligned.

Note: Discrete-time signals are denoted with square brackets (e.g., $n_R[i] = n_R(iT_s)$), omitting the explicit T_s.

Statistical Characterization Under H_0

Under H_0, the received signal consists solely of noise. Hence, the nth cell of the CAF in (4.3) is

$$R_n = R(\hat{\tau}_n, \hat{F}_{d,n}) = \frac{1}{L}\sum_{i=1}^{L}\Big(n_R[i] + j\, n_I[i]\Big)c_0[i-\hat{\tau}_n]\exp\Big(-j2\pi\hat{F}_{d,n}i\Big), \qquad (7.2)$$

where $n_R[i]$ and $n_I[i]$ are the real and imaginary parts of the noise, assumed i.i.d. Gaussian with zero mean and variance $\sigma^2 = \frac{N_0}{2}$ (N_0 is the one-sided noise spectral density).

By reformulating (7.2) as in (4.5), we can evaluate the variance of the real and imaginary part as [30]

$$\begin{aligned}
\mathrm{var}[Y_{R,n}] &= \mathrm{var}\left\{\Re\left\{\frac{1}{L}\sum_{i=1}^{L}\Big(n_R[i] + j\, n_I[i]\Big)c_0[i-\hat{\tau}_n]e^{j2\pi\hat{F}_{d,n}i}\right\}\right\} \\
&= \frac{1}{L^2}\sum_{i=1}^{L}\mathrm{var}\Big\{n_R[i]\cos(2\pi\hat{F}_{d,n}i) - n_I[i]\sin(2\pi\hat{F}_{d,n}i)\Big\} \\
&= \frac{1}{L^2}\sum_{i=1}^{L}\Big[\sigma^2\cos^2(2\pi\hat{F}_{d,n}i) + \sigma^2\sin^2(2\pi\hat{F}_{d,n}i)\Big] = \frac{\sigma^2}{L}.
\end{aligned}$$

Similarly

$$\mathrm{var}\,[Y_{I,n}] = \frac{\sigma^2}{L}\ .$$

It follows that $Y_n = Y_{R,n}^2 + Y_{I,n}^2$ with variance $\sigma_Y^2 = \frac{\sigma^2}{L}$. Therefore, Y_n follows a central scaled chi-square distribution with two degrees of freedom:

$$Y_n \sim \sigma_Y^2\,\chi^2(2).$$

The non-coherent accumulation over N_c integrations then averages N_c independent scaled chi-squared random variables, resulting in another scaled chi-squared distribution with $2N_c$ degrees of freedom. The variance is $\sigma_{N_c}^2 = \frac{\sigma_Y^2}{N_c} = \frac{\sigma^2}{L\,N_c}$:

$$X_n = \frac{1}{N_c}\sum_{k=1}^{N_c} Y_{k,n} \ \sim\ \sigma_{N_c}^2\,\chi^2(2N_c).$$

The probability density function (PDF) under H_0 is then:

$$f_{X_n|H_0}(x) \ =\ \frac{1}{2\,\sigma_{N_c}^2}\Big(\tfrac{x}{2\,\sigma_{N_c}^2}\Big)^{N_c-1}\frac{1}{\Gamma(N_c)}\exp\Big(-\tfrac{x}{2\,\sigma_{N_c}^2}\Big) \quad \text{for } x \geq 0,$$

where $\Gamma(\cdot)$ is the gamma function.

Cell Probability of False Alarm The probability of false alarm P_{fa} for a single cell at a predefined threshold t is given by [31]:

$$P_{\text{fa}}(t) = \int_t^{\infty} f_{X_n|H_0}(x)\, dx = \frac{\Gamma\left(N_c, \frac{t}{2\sigma^2_{N_c}}\right)}{\Gamma(N_c)}, \tag{7.3}$$

where $\Gamma(s, x)$ is the upper incomplete gamma function.

Statistical Characterization Under H_1

Under the H_1 hypothesis, we consider the signal in the cell A, where the signal is present and correctly aligned. In this case, the CAF in cell A can be defined as:

$$R_A = \frac{1}{L}\sum_{i=1}^{L}\left(c_r[i-\tau]e^{j(2\pi F_d i+\Phi)} + n_R[i] + jn_I[i]\right) c_0[i-\tau_A]e^{-j2\pi\hat{F}_{d,A}i} \tag{7.4}$$

where Φ is an unknown but constant carrier phase offset during the observation interval. The term c_r represents the possible code pattern in the observed signal resulting from the unknown serial combination of $\underline{c_0}$ and $\underline{c_1}$. The possibilities of which will be discussed in detail in the following sections.

Under this hypothesis, the real and imaginary parts of R_A, denoted by $Y_{R,A}$ and $Y_{I,A}$, respectively, are no longer zero-mean. To show it, we begin by expressing the expectation of the real part as

$$\begin{aligned}
E[Y_{R,A}] &= E\left[\mathcal{R}\left\{\frac{1}{L}\sum_{i=1}^{L}\Big(c_r[i-\tau]\, e^{j(2\pi F_d i+\Phi)} + n_R[i] + j\, n_I[i]\Big) c_0[i-\tau_A]\, e^{-j2\pi\hat{F}_{d,A}i}\right\}\right] \\
&\overset{H_1}{=} E\left[\mathcal{R}\left\{\frac{1}{L}\sum_{i=1}^{L} c_r[i-\tau]\, e^{j(2\pi F_d i+\Phi)}\, c_0[i-\tau]\, e^{-j2\pi F_d i}\right\}\right] \\
&= \frac{1}{L}\sum_{i=1}^{L} c_r[i-\tau]\, c_0[i-\tau]\, \mathcal{R}\Big\{e^{j(2\pi F_d i+\Phi)}\, e^{-j2\pi F_d i}\Big\} \\
&= \frac{1}{L}\sum_{i=1}^{L} c_r[i-\tau]\, c_0[i-\tau]\, \mathcal{R}\Big\{e^{j\Phi}\Big\} \\
&= \frac{1}{L}\sum_{i=1}^{L} c_r[i-\tau]\, c_0[i-\tau]\, \cos(\Phi)\,.
\end{aligned} \tag{7.5}$$

where (7.5) follows from the H_1 assumption that $\hat{F}_{d,A} = F_d$ and $\tau_A = \tau$.

Similarly, for the imaginary part we get

$$E[Y_{I,A}] = \frac{1}{L}\sum_{i=1}^{L} c_r[i-\tau]c_0[i-\tau]\sin(\Phi) \ .$$

Now, due to the presence of the alternative codes $\underline{c_1}$ in the pilot channel, $\underline{c}_r$ depends on the window where coherent integration is considered. We define $\underline{c}_{r,k}$ as the pattern found within the k-th coherent integration of the non-coherent accumulation, and we introduce the parameter:

$$\alpha_k = \frac{1}{L}\sum_{i=1}^{L} c_{r,k}[i-\tau]c_0[i-\tau] \tag{7.6}$$

The variance of $Y_{R,A}$ and $Y_{I,A}$ is not affected by the presence of the useful signal (a deterministic component). Hence:

$$Y_{R,A} \sim \mathcal{N}(\alpha_k \cos(\Phi), \frac{\sigma^2}{L}), \tag{7.7}$$

and

$$Y_{I,A} \sim \mathcal{N}(\alpha_k \sin(\Phi), \frac{\sigma^2}{L}). \tag{7.8}$$

Since the sum of the squares of two non-zero mean independent Gaussian random variables leads to a non-central χ^2 distribution, we have:

$$Y_A = Y_{R,A}^2 + Y_{I,A}^2$$

$$Y_A \sim \chi^2_{nc,2}(\lambda_k, \frac{\sigma^2}{L}). \tag{7.9}$$

where:

$$\begin{aligned} \lambda_k &= E^2\Big[Y_{R,A}\Big] + E^2\Big[Y_{I,A}\Big] \\ &= \left(\frac{1}{L}\sum_{i=1}^{L} c_{r,k}[i-\tau]c_0[i-\tau]\right)^2 \end{aligned} \tag{7.10}$$

Therefore, the final random variable X_A, which is the output of the non-coherent accumulation in cell A, is the average of N_c non-central χ^2 random variables, each with 2 degrees of freedom. This results in a non-central χ^2 variable with $2N_c$ degrees of freedom and a non-centrality parameter:

$$\lambda = \frac{1}{N_c}\sum_{k=1}^{N_c} \lambda_k, \tag{7.11}$$

where λ_k is given in (7.10).

Possible Scenarios of $\underline{c_r}$

To compute the non-centrality parameter of X_A, it is necessary to account for all possibilities of $\underline{c_r}$ within the coherent integration time and consequently for λ_k.

For a generic pilot channel constructed using Serial DSSS, three distinct scenarios of $\underline{c_r}$ are identified. These scenarios, labeled 1, 2, and 3 in Fig. 7.1, correspond to $\lambda^{(1)}$, $\lambda^{(2)}$, and $\lambda^{(3)}$, respectively.

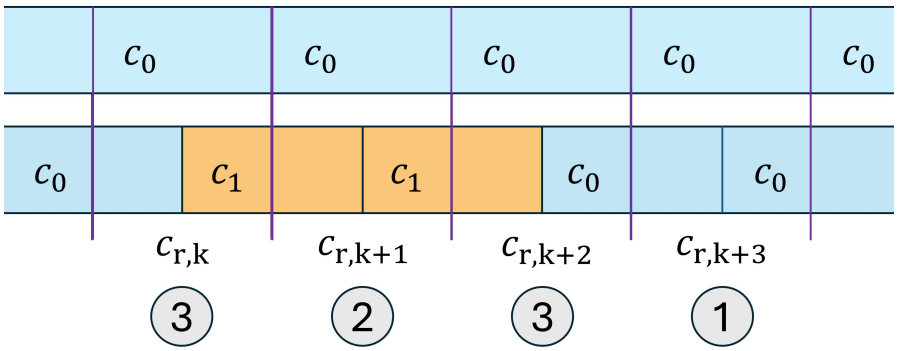

Figure 7.1: Illustration of the three possible scenarios of $\underline{c_r}$ within the coherent integration time.

1. **Cyclic Shift of $\underline{c_0}$**: In this case:

$$\lambda^{(1)} = \left(\frac{1}{L} \sum_{i=1}^{L} c_{0,i}^2 \right)^2 = 1.$$

2. **Cyclic Shift of $\underline{c_1}$**: The value of $\lambda^{(2)}$ in this case depends on the cross-correlation between $\underline{c_0}$ and $\underline{c_1}$, and can be expressed as:

$$\begin{aligned} \lambda^{(2)} &= \left(\frac{1}{L} \sum_{i=1}^{L} S^{-\tau} \left(S^{\tau} c_{1,i} \right) c_{0,i} \right)^2 \\ &= \left(\frac{1}{L} \sum_{i=1}^{L} c_{1,i} c_{0,i} \right)^2 = \rho_{01}^2. \end{aligned} \tag{7.12}$$

   where $S^{\tau}\underline{c_1}$ denotes the cyclic shift of length τ of $\underline{c_1}$ and ρ_{01} is the normalized cross-correlation between $\underline{c_0}$ and $\underline{c_1}$.

3. **Leakage from $\underline{c_1}$:**

For this scenario, the amount of leakage clearly depends on the true delay τ. We also notice that whenever $\underline{c_1}$ exists, there is leakage from $\underline{c_1}$ onto $\underline{c_0}$, as well as leakage from $\underline{c_0}$ onto $\underline{c_1}$. The corresponding non-centrality parameters, $\lambda^{(3)}_{(0\to1)}$ and $\lambda^{(3)}_{(1\to0)}$, are computed for these leakages. These scenarios are labeled as 3 in Fig. 7.1. This leakage is independent of the length of runs of the alternative code $\underline{c_1}$.

We define:

$$\underline{c_{01}} = (\underline{c_0}, \underline{c_1}) = (c_{0,1}, \ldots, c_{0,i}, \ldots, c_{0,L}, c_{1,1}, \ldots, c_{1,i}, \ldots, c_{1,L}), \tag{7.13}$$

where $\underline{c_0}$ and $\underline{c_1}$ are the short spreading codes. The cyclic shift by τ of $\underline{c_{01}}$ is denoted as $S^\tau \underline{c_{01}}$. For example:

$$S^1\underline{c_{01}} = (c_{1,L}, c_{0,1}, \ldots, c_{0,i}, \ldots, c_{0,L}, c_{1,1}, \ldots, c_{1,i}, \ldots, c_{1,L-1}). \tag{7.14}$$

We denote $S^\tau_{L,1}\underline{c_{01}}$ as the first L entries of the cyclic shift of length τ of $\underline{c_{01}}$, and we similarly denote $S^\tau_{L,2}\underline{c_{01}}$ as the second L entries.

We define the leakage $l(\tau)$ as follows:

$$l(\tau) = \lambda^{(3)}_{0\to1} + \lambda^{(3)}_{1\to0},$$

and

$$l(\tau) = \left(\frac{1}{L}\sum_{i=1}^{L} S^{-\tau}\left(S^\tau_{L,1}c_{01,i}\right)c_{0,i}\right)^2 + \left(\frac{1}{L}\sum_{i=1}^{L} S^{-\tau}\left(S^\tau_{L,2}c_{01,i}\right)c_{0,i}\right)^2 \tag{7.15}$$

The first term represents the cross product between the first L entries of the cyclic shift of $\underline{c_{01}}$ by τ, where only these L entries are further cyclically shifted by $-\tau$, and the legitimate code $\underline{c_0}$. The second term is computed in exactly the same way but uses the second L entries of the τ-shifted $\underline{c_{01}}$.
The leakage characterizes the normalized cross-correlation between the legitimate code $\underline{c_0}$ and the received mixed code for a given delay τ (with the delay determining the amount of the leakage), within cell A, where the legitimate code itself is cyclically shifted by τ.

The term $l(\tau)$ is defined for the two cases of leakage together ($1 \to 0$ and $0 \to 1$) because they always coexist.

Occurrence of Scenarios

the non-centrality parameter of the random variable characterizing the cell A in the output of non-coherent integration depends on the occurrence of each scenario, denoted N_1 (number of occurrences of scenario 1), N_2 (number of occurrences of scenario 2), and N_2 (number of occurrences of scenario 3), depends on N_c, the number of runs of codes $\underline{c_1}$, denoted N_{c_1}, and the length of each run denoted $L_{c_1,i}$ (the length of the i-th run of alternative codes). These quantities are related by the following equations:

$$N_3 = N_{c_1}, \tag{7.16}$$

$$N_2 = \sum_{i=1}^{N_{c_1}} \Big(L_{c_1,i} - 1 \Big), \tag{7.17}$$

$$N_1 = N_c - 2N_3 - N_2. \tag{7.18}$$

Therefore, the non-centrality parameter $\lambda(\tau)$ becomes:

$$\begin{aligned} \lambda(\tau) &= \frac{1}{N_c} \left(N_1 \lambda^{(1)} + N_3 \lambda^{(3)} + N_2 \lambda^{(2)} \right) \\ &= \frac{1}{N_c} \left(N_1 + N_3 l(\tau) + N_2 \rho_{01}^2 \right), \end{aligned} \tag{7.19}$$

Since the delay τ is equally probable for any value, $\lambda(\tau)$ has a probability of $\frac{1}{L}$ for each τ.

Having defined the non-centrality parameters and the number of occurrences for each scenario, we now note that the number of occurrences N_1, N_2, and N_3 depends on the specific segment of the pilot channel $\underline{s}$ being considered.

We extract from the pilot channel $\underline{s}$ all possible segments $\underline{y}$ of length N_c short codes, aligned with the short codes. For each segment $\underline{y}^m$, we compute $N_{c_1}^m$, representing the number of runs of the alternative code $\underline{c_1}$ within the segment, and $L_{c_1,i}^m$, denoting the length of each run in segment $\underline{y}^m$. The total number of segments is K, which corresponds to the number of short codes in $\underline{s}$. The probability of each segment is then by $\frac{1}{K}$.

For each $\underline{y}^m$, we then compute:

$$\lambda^m(\tau) = \frac{1}{N_c} \left(N_1^m + N_3^m l(\tau) + N_2^m \rho_{01}^2 \right) \quad \forall \tau$$

where N_1^m, N_3^m, and N_2^m are computed using equations (7.18), (7.16), and (7.17) respectively. Thus, the probability density function of the random variable X_A is given by:

$$f_{X_A}(x) = \frac{1}{K}\sum_{m=1}^{K}\frac{1}{L}\sum_{\tau=1}^{L}\frac{1}{2\sigma^2/(LN_c)}\left(\frac{x}{\lambda^m(\tau)}\right)^{(N_c-1)/2}$$

$$\exp{-\frac{x+\lambda^m(\tau)}{2\sigma^2/(LN_c)}}I_{N_c-1}\left(\frac{\sqrt{x\lambda^m(\tau)}}{\sigma^2/(LN_c)}\right) \tag{7.20}$$

$$x \geq 0;$$

Important Note: When an alternative code appears at the edges of the non-coherent accumulation window, each type of leakage may be introduced in two different windows. Our analysis, however, combines both types of leakage within a single window, leading to a slight overestimation of one non-centrality parameter and a slight underestimation of the other. Despite this, the impact on the overall non-centrality parameter remains minimal, particularly for long non-coherent accumulation periods. Notably, when the non-coherent accumulation spans the entire pilot channel, our analysis is exact since, in this case, shifts in the segments are truly cyclic.

Cell Probability of Detection

Finally, we are able to compute the probability of detection P_d for a single cell for a predefined threshold t:

$$P_d(t) = \int_t^{+\infty} f_{X_A}(x)\,dx$$

$$P_d(t) = \frac{1}{K}\sum_{m=1}^{K}\sum_{\tau=1}^{L}\frac{1}{L}Q_{N_c}\left(\sqrt{\frac{\lambda^m(\tau)}{\sigma^2/(LN_c)}}, \sqrt{\frac{t}{\sigma^2/(LN_c)}}\right) \tag{7.21}$$

where Q_{N_c} is the Marcum Q-function of order N_c.

7.2.3 Decision Probabilities

Building on the single-cell detection and false alarm probabilities P_d and P_{fa}, we now derive the overall decision probabilities using the maximum search strategy.

Missed Detection Probability

A miss-detection occurs when the satellite is present but it is not detected. This happens when no cell value exceeds the threshold, corresponding to the event that all the random variables X_n are lower than the threshold t.

The miss-detection probability is given by

$$P_{\mathrm{MD}}(t) = \prod_{n=1}^{M} P(X_n < t)$$

where

$$P(X_n < t) = \begin{cases} 1 - P_{\mathrm{d}}(t) & \text{when } X_A \neq X_n, \\ 1 - P_{\mathrm{fa}}(t) & \text{when } X_A = X_n, \end{cases}$$

Where $P_d(t)$ and $P_{fa}(t)$ are the single cell probabilities derived in 7.21 and 7.3 respectively. The miss-detection probability becomes:

$$\begin{aligned} P_{\mathrm{MD}}(t) &= [1 - P_d(t)] \prod_{n=1}^{M-1} [1 - P_{\mathrm{fa}}(t)] \\ &= [1 - P_{\mathrm{fa}}(t)]^{M-1} [1 - P_d(t)] \end{aligned} \tag{7.22}$$

Detection Probability

The overall detection probability $P_D(t)$, based on the maximum search strategy, is:

$$P_D(t) = P\left(X_A = \max_n \{X_n\}, X_A > t\right), \tag{7.23}$$

$P_D(t)$ can then be expressed as [30]:

$$P_D(t) = \int_t^{+\infty} (1 - P_{fa}(x))^{M-1} f_{X_A}(x)\, dx \tag{7.24}$$

Assuming small false alarm probabilities, Eq.(7.24) reduces to:

$$P_D(t) \approx \int_t^{+\infty} f_{X_A}(x)\, dx = P_d(t) \tag{7.25}$$

False Alarm Probability

It is important to distinguish between the probability of false alarm of the decision when the signal is absent P^a_{FA} and when the signal is present P^p_{FA}. The threshold t is chosen based on P^a_{FA} since it represents a more critical system performance indicator [30]:

$$P^a_{\mathrm{FA}}(t) \geq P^p_{\mathrm{FA}}(t) \quad \forall t. \tag{7.26}$$

The probability P^a_{FA}, the false alarm probability of the decision adopting the maximum strategy, is:

$$P^a_{FA}(t) = P\left(\max_n(X_n) > t\right) = 1 - P\left(\max_n(X_n) < t\right)^M$$

$$= 1 - (1 - P(X_n > t))^M = 1 - (1 - P_{fa}(t))^M \tag{7.27}$$

$$P^a_{\mathrm{FA}}(t) = 1 - (1 - P_{\mathrm{fa}}(t))^M \tag{7.28}$$

The probability of false alarm of the decision when the signal is present P^p_{FA}can be obtained by:

$$P^{\mathrm{p}}_{\mathrm{FA}}(t) = 1 - P_D(t) - P_{\mathrm{MD}}(t),$$

7.2.4 Simulation Results

MEO GNSS Pilot Channel

To validate the theoretical analysis, we performed simulations to estimate both the false alarm probability P_{FA} and the detection probability P_{D}.

Probability of False Alarm Figure 7.2 shows the simulation results for P_{FA} alongside the analytical curve. The close agreement between the simulated and theoretical results confirms the accuracy of the model.

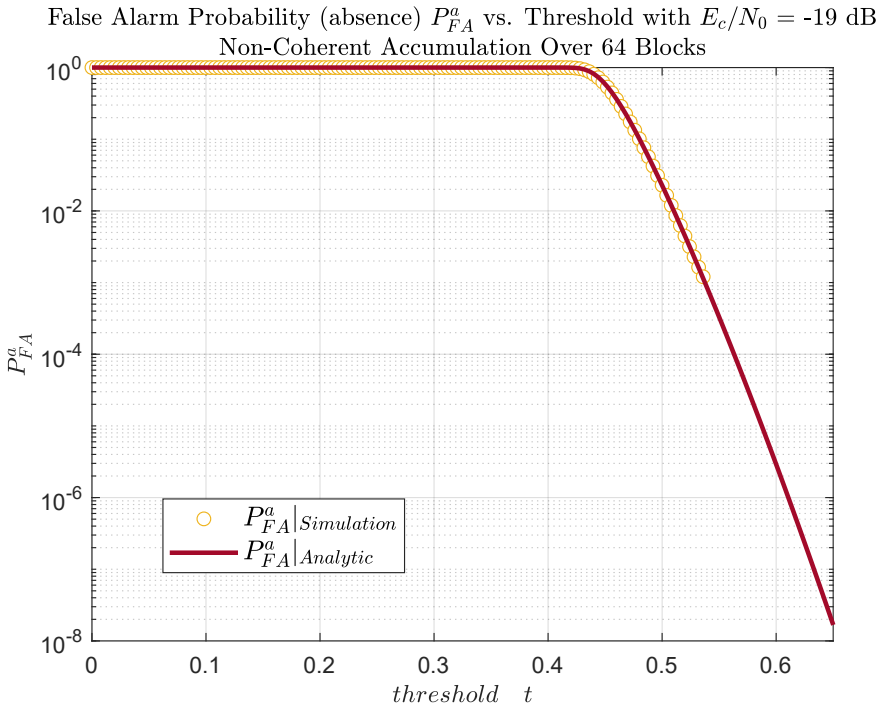

Figure 7.2: Simulation results for P^a_{FA} compared with the analytical curve.

Probability of Detection Figure 7.3 presents the simulation results for P_{D} together with the theoretical curve. Once again, the perfect alignment between the two indicates that the derived expressions accurately predict system performance.

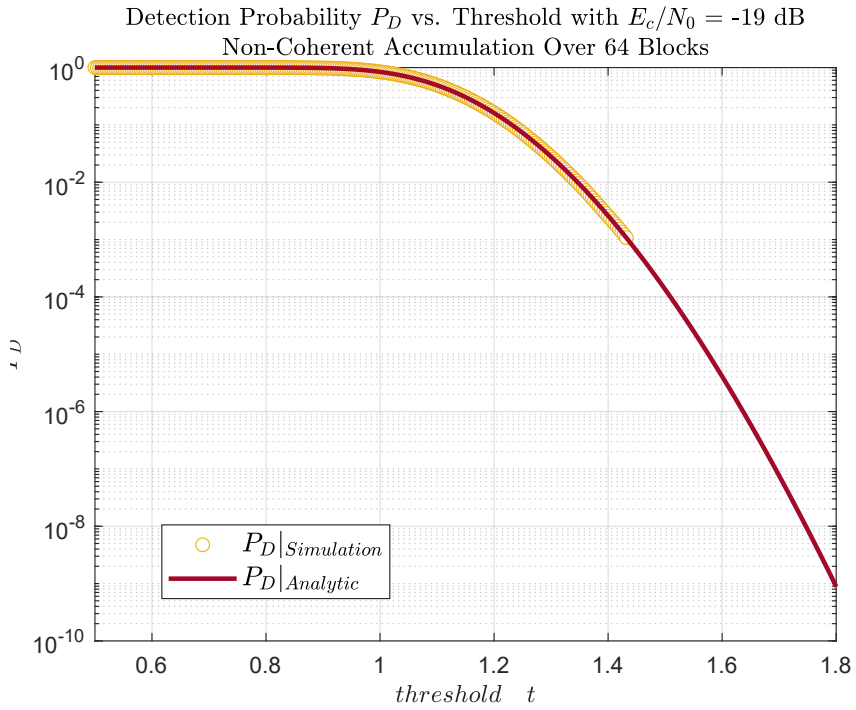

Figure 7.3: Simulation results for P_{D} compared with the analytical curve.

LEO GNSS Pilot Channel

We also conducted simulations for the LEO GNSS pilot channel to validate our theoretical predictions of P_{FA} and P_{D}.

Probability of False Alarm Figure 7.4 illustrates the simulated P_{FA} values alongside the corresponding analytical curve. The two show excellent alignment, thereby confirming the validity of our model in a LEO scenario as well.

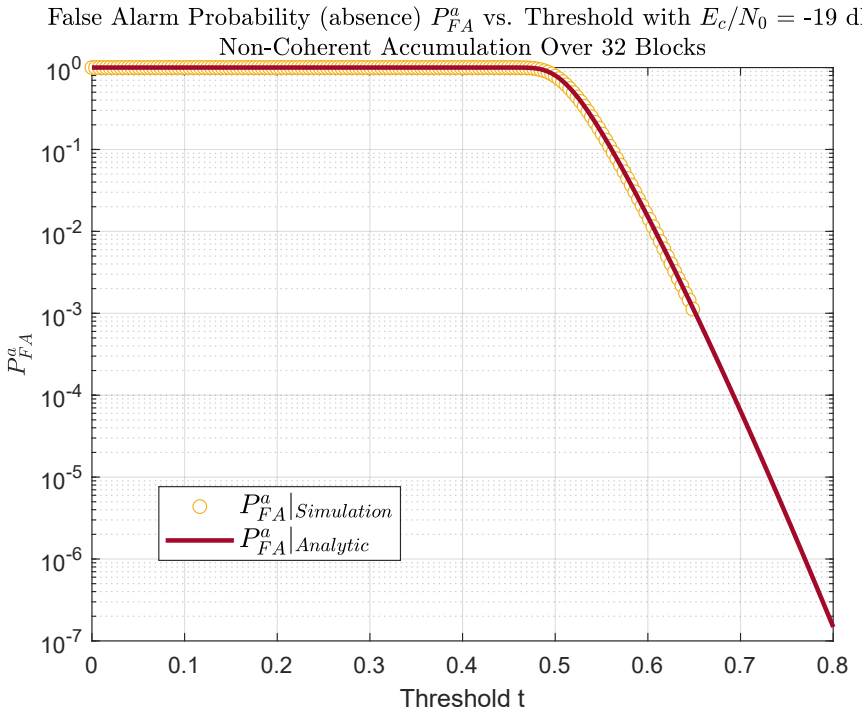

Figure 7.4: Simulation results for P^a_{FA} compared with the analytical curve.

Probability of Detection Figure 7.5 displays the simulation outcomes for P_{D} together with the analytical results. The agreement between the curves verifies the robustness of the analytical model for a LEO environment.

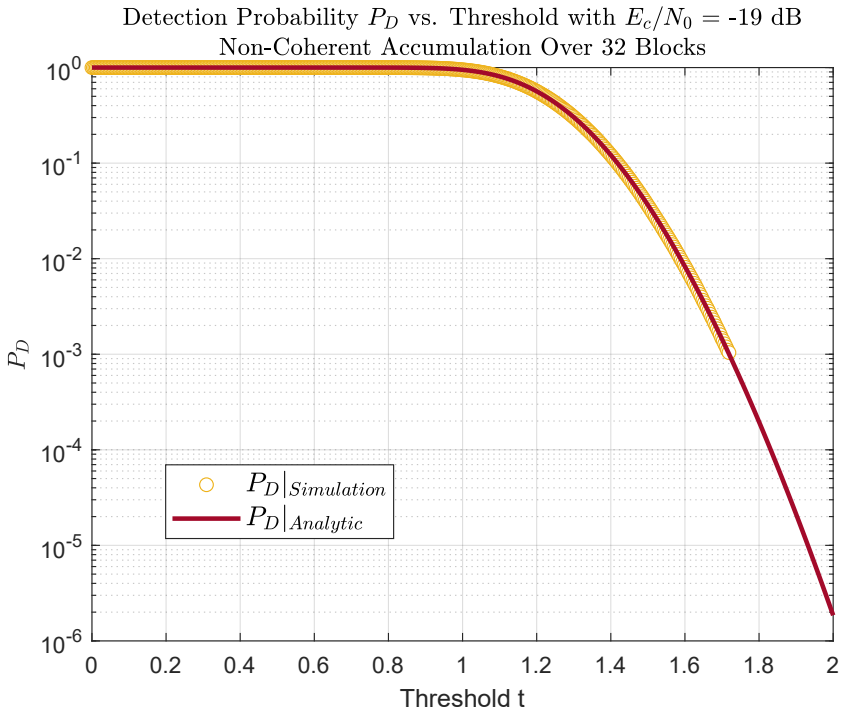

Figure 7.5: Simulation results for P_{D} compared with the analytical curve.

Chapter 8

Design of Pilot Channels for MEO GNSS Systems

8.1 Introduction

In the previous chapters, we examined the construction and performance of pilot channels for MEO GNSS systems based on the Serial Bicode DSSS approach as presented by Garello [1]. While the existing designs are effective in resolving code ambiguity, there is potential for exploring alternative pilot channel designs.

This chapter introduces well-considered alternative pilot channels designs that aim to provide a balanced approach to both block transition detection and acquisition processes. These alternatives focus on achieving distinct patterns with sufficient Hamming distances while maintaining efficient acquisition through thoughtful management of the number of alternative codes.

8.2 Design Considerations for New Pilot Channels

The design of the pilot channels is guided by three primary considerations:

1. **Transition Detection Distinctiveness:** The pilot channel is structured into b blocks, the detection of each block allows the detection of a transition. To ensure clear detection, the minimum Hamming distance is maximized between each block pattern and all possible segments of the same length, enhancing the distinctiveness of block.

2. **Minimization of Alternative Codes:** Fewer occurrences of the alternative code c_1 within the channel are preferred, as this improves acquisition

performance.

3. **Reduction of Consecutive Alternative Code Runs:** Reducing consecutive runs of the alternative code (c_1) contributes to improved acquisition performance.

Balancing Trade-Offs A reduction in the alternative code count, while beneficial for acquisition, tends to lower the minimum Hamming distance between each transition pattern and all possible segments, potentially impacting transition detection accuracy. However, through careful channel design, it is possible to find a balance that achieves satisfactory performance in both areas.

8.2.1 Optimization-Based Design Approach

The pilot channel design is framed as an optimization problem. The optimization goal is to maximize the minimum Hamming distance between each of the 1-block patterns and all possible shifts of equal length, enhancing transition distinctiveness. For acquisition efficiency, rather than minimizing the average number of alternative code runs (which would complicates the problem), the focus is on reducing the overall count of alternative codes (c_1) within each block, with transition detection optimized under this constraint.

The result is a binary pattern when mapped to legitimate and alternative codes per Serial DSSS principles, it forms the pilot channel.

8.2.2 Modeling of the Problem

The pilot channel optimization problem is formulated using the following parameters, decision variables, and constraints:

8.2.3 Parameters

- K: Length of the binary pattern $\underline{p}$.
- B: Block length within the binary pattern.
- m: Number of ones per block.
- $b = \frac{K}{B}$: Number of blocks.

8.2.4 Decision Variables

- $\underline{p}$: Binary pattern with p_i representing the i-th bit, where $p_i \in \{0, 1\}$ for $i = 1, 2, \ldots, K$.

8.2.5 State Variables

- $\mathbf{P}$: Matrix where each row is a 1-block pattern:

$$\mathbf{P} = \begin{pmatrix} p_1 & \cdots & \cdots & \cdots & \cdots & p_B \\ p_{B+1} & \cdots & \cdots & \cdots & \cdots & p_{2B} \\ \vdots & \vdots & \vdots & \vdots & \vdots & \vdots \\ p_{(b-1)B+1} & \cdots & \cdots & \cdots & \cdots & p_{bB} \end{pmatrix}$$

- $\mathbf{S}$: Matrix containing all segments of length B in $\underline{p}$:

$$\mathbf{S} = \begin{pmatrix} p_1 & \cdots & \cdots & p_B \\ p_2 & \cdots & \cdots & p_{B+1} \\ \vdots & \vdots & \vdots & \vdots \\ p_{(b-1)B+1} & \cdots & p_{bB} & p_1 \\ \vdots & \vdots & \vdots & \vdots \\ p_{bB} & p_1 & \cdots & p_{B-1} \end{pmatrix}$$

- $Z \in \mathbb{Z}$: Integer for the maximum dot product between any 1-block pattern and any 1-block long shift of $\underline{p}$ (excluding itself).

8.2.6 Problem Formulation

$$\min Z$$

subject to:

$$\sum_{j=iB+1}^{(i+1)B} p_j = m, \quad \forall i = 0, 1, \ldots, (b-1),$$

$$Z \geq \mathbf{P}_i \cdot \mathbf{S}_j^{\mathrm{T}}, \quad \forall i = 1, 2, \ldots, b, \quad \forall j = 1, \ldots, K, \quad j \neq (i-1)B + 1.$$

8.3 Pilot Channel Presentation

For the presented pilot channel, the following parameters were selected:

- $K = 320$: Total length of the binary pattern.
- $B = 64$: Length of each block within the binary pattern.

- $b = \frac{K}{B} = 5$: Total number of blocks.

The pilot channel optimization problem was solved using the Gurobi optimizer with a time limit given the challenge of achieving optimal convergence due to the problem's complexity. The solutions presented here, while not optimal, provide considerable improvements over the original channel.

We introduce three distinct pilot channel designs:

- **Channel A: Enhanced Acquisition** - This design prioritizes acquisition performance with $m = 8$ (ones per block), facilitating improved signal acquisition.
- **Channel B: Enhanced Transition Detection** - Focused on block transition distinctiveness, this design sets $m = 12$, enhancing detection accuracy for transitions.
- **Channel C: Balanced Design** - This design balances acquisition efficiency and transition detection accuracy, setting $m = 10$ to achieve a compromise between the two objectives.

The three pilot channel designs are illustrated in Fig. 8.1, where orange indicates a '1' and blue indicates a '0'. In these designs, '1' is mapped to the alternative code ($\underline{c_1}$), and '0' is mapped to the legitimate code ($\underline{c_0}$), forming the complete pilot channel.

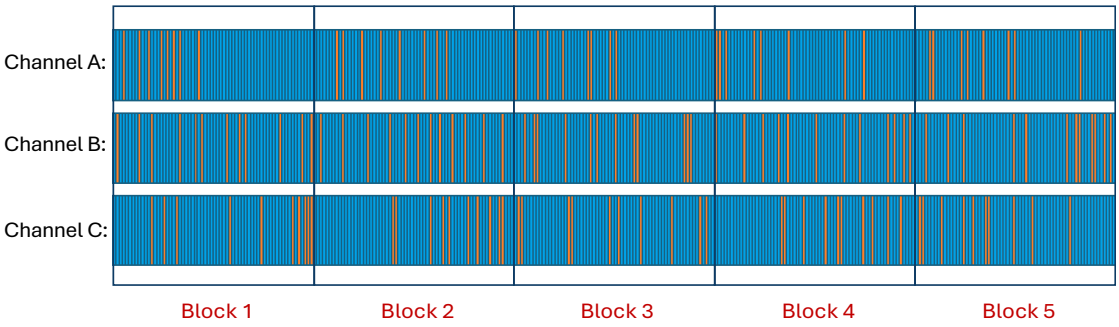

Figure 8.1: Visualization of the three pilot channel designs: Channel A, Channel B, and Channel C. Orange represents '1' (mapped to the alternative code), and blue represents '0' (mapped to the legitimate code).

8.3.1 Channel A: Enhanced Acquisition

Channel A is tailored to improve acquisition by reducing the presence of alternative codes (c_1) in each block. With $m = 8$, this design facilitates efficient acquisition

performance by limiting the number of ones. Although fewer runs of c_1 codes could further enhance acquisition, this would increase optimization complexity as discussed before. Instead, the focus here remains on minimizing the maximum dot product to aid in block transition detection.

Performance of Channel A The ROC curve in Fig. 8.2 compares Channel A's transition detection performance to the original pilot channel.

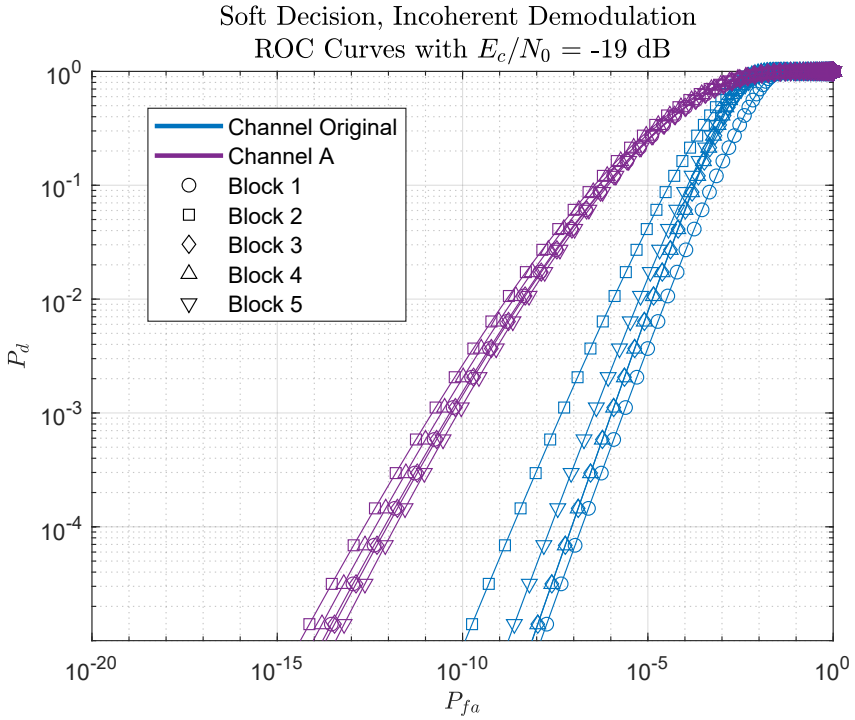

Figure 8.2: ROC curve for Channel A, comparing transition patterns with the original channel.

The acquisition performance of Channel A, shown in Fig. 8.3, illustrates its balance between detection accuracy and acquisition efficiency, highlighting its effective compromise.

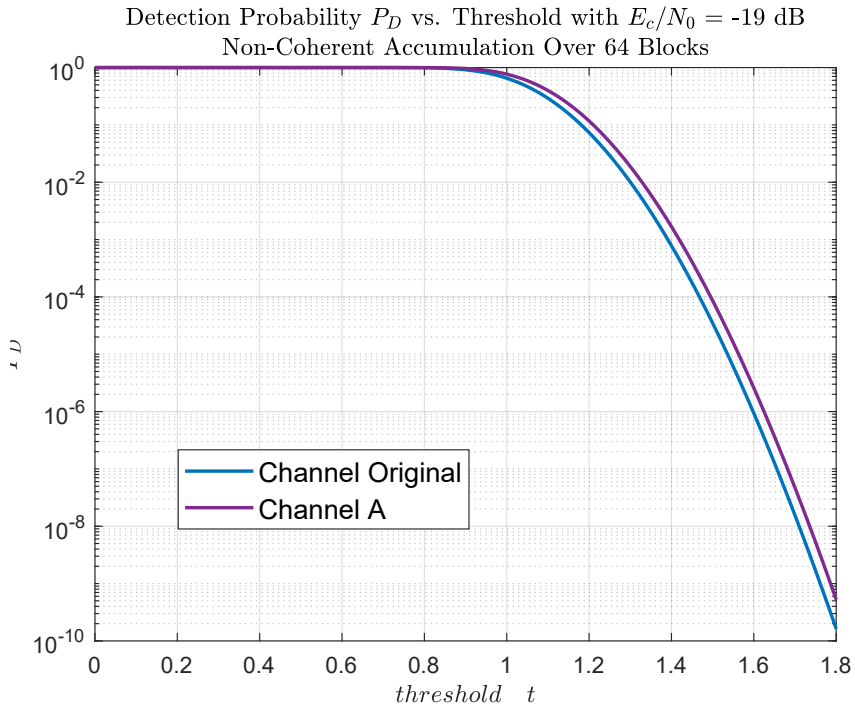

Figure 8.3: Acquisition performance comparison between the original and Channel A, showing detection probability (P_D).

8.3.2 Channel B: Improved Block Transition Detection

Channel B is designed to maximize the distinctiveness of block transitions, with $m = 12$ to ensure highly distinguishable transitions for accurate detection.

Performance Comparison The ROC curve in Fig. 8.4 compares Channel B's transition detection performance to the original pilot channel, highlighting its enhanced distinctiveness for block transitions.

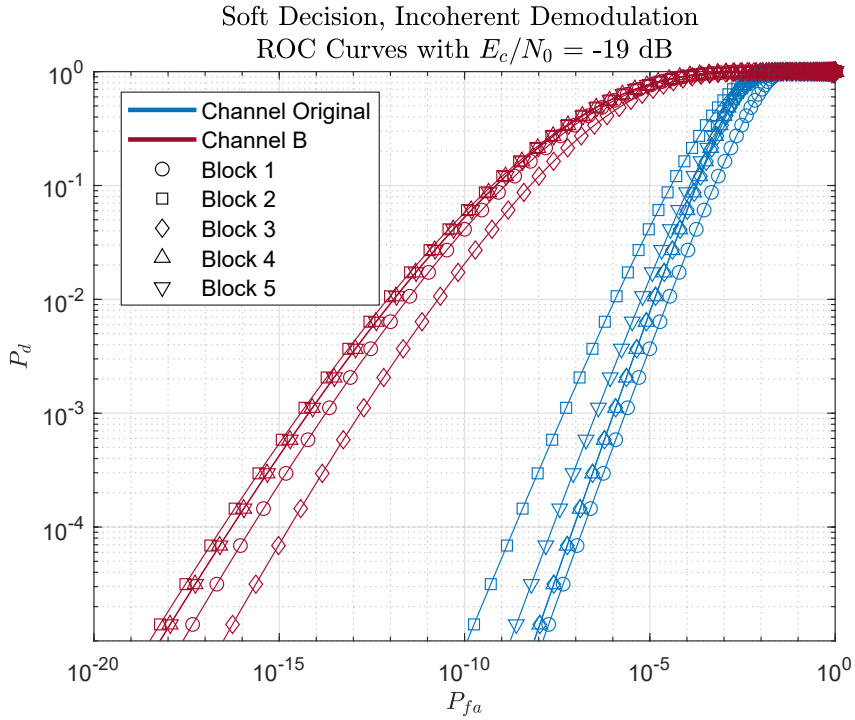

Figure 8.4: ROC curve for Channel B, comparing transition patterns with the original channel.

The acquisition performance of Channel B, shown in Fig. 8.5, illustrates the trade-off, where enhanced transition detection slightly impacts acquisition performance.

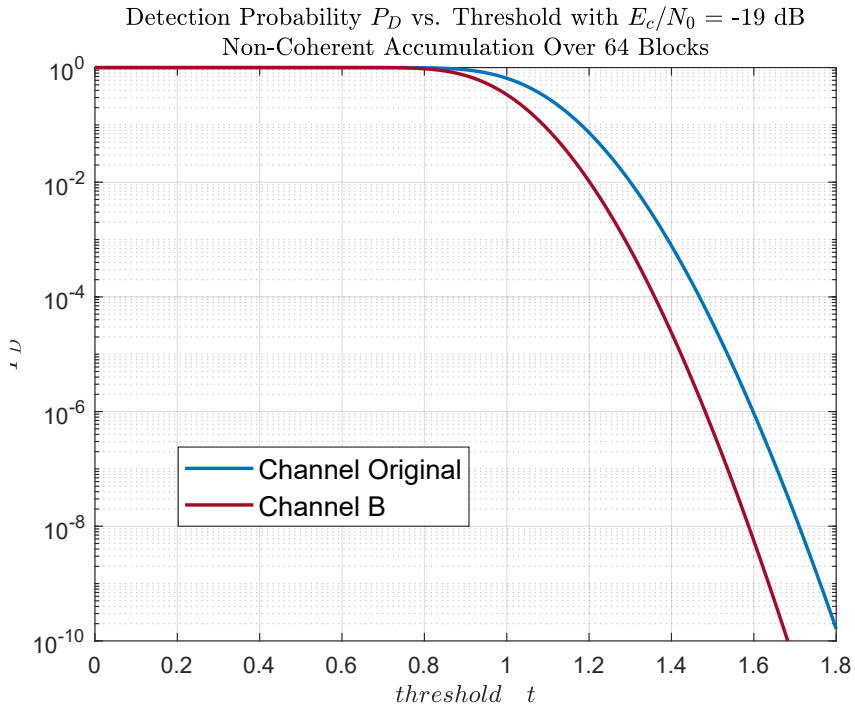

Figure 8.5: Acquisition performance comparison between the original and Channel B, showing detection probability (P_d).

8.3.3 Channel C: Balanced Approach

Channel C provides a compromise between acquisition efficiency and transition detection accuracy, with $m = 10$ to balance both aspects.

Performance Comparison The ROC curve in Fig. 8.6 compares Channel C's transition detection performance to the original pilot channel, highlighting its balance between distinct transitions and acquisition efficiency.

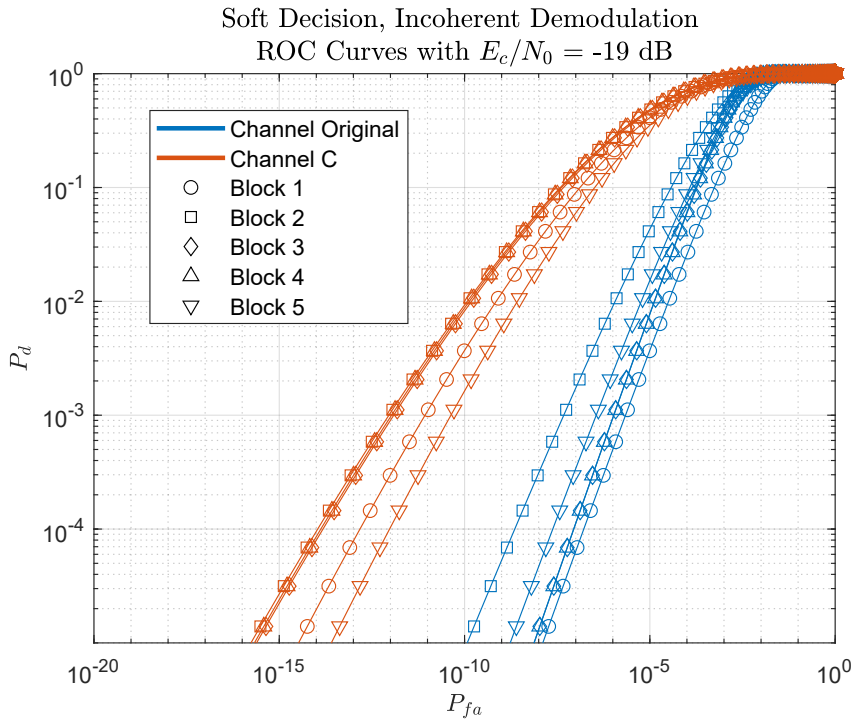

Figure 8.6: ROC curve for Channel C, comparing transition patterns with the original channel.

The acquisition performance for Channel C, shown in Fig. 8.7, illustrates its balanced approach, maintaining reasonable performance in both acquisition and transition detection.

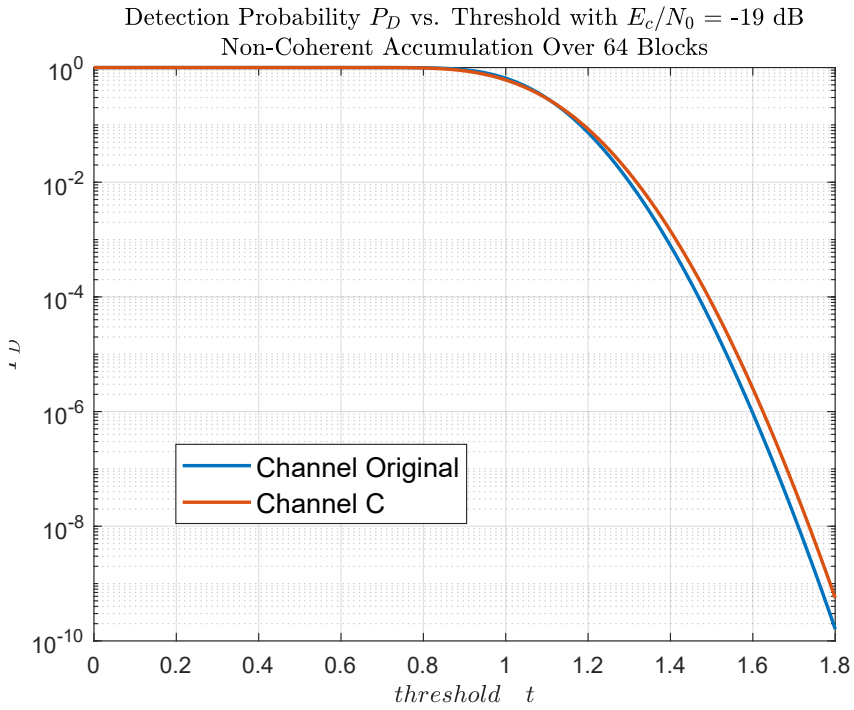

Figure 8.7: Acquisition performance comparison between the original and Channel C, showing detection probability (P_d).

Chapter 9

Conclusion and Future Work

This thesis has presented a comprehensive treatment of Serial Bicode/Multicode DSSS pilot channels, including derivations of error performance under coherent demodulation, analytical frameworks to evaluate the performance of pilot channels employing Serial Bicode DSSS, and a novel approach to channel design by treating the design as an optimization task. The results confirm the potential of embedding additional codes within a single pilot channel to expedite synchronization tasks, particularly under challenging satellite navigation conditions in both MEO and LEO orbits.

While the proposed design methodology demonstrates significant performance gains, there remain several avenues for refinement and further research:

- **Enhanced Optimization:** The proposed Algorithm for selecting the code blocks may be improved by adopting refined solvers or heuristics. Alternatively, more advanced techniques—such as integer programming or metaheuristics—could be explored.
- **Machine Learning for Transition Detection:** Transition detection in block-structured pilot signals may benefit from modern machine learning techniques. Neural network architectures, or lightweight denoising models coupled with conventional correlators, could potentially reduce false alarms and improve performance under various conditions.
- **Personalized Local Code for Extended Coherent Integration:** A carefully optimized local reference code, tailored for the bicode structure, could enable extended coherent integration times in the cross ambiguity function. Increasing coherent processing intervals could further enhance acquisition performance in low-SNR scenarios.

Collectively, these proposed directions promise to further advance the design and performance of Serial Bicode/Multicode DSSS pilot channels, offering new ways to meet the requirements of next-generation satellite navigation systems.

Bibliography

[1] R. Garello. «Serial Multicode Direct Sequence Spread Spectrum with Applications to Satellite Navigation Pilot Channels». In: *IEEE Transactions on Communications* (2023) (cit. on pp. ii, 1, 2, 4–6, 8, 27, 28, 30, 31, 73, 88).

[2] Elliott D. Kaplan and Christopher J. Hegarty. *Understanding GPS/GNSS: Principles and Applications*. 3rd. Artech House, 2017 (cit. on pp. 1, 22, 26).

[3] Peter Teunissen and Oliver Montenbruck. *Springer handbook of global navigation satellite systems*. Springer, 2017 (cit. on p. 1).

[4] Daniele Borio. «GNSS Data/Pilot Combining with Extended Integrations for Carrier Tracking». In: *Sensors* 23.8 (2023). DOI: 10.3390/s23083932 (cit. on p. 1).

[5] Kannan Muthuraman. «Tracking Techniques for GNSS Data/Pilot Signals». PhD thesis. Calgary, Canada: University of Calgary, Jan. 2010 (cit. on p. 1).

[6] Stefan Wallner et al. «Quasi-Pilot Signal Design – Facilitating New Signal Processing Concepts». In: *Proceedings of the 34th International Technical Meeting of the Satellite Division of The Institute of Navigation (ION GNSS+ 2021)*. 2021, pp. 1859–1876. DOI: https://doi.org/10.33012/2021.17981 (cit. on p. 1).

[7] Marco Anghileri, Matteo Paonni, Stefan Wallner, Jose-Angel Avila-Rodriguez, and Bernd Eissfeller. «Estimating the Time-To-First-Fix for GNSS Signals Theory and Simulation Results». In: *European Navigation Conference (ENC GNSS) Proceedings*. Toulouse, France, Jan. 2008 (cit. on p. 1).

[8] Don Torrieri. *Principles of Spread-Spectrum Communication Systems*. Switzerland AG 2022: Springer Cham, 2022. DOI: https://doi.org/10.1007/978-3-030-75343-6 (cit. on p. 1).

[9] Chih-Lin I and R.D. Gitlin. «Multi-code CDMA wireless personal communications networks». In: *Proceedings IEEE International Conference on Communications ICC '95*. Vol. 2. 1995, 1060–1064 vol.2. DOI: 10.1109/ICC.1995.524263 (cit. on p. 1).

[10] Dong In Kim. «Optimum packet data transmission in cellular multirate CDMA systems with rate-based slot allocation». In: *IEEE Transactions on Wireless Communications* 3.1 (2004), pp. 165–175. DOI: 10.1109/TWC.2003.821160 (cit. on p. 1).

[11] Rajan Kapoor and Preetam Kumar. «Multicode CDMA/CI for multimedia services over LEO satellite channel». In: *2014 International Conference on Advances in Computing, Communications and Informatics (ICACCI)*. 2014, pp. 301–304. DOI: 10.1109/ICACCI.2014.6968464 (cit. on p. 1).

[12] Sagheer Khan, Muhammad Zeeshan, and Yasar Ayaz. «Implementation and analysis of MultiCode MultiCarrier Code Division Multiple Access (MC–MC CDMA) in IEEE 802.11ah for UAV Swarm communication». In: *Physical Communication* 42 (2020), p. 101159. ISSN: 1874-4907. DOI: https://doi.org/10.1016/j.phycom.2020.101159 (cit. on p. 1).

[13] D. Torrieri. *Principles of Spread-Spectrum Communication Systems*. Springer, 2005 (cit. on pp. 3, 5).

[14] John G. Proakis and Masoud Salehi. *Digital Communications*. 5th. McGraw-Hill, 2007. ISBN: 978-0072957167 (cit. on pp. 7, 14).

[15] Pratap Misra and Per Enge. *Global Positioning System: Signals, Measurements and Performance*. 2nd. Ganga-Jamuna Press, 2006 (cit. on p. 22).

[16] Kai Borre, Dennis M. Akos, Nicolaj Bertelsen, Peter Rinder, and Soren Holdt Damm. *A Software-Defined GPS and Galileo Receiver: A Single-Frequency Approach*. Birkhauser, 2007 (cit. on p. 22).

[17] B. Hofmann-Wellenhof, H. Lichtenegger, and E. Wasle. *GNSS - Global Navigation Satellite Systems: GPS, GLONASS, Galileo & more*. Springer, 2008 (cit. on p. 22).

[18] James Bao-Yen Tsui. *GPS Fundamentals and Applications*. John Wiley & Sons, 2005 (cit. on p. 22).

[19] European Space Agency (ESA). *Front End*. Navipedia. 2024. URL: https://gssc.esa.int/navipedia/index.php/Front_End (cit. on p. 23).

[20] J. Leclère. «Resource-efficient parallel acquisition architectures for modernized GNSS signals». Ph.D. Thesis. PhD thesis. Ecole Polytechnique Fédérale de Lausanne (EPFL), 2014 (cit. on p. 23).

[21] B. Motella and L. Lo Presti. «The Math of Ambiguity: What is the acquisition ambiguity function and how is it expressed mathematically?» In: *Inside GNSS* 5 (2010), pp. 20–28 (cit. on p. 23).

[22] M. Foucras, J. Leclère, C. Botteron, O. Julien, C. Macabiau, et al. «Study on the cross-correlation of GNSS signals and typical approximations». In: *GPS Solutions* (2016). hal-01353985. DOI: 10.1007/s10291-016-0556-7 (cit. on p. 23).

[23] Phillip W. Ward, John W. Betz, and Christopher J. Hegarty. *Satellite Signal Acquisition, Tracking, and Data Demodulation*. Vol. 1. Understanding GPS Principles and Applications. Within Understanding GPS Principles and Applications, edited by Elliott D. Kaplan and Christopher J. Hegarty. Artech House, 2006 (cit. on p. 24).

[24] M. L. Psiaki, H. Jung, and P. M. Kintner. «Design of a GPS Software Receiver: A Case Study». In: *GPS Solutions* 4.4 (2001), pp. 30–46. DOI: 10.1007/PL00012854 (cit. on p. 24).

[25] Fabio Dovis. *GNSS Interference Threats and Countermeasures*. Artech House, 2015. ISBN: 978-1608078100 (cit. on pp. 24, 26).

[26] Pratap Misra and Per Enge. *Global Positioning System: Signals, Measurements, and Performance*. 2nd. Ganga-Jamuna Press, 2011. ISBN: 978-0970954428 (cit. on p. 26).

[27] A. J. Van Dierendonck. «GPS Receivers». In: *Global Positioning System: Theory and Applications*. Ed. by Bradford W. Parkinson and James J. Spilker. Vol. 1. American Institute of Aeronautics and Astronautics, 1996, pp. 329–407 (cit. on p. 26).

[28] Il Heung Choi, Sang Hyun Park, Deuk Jae Cho, Sang Jun Yun, Young Baek Kim, and Sang Jeong Lee. «A novel weak signal acquisition scheme for assisted GPS». In: *Proceedings of the 15th International Technical Meeting of the Satellite Division of The Institute of Navigation (ION GPS 2002)*. Sept. 2002 (cit. on p. 26).

[29] Steven M. Kay. *Fundamentals of Statistical Signal Processing, Volume 2: Detection Theory*. Prentice Hall, 1998. ISBN: 978-0135041352 (cit. on p. 34).

[30] Daniele Borio. «A Statistical Theory for GNSS Signal Acquisition». Ph.D. Thesis. PhD thesis. Department of Electronics and Telecommunications: Politecnico di Torino, Jan. 2007 (cit. on pp. 75, 82, 83).

[31] L. Musumeci, F. Dovis, Pedro F. Silva, Hugo D. Lopes, and João S. Silva. «Design of a very High Sensitivity acquisition system for a space GNSS receiver». In: *2014 IEEE/ION Position, Location and Navigation Symposium - PLANS 2014*. 2014, pp. 556–568. DOI: 10.1109/PLANS.2014.6851417 (cit. on p. 76).

[32] Cillian O'Driscoll. «Performance Analysis of the Parallel Acquisition of Weak GPS Signals». Ph.D. Thesis. PhD thesis. Department of Electrical and Electronic Engineering: National University of Ireland, Cork, Jan. 2007.

[33] Elliott Kaplan and Christopher Hegarty. *Understanding GPS: principles and applications*. Artech House, 2005.

[34] Elliott Kaplan and Christopher Hegarty. *Understanding GPS/GNSS: Principles and Applications*. Artech House, 2017.

[35] Roberto Garello. «Serial Multicode Direct Sequence Spread Spectrum With Applications to Satellite Navigation Pilot Channels». In: *IEEE Communications Letters* 28.11 (2024), pp. 2603–2607. DOI: 10.1109/LCOMM.2024.3457693.

[36] P. Henkel. «Precise Point Positioning with Kepler». In: *2019 IEEE 90th Vehicular Technology Conference (VTC2019-Fall)*. 2019, pp. 1–5.

[37] B. T. Fang. «Geometric dilution of precision in Global Positioning System navigation». In: *Journal of Guidance and Control* 4.1 (1981), pp. 92–94. DOI: 10.2514/3.19719.

[38] Peter Teunissen and Oliver Montenbruck, eds. *Springer Handbook of Global Navigation Satellite Systems*. Cham, Switzerland: Springer, 2017.

[39] Philip Mayne Woodward. *Probability and Information Theory, with Applications to Radar*. Dedham, Mass.: Artech House, 1980.

[40] Parisa Borhani-Darian, Haoqing Li, Peng Wu, and Pau Closas. «Deep Learning of GNSS Acquisition». In: *Sensors* 23.3 (2023), p. 1566. DOI: 10.3390/s23031566.